Université du Québec
à Rimouski

DYNAMIQUE SÉDIMENTAIRE ET CONDITIONS OCÉANIQUES DE SURFACE SUR LE TALUS DU MACKENZIE AU COURS DE L'HOLOCÈNE RÉCENT

Mémoire présentée

dans le cadre du programme de maîtrise en Océanographie

en vue de l'obtention du grade de maître ès sciences (M.Sc.)

PAR

© OMNAIN FRANCIS KUTOS YRIZA

Août 2019

Composition du jury :

Michel Gosselin, président du jury, UQAR-ISMER, Rimouski

Rochon André, directeur de recherche, UQAR-ISMER, Rimouski

Jean-Carlos Montero-Serrano, codirecteur de recherche, UQAR-ISMER, Rimouski

Elisabeth Levac, examinatrice externe, Université Bishop's

Dépôt initial le 19 juin 2019 Dépôt final 13 août 2019

REMERCIEMENTS

Tout d'abord, je souhaite remercier mon directeur de recherche, André Rochon qui m'a guidé tout au long de ce projet et qui a su éclairer ma démarche grâce à ces compétences sur le sujet. J’ai apprécié la clarté de ses explications, sa facilité à vulgariser et transmettre ses connaissances et sa passion sur la palynologie. Merci également à mon co-directeur Jean-Carlos Montero-Serrano qui m'a fait confiance et qui a appuyé ma candidature afin d’obtenir ce projet de maîtrise à l’ISMER. L’obtention de ce projet était une étape importante dans ma vie. André et Jean-Carlos m’ont également donné l’opportunité de participer à des congrès nationaux et internationaux qui ont enrichi mon expérience académique. Je leur en suis grandement reconnaissante. Merci aussi pour le soutien financier de l’UQAR-ISMER pour les cinq premières sessions et les bourses obtenues par Arctrain.

Un remerciement particulier à Thomas Richerol pour le soutien qu'il m'a apporté pour le comptage des dinokystes, ainsi que sa disponibilité lorsque j'avais des questions sur des points qui m'étaient particulièrement ambigus. Merci également à Charles-Édouard, Myriam, Maria Emilia, Adriana, Simon et Iliana pour leur aide tout au long de la maîtrise. Merci à l’équipe de géologie de m’avoir accueilli chaleureusement dès mon arrivée à Rimouski et notamment, à mes amies vénézuéliennes pour m’avoir fait sentir proche de mon pays. Merci Yan d’avoir été mon guide dans ce parcours et être là pour moi à tout moment.

Finalement, un grand merci à ma famille de m’avoir soutenu tout au long de cette aventure !

RÉSUMÉ

La composition minéralogique (fractions brute et argileuse) et géochimique, ainsi que les assemblages de kystes de dinoflagellés (dinokystes) ont été étudiés afin de reconstituer les apports détritiques et d'estimer les conditions des masses d'eau de surface liés à la variabilité hydroclimatique de l'Holocène récent au cours des derniers 2000 ans. Dans ce contexte, une carotte à boîte et une à gravité ont été prélevées sur le talus du Mackenzie (mer de Beaufort, Arctique canadien) et combinées en une séquence composite (AMD0214-03: 03CS).

Quatre principales zones géochimiques et de dinokystes ont été déterminées sur la base d'une analyse de regroupement hiérarchique: La **Zone I** (2700 – 2000 cal yr BP) montre une granulométrie et des valeurs de l'ensemble des éléments géochimiques relativement constantes. Cette zone est dominée par des espèces autotrophes (kyste de *Pentapharsodinium dalei* et *Operculodinium centrocarpum*), de palynomorphes d'eau douce et pré-quaternaires. Les valeurs élevées de flux de dinokystes et de réseaux organiques de foraminifères suggèrent des productivités primaires et benthiques élevées, alors que les palynomorphes d'eau douce et pré-quaternaires suggèrent des apports importants d'eau douce en provenance du fleuve Mackenzie. Les rapports minéralogiques élevés de illite/K-feldspath+plagioclase (I/Fsp) et bas de smectite+vermiculite/illite (S+V/I) suggèrent une provenance de sédiments du nord du bassin du fleuve Mackenzie en raison de fortes précipitations septentrionales, ce qui correspond à une configuration négative de l'oscillation décennale du Pacifique (ODP-) et à une faible dépression des Aléoutienne-ouest. La ODP- ainsi que la configuration positive de l'oscillation arctique (OA+; affaiblissement du gyre de Beaufort) au cours de cette période suggèrent également une augmentation des apports d'eau du Pacifique Nord (riche en nutriments); La **Zone II** (2000 – 200 cal yr BP) montre une diminution du taux de sédimentation (de 53 à 23 cm/ka), du flux des dinokystes ainsi que de l'ensemble des palynomorphes, ce qui suggère des conditions climatiques plus sèches en lien avec une diminution de la décharge du fleuve Mackenzie, ainsi qu'une productivité primaire diminuée. Les rapports I/Fsp et S+V/I indiquent une augmentation progressive des feldspaths et des smectites-vermiculites (minéraux caractéristiques du sud du bassin du fleuve Mackenzie). De plus, cette zone montre une diminution graduelle des espèces autotrophes vers la dominance des hétérotrophes qui devient plus marquée (productivité primaire possiblement dominée par des diatomées) dans une période qui correspond au début de l'Optimum climatique médiéval (OCM: ~ AD 800 – 1525) jusqu'à la fin du Petit âge glaciaire (PAG : ~ AD 1525 – 1865). L'OCM et le PAG sont marqués par l'augmentation de l'abondance relative de *Spiniferites elongatus/frigidus* (conditions relativement plus douces) et d'*Islandinium minutum* s.l. (conditions relativement plus froides), respectivement. Ces résultats sont en accord avec un signal plus faible de l'OA (gyre de Beaufort renforcé) et d'un

changement d'une phase ODP- (faible dépression des Aléoutiennes-ouest) à une phase ODP+ (forte dépression des Aléoutiennes-est) qui correspond à une diminution des précipitations au nord du Pacifique. Par contre, la Z**one III** (AD 1800 – 1950) montre une augmentation du Ts (jusqu'à 167 cm/ka), de certains rapports élémentaires (ex., Al/Ca, As/Al et Fe/Al) et minéralogiques (Argiles/Dol, I/Fsp et illite/kaolinite+chlorite) et une diminution du rapport S+V/I, ce qui indique une forte augmentation des apports sédimentaires du bassin nord du fleuve Mackenzie par rapport au bassin sud. Cependant, les valeurs relativement élevées en smectite et vermiculite (S+V/I) à la base de cette zone indiquent aussi une certaine contribution du bassin sud. Ceci est probablement contrôlé par une configuration ODP+ (forte dépression des Aléoutiennes-est), ce qui implique un transport d'humidité plus important vers le nord-ouest du continent nord-américain et à une augmentation des précipitations au sud du bassin du fleuve Mackenzie. Cette augmentation d'apport d'eau douce est également marquée par l'augmentation des flux de palynomorphes d'eau douce et pré-quaternaires. On y observe la co-dominance de taxons autotrophes et hétérotrophes. Finalement, la **Zone IV** (AD 1950 – moderne) est caractérisée par un taux de sédimentation élevé (143 cm/ka) et une augmentation de la taille des grains (2,7 à 4,1µm). Les espèces autotrophes (*Operculodinium centrocarpum* et kyste de *Pentapharsodinium dalei*) et les conditions oxiques (augmentation de Fe-oxides) dominent.

Les variations dans l'intensité des apports sédimentaires et d'eau douce du fleuve Mackenzie, ainsi que l'arrivée de masses d'eau en provenance du Pacifique sur le talus du Mackenzie, sont probablement dues au changement des modes de variabilité climatique du Pacifique. Ceci est semblable aux mécanismes actuels selon lesquels l'OA et l'ODP contrôlent la plupart des précipitations dans les bassins versants du fleuve Mackenzie et l'advection des eaux du Pacifique vers l'océan Arctique.

Mots-clés: Holocène récent; secteur canadien de la mer de Beaufort; talus du Mackenzie; Kystes de dinoflagellés; Minéralogie totale et des argiles; Géochimie élémentaire; Oscillation décennale du Pacifique; Oscillation Arctique; Dépression des Aléoutiennes.

ABSTRACT

Bulk and clay mineralogy and elemental geochemistry, together with dinoflagellate cyst (dinocyst) assemblages, were investigated in order to reconstruct detrital inputs and to estimate sea-surface conditions related to late Holocene ocean-climate variability over the last 2000 years. In this context, a box core (BC) and a trigger weight core (TWC) were recovered from the Mackenzie Slope (Beaufort Sea, Canadian Arctic) and combined into a composite sequence (AMD0214-03: 03CS).

Four main geochemical and dinocyst zones were determined based on constrained cluster analysis: **Zone I** (2700 – 2000 cal yr BP) reveals relatively constant values in grain size and all geochemical elements. This zone is dominated by autotrophic taxa (cyst of *Pentapharsodinium dalei* and *Operculodinium centrocarpum*), by freshwater and pre-Quaternary palynomorphs. High dinocyst and foraminifer organic lining influxes suggest important primary and benthic productivities, whereas freshwater and pre-Quaternary palynomorphs suggest important freshwater inputs from the Mackenzie River. The high illite/K-feldspar+plagioclase (I/Fsp) and smectite/vermiculite/illite (S+V/I) mineralogical ratios suggest northern Mackenzie Basin sediment sources due to strong northern precipitations, corresponding to a negative phase of the Pacific Decadal Oscillation (PDO-). A PDO- and a positive phase of the Arctic Oscillation (AO+; weak Beaufort Gyre) during this period also suggest an increase in North Pacific nutrient-rich waters; **Zone II** (2000 – 200 cal yr BP) shows a decrease of the sedimentation rate (from 53 to 23 cm/ka), dinocysts and all palynomorph influxes, suggesting drier weather conditions associated with a decrease in the Mackenzie River discharge, together with a reduced primary productivity. The mineralogical ratios I/Fsp and S+V/I show a gradual increase in the input of feldspars and smectite-vermiculite, which are characteristic minerals from the southern Mackenzie basin. Moreover, this zone shows a gradual decrease of autotrophic species in favor of heterotrophic taxa, which intensified (primary productivity possibly dominated by diatoms) in a period coinciding with the beginning of the Medieval Warm Period (MWP: ~ AD 800 – 1525) and the end of the Little Ice Age (LIA: ~ AD 1525 – 1865). The MWP and the LIA are marked by an increase in the relative abundances of *Spiniferites elongatus/frigidus* (relatively milder conditions) and *Islandinium minutum* s.l. (relatively colder conditions), respectively. These results agree with a weaker signal in AO (stronger Beaufort Gyre) and with changes from a the PDO- state (weak west Aleutian Low) to a PDO+ state (strong east Aleutian Low) which correspond with a gradual decrease in the amount of precipitation over the North Pacific. However, **Zone III** (AD 1800 – 1950) displays a sharp increase in the sedimentation rate (up to 167 cm/ka) and in certain elemental (e.g., Al/Ca, As/Al and Fe/Al), mineralogical (total clays/dolomite, I/Fsp and illite/kaolinite+chlorite) ratios, and a decrease in the S+V/I ratio, suggesting increasing detrital input from the northern basin of the Mackenzie River in relation to the southern basin. However, the beginning of the zone is marked by relatively

high values of smectite and vermiculite, which indicates some contribution from the southern basin. This is probably controlled by a PDO+ phase (strong east Aleutian Low), which induces more moisture to the northwestern North American continent and increased precipitation in the southern part of the Mackenzie River basin. The increasing freshwater input is concomitant with those of the freshwater and pre-Quaternary palynomorph influxes. The co-dominance of autotrophic and heterotrophic taxa is also observed. Finally, **Zone IV** (AD 1950 – modern) is characterized by a high sedimentation rate (143 cm/ka) and increasing grain size (2.7 to 4.1 µm). Autotrophic taxa (*Operculodinium centrocarpum* and cyst of *Pentapharsodinium dalei*) and oxic conditions (increase in Fe-oxides) dominate.

Sediment and freshwater input intensity variations from the Mackenzie River, as well as the entry of Pacific water over the Mackenzie Slope, are likely due to changing patterns of Pacific climate variability. This could be similar to the current mechanisms under which the PDO and the AO control most precipitations in the Mackenzie River basins and the Pacific water advection toward the Arctic Ocean.

Keywords: Late Holocene, Canadian Beaufort Sea; Mackenzie Slope; Dinoflagellate cysts; Bulk and clay mineralogy; Geochemistry; Pacific Decadal Oscillation; Arctic Oscillation; Aleutian Low.

TABLE DES MATIÈRES

LISTE DES TABLEAUX

LISTE DES FIGURES

LISTE DES ABRÉVIATIONS, DES SIGLES ET DES ACRONYMES

CODE	SIGNIFICATION EN FRANÇAIS
AD	Anno Domini
AL	Dépression des Aléoutiennes
BC	Carottier à boîte
BP	Before present (before 1950)
C	Chlorite
CS	**S**équence composite
Dol	Dolomite
DTP	Dérive Transpolaire
et al.	Et alii (et collaborateurs)
ex.	Par example
I	Illite
ISMER	Institut des sciences de la mer de Rimouski
K	Kaolinite
ka	Millier(s) d'années
OA	Oscillation Arctique

OCM	Optimum climatique médiéval
ODP	Oscillation décennale du Pacifique
PAG	Petite âge glaciaire
^{210}Pb	Plomb-210
PC	Carottier à piston
S	Smectite
TWC	Carottier déclencheur
UCV	Universidad Central de Venezuela
UQAR	Université du Québec à Rimouski
V	Vermiculite
yr	an

CODE	**SIGNIFICATION EN ANGLAIS**
AD	Anno Domini
AL	Aleutian Low
AO	Arctic Oscillation
BC	Box core
C	Chlorite
CAA	Canadian Arctic Archipelago
cal	Calibrated years

CS	Composite core
Dol	Dolomite
EF	Enrichment Factors
e.g	Exempli gratia (for example)
et al.	Et alii (and others)
Fsp	K-Feldspath+Plagioclase
HCl	Hydrochloric acid
HF	Hydrofluoric acid
I	Illite
K	Kaolinite
LIA	Little Ice Age
MAT	Modern Analogue Technique
MWP	Medieval Warm Period
PAAS	Post-Archaean Average Shale
^{210}Pb	Lead-210
PC	Piston core
PDO	Pacific Decadal Oscillation
S	Smectite
SSS	Sea-surface salinity
SST	Sea-surface temperature

TPD	Transpolar Drift
TWC	Trigger weight core
UCV	Universidad Central de Venezuela
V	Vermiculite
yr	year

AVANT-PROPOS

Ce mémoire de maîtrise est présenté en trois parties : une introduction générale rédigée en français, d'un chapitre principal rédigé en anglais sous forme d'article scientifique en prévision d'être soumis pour publication à la revue internationale «*Quaternary Research*», et une brève conclusion générale rédigée en français.

Contributions et autres réalisations

L'article présenté dans ce mémoire de maîtrise a été rédigé par moi-même sous la supervision des professeurs André Rochon et Jean-Carlos Montero-Serrano de l'UQAR-ISMER. En tant que premier auteur, ma contribution de ce travail fut la réalisation des analyses de laboratoire des différents traceurs minéralogiques, géochimiques et palynologiques et la rédaction de l'article. Les professeurs André Rochon et Jean-Carlos Montero-Serrano ont fourni l'idée originale, l'implémentation du développement de la méthode et la formation nécessaire pour réaliser les analyses de laboratoire, et ont contribué à la révision de l'article. Thomas Richerol a validé le comptage des échantillons palynologiques. La datation au ^{210}Pb a été effectuée par les techniciens du centre de recherche GEOTOP.

Au cours ma maîtrise j'ai eu l'opportunité de présenter les principaux résultats de ce projet de recherche dans cinq congrès nationaux et internationaux :

Kutos, O., Rochon, A., Montero-Serrano, J.-C., 2018. Late Holocene surface ocean conditions on the Mackenzie Slope - Beaufort Sea, Canadian Arctic. Congrès des étudiants du GEOTOP 2018, La Malbaie, Québec, Canada, 21 au 23 mars.

Kutos, O., Rochon, A., Montero-Serrano, J.-C., 2017. Multi-proxy study in Arctic Late Holocene sediment cores on the continental margin of the western Canadian Beaufort Sea. DINO11 - 11th International conference on modern and fossil dinoflagellates, 17-21 juillet, Bordeaux, France.

Kutos, O., Rochon, A., Montero-Serrano, J.-C., 2017. Late Holocene sediment dynamics and surface ocean conditions on the Mackenzie Slope - Beaufort Sea, Canadian Arctic. ArcTrain 4th Annual meeting, 18-20 September, Bremen, Allemagne.

Kutos, O., Rochon, A., Montero-Serrano, J.-C., 2017. Multi-proxy reconstruction of late Holocene palaeoceanography and sediment dynamic over the Mackenzie Slope (Beaufort Sea, Canadian Arctic). Arctic Change meeting, 11-15 December, Quebec, Canada.

Kutos, O., Rochon, A., Montero-Serrano, J.-C., 2017. Dynamique sédimentaire et conditions océaniques de surface sur le talus du Mackenzie au cours de l'Holocène récent - Mer de Beaufort, Arctique canadien. Congrès des étudiants du GEOTOP 2017, Forêt Montmorency, Québec, Canada, 24 au 26 mars.

Financements et bourses obtenus :

- Soutien financier d'André Rochon et Jean-Carlos Montero-Serrano à travers des subventions d'ArcticNet et le Conseil de recherches en sciences naturelles et en génie du Canada (CRSNG).
- Soutien financier de l'UQAR-ISMER pour les premières cinq sessions (1000$/session)
- Bourses d'Arctrain pour déplacements aux congrès internationaux (2625$, 2000$).

INTRODUCTION GÉNÉRALE

L'introduction générale de ce mémoire présente dans un premier temps la problématique du projet de recherche et une revue de littérature sur les changements environnementaux, les caractéristiques sédimentologiques et la composition palynologique de la partie canadienne de la mer de Beaufort au cours de l'Holocène récent. Dans un second temps, les objectifs de recherche, l'approche méthodologique et un résumé des principaux résultats obtenus sont exposés.

Contexte scientifique et problématique

Le climat de la planète est clairement en voie de changement. Depuis l'ère industrielle, les activités humaines ont conduit à l'augmentation des concentrations de gaz à effet de serre, ce qui entraine des perturbations du climat à l'échelle globale. Les prédictions des modèles de simulation du climat montrent que le réchauffement climatique sera perçu en premier dans les régions subarctique et arctique (ex., Walsh et Crane, 1992; Cohen et al., 2014). Ce réchauffement est ainsi plus intense et rapide en Arctique qu'aux basses latitudes dû à la transformation directe de l'énergie solaire en réchauffement atmosphérique, tandis qu'aux basses latitudes il se produit plutôt de l'évaporation (McBean et al., 2005; Serreze et Francis, 2006). En effet, l'ensemble des données climatiques de l'océan Arctique des dernières décennies a démontré une évolution rapide sous l'effet des changements globaux, ainsi qu'une hétérogénéité spatiale de cet océan (McLaughlin et al., 2002), contrairement à la stabilité qu'on lui attribuait auparavant (Treshnikov et al., 1977). De nos jours, la partie centrale de l'océan Arctique est couverte de glaces permanentes, tandis qu'en périphérie les cycles saisonniers permettent la formation et la fonte de la glace (Bourke et Garrett, 1987).

En général, les données instrumentales des 30 dernières années ont démontré une réduction accélérée du couvert de glace en Arctique, ainsi qu'une diminution globale du volume, de l'épaisseur et de l'étendue de la glace (Rothrock et al., 1999; Dumas et al., 2005; Lindsay et Schweiger, 2015; Serreze et Meier, 2018) dues au réchauffement climatique. Une

diminution du couvert de glace entraine une augmentation de la lumière dans la colonne d'eau qui favorise le développement du phytoplancton, ce qui entraine également une réduction des algues de glace comme nourriture pour les organismes benthiques et pélagiques (Carmack et Macdonald, 2002). Une diminution de l'étendue du couvert de glace peut également entrainer un mélange vertical de la colonne d'eau, et aussi peut accélérer l'érosion côtière, laquelle est déjà affectée par la fonte du pergélisol (Carmack et Macdonald, 2002; Manson et Solomon, 2007).

Cependant, pour mettre en perspective la diminution de l'étendue de la glace de mer en Arctique (réduction de plus de 15 x 10^3 km^2 yr^{-1} au cours des 30 dernières années; Cavalieri and Parkinson, 2012), il est nécessaire de connaître son histoire dans le passé géologique récent. Dans ce contexte, les enregistrements sédimentaires apparaissent essentiels pour étudier la variabilité climatique et océanographique naturelle dans l'ouest de l'Arctique canadien (mer de Beaufort), pour des périodes antérieures à celles des données historiques (> 150 ans). En effet, de nombreux indicateurs minéralogiques, géochimiques et micropaléontologiques préservés dans ces enregistrements sédimentaires peuvent donner des informations sur cette variabilité au cours de l'Holocène (derniers 10 000 ans), que l'on peut comparer aux changements récents. L'Holocène est considéré comme une période relativement stable (Dansgaard et al., 1993) même si l'Optimum climatique médiéval (OCM; ~ AD 800 – 1525) et le Petit âge glaciaire (PAG : ~ AD 1525 – 1865; Lamb, 1965; Robock, 1979; Bradley et Jonest, 1993; Crowley et Lowery, 2000; Podritske et Gajewski, 2007) font partie des fluctuations climatiques qui le démarquent, mais sans avoir la même ampleur que, par exemple, le Dryas récent (~ 12 900 – 11 600 cal yr BP; Rasmussen et al., 2006).

Les régions marginales en Arctique formées par des vastes plateaux continentaux ont un comportement similaire aux grands estuaires. Ce type d'écosystème dans lequel les eaux sont constituées d'un mélange d'eaux d'origine Atlantique, Pacifique, des fleuves et de la fonte de la glace de mer est considéré très dynamique (Ekwurzel et al., 2001; Carmack and Wassmann, 2006). En effet, la sédimentation sur la marge continentale canadienne de la mer de Beaufort est à la fois influencée par le gyre de Beaufort et la dérive transpolaire (DTP;

Darby et Bischof, 2004), ainsi que par une circulation profonde provenant des océans Pacifique et Atlantique (Pickart, 2004). L'ensemble de cette circulation est influencé par la décharge sédimentaire du fleuve Mackenzie (Gamboa et al., 2017) et par des variations climatiques à court terme, telles que l'oscillation Arctique (OA), l'oscillation décennale du Pacifique (ODP) et la dépression des Aléoutiennes (AL) (Darby et al., 2012; Durantou et al., 2012; Brugler et al., 2014), et à long terme par la fonte des calottes glaciaires Laurentidienne et Inuitienne (Bischof et al., 1996). L'OA contrôle le gyre de Beaufort et la dérive transpolaire (DTP; Darby et Bischof, 2004) dans l'Arctique (Figure 1). Au cours de la phase négative de l'OA, la DTP se déplace vers l'est et le gyre de Beaufort s'agrandit et se renforce, tandis que pendant sa phase positive, la DTP se déplace vers l'ouest et le gyre de Beaufort est affaibli, ce qui favorise la pénétration d'eaux du Pacifique Nord par le détroit de Béring (ex., McLaughlin et al., 2002). Ainsi, la dynamique du gyre de Beaufort et de la DTP affectent la sédimentation dans l'Arctique (ex., Darby et al., 2012). D'autre part, l'ODP est l'un des principaux modes de variabilité climatique du Pacifique Nord et contrôle la plupart des précipitations dans les bassins des fleuves Mackenzie et Yukon (Cassano et Cassano, 2010) ainsi que l'advection des eaux du Pacifique Nord vers l'Arctique par le détroit de Béring (Danielson et al., 2011). Pendant la phase positive de la PDO, la température des eaux de surface a tendance à être anormalement fraîche dans le centre du Pacifique Nord et anormalement chaude le long de la côte ouest de l'Amérique du Nord. Cela favorise des précipitations importantes dans les bassins des rivières Mackenzie et Yukon (ex., Okkonen et al. 2004; Pickart et al. 2009; Bringué et Rochon 2012; Durantou et al. 2012). Ces conditions sont inversées pendant les phases de PDO négatives (MacDonald et Case, 2005). Plusieurs études paléoclimatiques basées sur des enregistrements lacustres (Moon Lake et Jellybean Lake) à l'ouest nord-américain suggèrent un changement du signal de la PDO (phase négative à une phase positive) vers 1000 cal yr BP (ex., Laird et al., 1998; Anderson et al., 2005,2016; MacDonald and Case, 2005; Barron and Anderson, 2011; Bird et al., 2017).

Le fleuve Mackenzie est le troisième fleuve en importance dans l'Arctique, en termes de débit d'eau douce (280 km^3/yr ± 25 %; Melling, 2000) et le plus important en termes de charge sédimentaire (environ 127 Mt/an; Macdonald et al., 2004; O'Brien et al., 2006). Par

conséquent, les taux de sédimentation élevés (~ 10 à 200 cm/ka; Barletta et al., 2008; Durantou et al., 2012, Deschamps et al., 2018b) et les sédiments postglaciaires relativement fins déposés dans la portion canadienne de la mer de Beaufort (Gamboa et al., 2017) renferment des archives importantes pour la reconstitution des conditions climatiques et océanographiques du passé récent et de la dynamique des sédiments à des échelles centennale à milléniale.

De nombreux travaux utilisant les assemblages de kystes de dinoflagellés ont été réalisés en mer de Beaufort afin de documenter la variabilité dans les conditions océaniques de surface au cours de l'Holocène récent (ex., Richerol et al., 2008a,b; Bringué et Rochon, 2012; Durantou et al., 2012). Les dinoflagellés sont des protistes de 10 à 100 µm de longueur qui vivent dans les milieux marins et en eau douce. Au cours de leur cycle de vie, lorsque les conditions sont propices, certaines espèces produisent des kystes (dinokystes) très résistants qui vont éventuellement se retrouver dans les sédiments et qui peuvent être préservés durant des millions d'années si les conditions le permettent. Contrairement aux organismes silicatés et carbonatés, la dissolution n'affecte pas les dinokystes due à leur paroi résistante (polymère aliphatique riche en liaisons C-O; Versteegh et al., 2012). Les assemblages de dinokystes sont représentatifs des conditions marines dans lesquelles ils se développent et varient, en composition et en abondance, avec les changements climatiques. Ces assemblages permettent de reconstituer l'évolution des conditions océaniques de surface (température, salinité, productivité et durée du couvert de glace; de Vernal et al., 2001). Des informations supplémentaires sur les dinokystes comme indicateurs paléo-environnementaux se retrouvent dans les sections 3.2.2 et 3.3 de ce mémoire.

Des études dans la mer de Beaufort (ouest de l'Arctique) ont montré que l'abondance des dinokystes est relativement élevée en dehors du panache du fleuve Mackenzie et augmente progressivement vers le golfe d'Amundsen (Richerol et al., 2008a). De plus, Richerol et al. (2008b) suggèrent une augmentation de la productivité au cours des dernières 600 années jusqu'à AD 1850. Durantou et al. (2012) suggèrent une phase de décharge réduite (1858 – 1902), intermédiaire (1900 – 1976) et maximale pour le fleuve Mackenzie (1976 – 2004) au

cours des 150 dernières années sur la base d'assemblages de palynomorphes d'eau douce. Bringué et Rochon (2012) enregistrent des refroidissements épisodiques entre 700 et 1820 AD, possiblement reliés à l'advection d'eau pacifique froide liée à une phase négative de la PDO. De plus, les données sur les isotopes $\delta^{15}N_{total}$ d'une séquence sédimentaire composite prélevée sur le talus du Mackenzie montrent l'influence des eaux du Pacifique dans la mer de Beaufort entre 1300 et 4600 cal yr BP, probablement associée aux changements séculaires de l'OA (Bringué et Rochon, 2012).

Les caractéristiques hydrologiques et la dynamique sédimentaire sur le plateau de la mer de Beaufort sont influencées par le débit d'eau douce et l'apport de sédiments du fleuve Mackenzie (Richerol et al., 2008a; Gamboa et al., 2017; Deschamps et al., 2018a). Le panache du fleuve s'étend vers le large apportant un important volume d'eau douce, de sédiments et de nutriments dans le secteur canadien de la mer de Beaufort (Carmack et Macdonald, 2002). Les affluents du Mackenzie recueillent les eaux de ruissellement provenant de différents bassins versants et les particules détritiques en suspension transportés sont caractéristiques des zones drainées. En effet, la lithologie des bassins versants des principaux tributaires du fleuve Mackenzie est composée d'un mélange de roches argileuses et ignées contenant différents assemblages de minéraux et signatures géochimiques (Millot et al., 2003; Dellinger et al., 2017; Gamboa et al., 2017). Par conséquent, les signatures minéralogiques et géochimiques des particules détritiques transportées par le fleuve Mackenzie peuvent donner des informations sur la provenance des sédiments dans le bassin du fleuve Mackenzie et sur les variations hydrologiques qui affectent le nord-ouest de l'Amérique du Nord (ex., Deschamps et al., 2018a). Cependant, malgré ces caractéristiques sédimentaires, peu d'études sur le système océan-continent ont été réalisées sur le plateau et le talus canadien de la mer de Beaufort afin d'expliquer les conditions paléo-environnementales durant l'Holocène récent.

Objectifs de recherche et approche méthodologique

L'objectif principal de ce projet de maîtrise est de reconstituer et documenter la variabilité hydrologique sur le talus du Mackenzie au cours de l'Holocène récent (spécifiquement les derniers 2000 ans), et son influence sur la dynamique sédimentaire. Pour ce faire, ce projet de recherche s'appuie sur deux objectifs spécifiques qui impliquent une approche utilisant plusieurs traceurs: **(1)** estimer les changements à long terme des conditions des masses d'eau de surface ainsi que la variabilité de la décharge du fleuve Mackenzie au cours de l'Holocène récent en utilisant les assemblages de dinokystes et autres palynomorphes, et **(2)** reconstituer les changements de sources dans les apports sédimentaires et la dynamique sédimentaire dans la mer de Beaufort au cours de l'Holocène récent à l'aide de la distribution granulométrique, de la minéralogie (fractions totale et argileuse) et de la géochimie élémentaire des sédiments.

Pour ce projet de recherche, une carotte à boîte de 45 cm (AMD0214-03BC) et une carotte à gravité de 172 cm (AMD0214-03TWC) ont été prélevées sur le talus du plateau du Mackenzie, au sud-ouest de la mer de Beaufort (Figure 1). Les carottes sédimentaires ont été prélevées à l'été 2014 lors de la mission ArcticNet à bord du brise-glace de la Garde côtière canadienne NGCC Amundsen (Leg 2a; Montero-Serrano et al., 2014).

La chronologie a été estimée à partir de mesures de ^{210}Pb sur la carotte à boîte (BC) (premiers 20 cm). La datation au ^{210}Pb a été effectuée au centre de recherche GEOTOP (Montréal, Canada). Le modèle à taux d'approvisionnement constant (modèle CRS; Appleby et Oldfieldz, 1983; Ruiz-Fernández et Hillaire-Marcel, 2009) a été utilisé pour calculer le taux de sédimentation (Figure 2). Pour la carotte à gravité (TWC), la chronologie a été estimée sur la corrélation des propriétés physiques (a*) et paléomagnétiques (inclination et déclinaison) avec une carotte à piston voisine bien datée (Deschamps et al., 2018b). Les carottes BC et TWC ont été combinées en une séquence composite (appelée 03CS) afin d'obtenir une séquence sédimentaire complète couvrant les 2000 dernières années. Une approche bayésienne, en utilisant le logiciel BACON, a été utilisée pour créer un modèle chronostratigraphique de la séquence composite (Blaauw and Christen, 2011).

Sommaire des principaux résultats

Quatre zones principales de distribution d'éléments chimiques et de dinokystes ont été déterminées sur la base d'une analyse de regroupement hiérarchique de l'abondance relative des données des éléments majeurs et des dinokystes, utilisant les applications *"cluster"* (Maechler et al., 2018), "rioja" (Juggins, 2019) et la méthode de regroupement *"Ward"* (Ward, 1963) sous le logiciel R.

La **Zone I** (2700 – 2000 cal yr BP) montre une granulométrie et des valeurs de l'ensemble des éléments géochimiques relativement constantes. Cette zone est dominée par des espèces autotrophes (kyste de *Pentapharsodinium dalei* et *Operculodinium centrocarpum*), et des palynomorphes d'eau douce et pré-quaternaires. Les valeurs élevées de flux de dinokystes et de réseaux organiques de foraminifères suggèrent des productivités primaires et benthiques élevées, alors que les palynomorphes d'eau douce et pré-quaternaires suggèrent des apports importants d'eau douce et de sédiments en provenance du fleuve Mackenzie. Les rapports minéralogiques élevés d'illite/K-feldspath+plagioclase (I/Fsp) et faible de smectite+vermiculite/illite (S+V/I) suggèrent une provenance de sédiments du nord du bassin du fleuve Mackenzie probablement liée à de fortes précipitations septentrionales induites par une configuration ODP- et à une faible dépression des Aléoutiennes-ouest. L'ODP- ainsi que l'OA+ (indicatif d'un affaiblissement du gyre de Beaufort; Darby et al., 2012) au cours de cette période suggèrent également une augmentation des apports d'eaux du Pacifique Nord (riches en nutriments).

La **Zone II** (2000 – 200 cal yr BP) montre une diminution du taux de sédimentation (de 53 à 23 cm/ka) et de l'ensemble des palynomorphes, ce qui suggère des conditions climatiques plus sèches en lien avec une diminution de la décharge du fleuve Mackenzie, ainsi qu'une productivité primaire réduite. Les rapports I/Fsp et S+V/I indiquent une augmentation progressive des feldspaths et des smectites-vermiculites (minéraux caractéristiques du sud du bassin du fleuve Mackenzie). De plus, cette zone montre une

diminution graduelle des espèces autotrophes vers la dominance des hétérotrophes qui devient plus marquée (productivité primaire possiblement dominée par des diatomées) dans une période qui s'étend du début de l'OCM (~ AD 800 – 1525) jusqu'à la fin du PAG (~ AD 1525 – 1865). L'OCM et le PAG sont marqués par l'augmentation de l'abondance relative de *Spiniferites elongatus/frigidus* (condition plus douces) et d'*Islandinium minutum* s.l. (conditions plus froides), respectivement. Ces résultats sont en accord avec un signal plus faible de l'OA (indicatif d'un gyre de Beaufort renforcé) et du passage d'une phase ODP- (faible dépression des Aléoutiennes-ouest) à une phase ODP+ (forte dépression des Aléoutiennes-est). L'ensemble de ces conditions favorisent une diminution des précipitations au nord du Pacifique.

Par contre, la Z**one III** (AD 1800 – 1950) montre une augmentation du taux de sédimentation (jusqu'à 167 cm/ka), de certains rapports élémentaires (ex., Al/Ca, As/Al et Fe/Al) et minéralogiques (Argiles/Dol, I/Fsp et illite/kaolinite+chlorite) et une diminution du rapport S+V/I, ce qui indique une forte augmentation des apports sédimentaires en provenance de la partie nord du bassin versant du fleuve Mackenzie par rapport à la partie au sud. Les valeurs relativement élevées en smectite et vermiculite (S+V/I) au début de cette zone indiquent néanmoins une certaine contribution du sud du bassin. Ceci est probablement contrôlé par une configuration ODP+ (forte dépression des Aléoutiennes-est), ce qui implique un plus important transport d'humidité vers le nord-ouest du continent nord-américain et à une augmentation des précipitations au sud du bassin du fleuve Mackenzie. Cette augmentation d'apport d'eau douce est également marquée par l'augmentation des flux de palynomorphes d'eau douce et pré-quaternaires. On observe dans la zone III la co-dominance de taxons autotrophes et hétérotrophes.

Finalement, la **Zone IV** (AD 1950 – moderne) est caractérisée par un taux de sédimentation élevé (143 cm/ka) et une augmentation de la taille des particules sédimentaires (2,7 à 4,1 µm). Les espèces autotrophes (*Operculodinium centrocarpum* et kyste de *Pentapharsodinium dalei*) dominent.

Dans l'ensemble, la granulométrie, les signatures minéralogiques et géochimiques et les assemblages de dinokystes révèlent des conditions relativement stables dans la zone d'étude au cours des 2000 dernières années. Cependant, le taux de sédimentation, la taille des grains, les flux de dinokystes et de palynomorphes d'eau douce et pré-quaternaires montrent une forte augmentation vers AD 1900. Au cours de la même période, les données géochimiques élémentaires indiquent des variations importantes de certains rapports élémentaires (ex., Al/Ca, As/Al et Fe/Al), et les rapports minéralogiques (Argiles/Dol, S+V/I) indiquent une augmentation des apports en eau douce du fleuve Mackenzie.

Les différents traceurs analysés dans cette étude ont été comparés à d'autres traceurs climatiques et océanographiques obtenus lors d'études antérieures en mer de Beaufort (ex., Richerol et al., 2008b; Bringué et Rochon, 2012; Darby et al., 2012; Durantou et al., 2012). Les résultats suggèrent que les variations dans l'intensité de l'apport sédimentaire et d'eau douce du fleuve Mackenzie, ainsi que l'arrivée des masses d'eau en provenance du Pacifique sur le talus du Mackenzie, sont probablement le résultat des changements dans les modes de circulation atmosphérique régionale, tels que l'OA et l'ODP. En effet, une phase positive de l'OA affaiblit le gyre de Beaufort et favorise l'arrivée des masses d'eau du Pacifique, tandis que l'ODP en phase positive favorise les précipitations dans le bassin versant du fleuve Mackenzie ainsi qu'une advection moindre d'eaux pacifiques vers l'océan Arctique.

Des études utilisant les mêmes traceurs des conditions de surface et de la dynamique sédimentaire sur d'autres carottes voisines pourront contribuer à documenter la variabilité passée en confirmant les hypothèses avancées dans le présent mémoire. Il faudrait améliorer la base de données dans la mer de Beaufort pour réussir à utiliser les reconstructions des paramètres des conditions de surface. Aussi, le modèle d'âge de ce mémoire pourrait être amélioré avec les données obtenues à partir des analyses de ^{14}C. En particulier, il serait intéressant d'avoir une meilleure résolution afin de mieux documenter les modes de variabilités hydroclimatiques.

CHAPITRE 1

EVOLUTION OF PALEO SEA-SURFACE CONDITIONS AND SEDIMENT DYNAMICS OVER THE LAST 2000 YEARS ON THE MACKENZIE SLOPE, BEAUFORT SEA (CANADIAN ARCTIC)

Omnain Kutos[1]*, André Rochon[1], Jean-Carlos Montero-Serrano[1]

[1] Institut des sciences de la mer de Rimouski (ISMER), Université du Québec à Rimouski, GEOTOP, Québec-Océan and ArcTrain, 310 allée des Ursulines, Rimouski, QC, G5L 3A1, Canada

*Corresponding author: O. Kutos. E-mail address: Omnain.kutos@gmail.com

1. INTRODUCTION

During the last decades, instrumental data have shown an increasing temperature and an accelerated reduction in the Arctic sea-ice cover in summer, together with an overall decline of ice volume and thickness (Rothrock et al., 1999; Dumas et al., 2005; Cohen et al., 2014; Lindsay and Schweiger, 2015; Serreze and Meier, 2018) as a result of climate warming. However, to place the reduction of Arctic sea-ice in perspective (~ 2.3 m or 65 % reduction in thickness in the last 30 years; Lindsay and Schweiger, 2015), it is necessary to know its history in the geological past. Thus, sedimentary records are of great importance to study climate and oceanographic changes for time periods prior to instrumental data (> 150 years). Indeed, micropaleontological, mineralogical and geochemical signatures preserved in these sedimentary records can provide information on hydroclimatic changes and in sediment dynamics that prevailed in the western Arctic Ocean during the Holocene, which in turn can be compared to recent changes.

The high sedimentation rates (~ 10-60 cm/ka; Barletta et al., 2008; Deschamps et al., 2018b) and the relatively fine-grained postglacial sediments deposited in the Canadian Beaufort Sea (Gamboa et al., 2017) offer valuable records for reconstructing past climate and oceanographic conditions and sediment dynamics at centennial to millennial time scales. In

this regard, previous palaeoceanographic investigations, especially those using Late Holocene dinocyst assemblages, have been conducted in the Canadian Beaufort Sea (e.g., Richerol et al., 2008a,b; Bringué and Rochon 2012; Durantou et al., 2012). Dinoflagellates are unicellular protists that live in both marine and freshwater environments. During their life cycle, under favorable environmental conditions, some species produce very resistant cysts (dinocysts) that will eventually sink to the sediments and be preserved for millions of years, if conditions allow. Dinocyst assemblages allow to reconstruct the evolution of sea-surface conditions (temperature, salinity, productivity, and sea-ice cover duration; de Vernal et al., 2001).

Studies in the Beaufort Sea (western Arctic) have determined that dinocyst abundances are relatively high outside the Mackenzie River plume and are increasing gradually towards the Amundsen Gulf (Richerol et al., 2008a). Likewise, based on freshwater palynomorphs, Durantou et al. (2012) suggested a low (AD 1858 – 1902), intermediate (AD 1900 – 1976) and maximum (AD 1976 – 2004) discharge phases for the Mackenzie River over the last 150 yr. Furthermore, $\delta^{15}N_{total}$ data from a composite sedimentary sequence collected in the Mackenzie Slope show the influence of Pacific waters in the Canadian Beaufort Sea between 1300 and 4600 cal yr BP, were likely associated with secular changes in the Arctic Oscillation (AO; Bringué and Rochon, 2012). In addition, the hydrological characteristics and sediment dynamics on the Canadian Beaufort Shelf are largely impacted by freshwater outflow and sediment supply from the Mackenzie River (Richerol et al., 2008a; Gamboa et al., 2017; Deschamps et al., 2018a). The Mackenzie tributaries collect runoff from different watersheds and carry suspended detrital particles that are characteristic of the drained areas. In fact, the watershed lithology of the main Mackenzie River tributaries is a mixture of shale and igneous rocks, containing different mineral assemblages and geochemical signatures (Millot et al., 2003; Dellinger et al., 2017; Gamboa et al., 2017). Therefore, the mineralogical and geochemical signatures of the detrital components transported by the Mackenzie River may provide information about the changes in sediment provenance within the Mackenzie River basin and on the hydrological variations that affected Northwestern North America through time (e.g., Deschamps et al., 2018a). However, land-sea linkage studies have rarely been

conducted on the Canadian Beaufort Shelf to elucidate Holocene paleoenvironmental conditions, in spite of these exceptional sedimentary characteristics.

In this context, using a multiproxy approach (including physical properties of sediments, grain size, bulk and clay mineralogy, elemental geochemistry and dinocyst assemblages) on a composite sediment core (AMD0214-03) recovered on the Mackenzie Slope in the Canadian Beaufort Sea, we aimed to (1) estimate the long-term changes in sea-surface conditions and detrital input related to late Holocene ocean-climate variability, and (2) provide new insights on the hydrological variations that affected Northwestern North America during the last 2000 years. The methodological approach to our study differs from that of other studies through better sampling resolution (~ 7 – 100 years) and the use of multiple proxies (combining mineralogical and elemental geochemistry with dinocyst assemblages).

2. REGIONAL SETTING

2.1. Regional morphology and hydrography

The Canadian Beaufort Shelf is a shallow platform located along the northwestern Canadian coast in the southeastern Beaufort Sea (Figure 1). It is bordered to the west by the Mackenzie Trough and to the east by Amundsen Gulf. This area is almost completely covered by sea-ice (pack-ice and landfast ice) from September/October to May (Barber and Hanesiak, 2004; Galley et al., 2008), with great annual and interannual variability in extent (e.g., Schell et al., 2008; Bringué and Rochon, 2012). In summer, freshet from the Mackenzie River, wind forcing, and rising air temperatures result in ice-free conditions over the shelf by late July and over the slope in August (O'Brien et al., 2006). During winter (November–April), a deep mixed layer (~ 100 m) is present over the shelf (~ 1.7 °C and salinity ~ 32; Mudie and Rochon, 2001). In summer, freshwater inputs leads to the formation of an upper mixed layer (~ 0 – 30 m; 1 – 10 °C and salinity 5 – 30) creating a strong stratification in the water column

(Dunton et al., 2006; O'Brien et al., 2006). Between 30 and 300 m in depth, halocline waters are formed by the nutrient rich Bering Sea's summer and winter waters, as well as the Alaskan Coastal Waters, all of Pacific origin. Relatively warm (> 0 °C), salty (> 34.9) Atlantic water is found downslope at depths greater than 300 m (Carmack et al., 2004; McLaughlin et al., 2004).

2.2. Geological settings of the Mackenzie Basin

The Mackenzie River drainage basin covers approximately 1.8×10^6 km^2 within the Canadian Northwest Territories (Carson et al., 1998; Hill et al., 2001). The upper crust drained by the main Mackenzie tributaries is composed of a mixture between shales and igneous rocks having a granodioritic to granitic composition (Millot et al., 2003; Dellinger et al., 2017; Gamboa et al., 2017). Three main geological units (Figure 1) are found in the Mackenzie River basin (Millot et al., 2003): (1) the North American Cordillera (including the Rocky and the Mackenzie Mountains) in the western part, characterized by volcanic and immature volcano-clastic sediments in the western Canadian orogenic belt (Stikine terrane) and carbonates and slates in the Mackenzie Mountains; (2) the Interior Platform (lowlands), composed of marine and non-marine sedimentary rocks (Cambrian to Cretaceous limestones, shales, and sandstones); and (3) the Canadian Shield in the eastern part, typified by old silicate rocks (Archean granites and gneisses) from the Slave Province (Padgham and Fyson, 1992). However, sediments transported by the Mackenzie River derive mostly from the tributaries of the Interior Platform, with the northern Rockies and Mackenzie Mountains as secondary sources (Millot et al., 2003; Gamboa et al., 2017; Deschamps et al., 2018a).

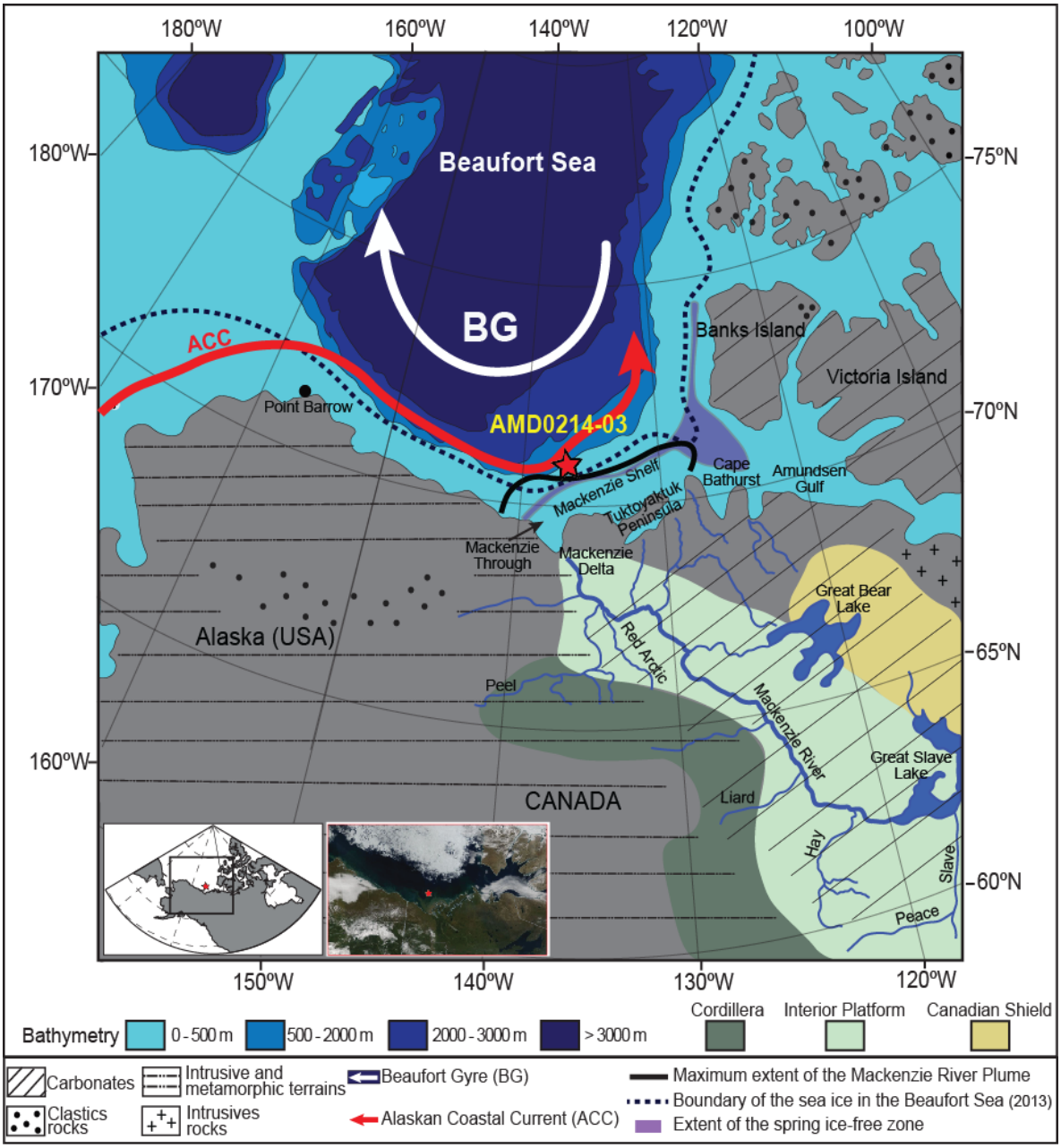

Figure 1. Bathymetric (Jakobsson et al., 2012) and geological (Millot et al., 2003; Fagel et al., 2014) setting map of the western Arctic Ocean (Southeastern Beaufort Sea) and location of the coring site studied here (AMD0214-03 = 03CS: red star). Moderate-Resolution Imaging Spectroradiometer (MODIS) of August 2014 from NASA Worldview application (https://worldview.earthdata.nasa.gov) and coring location. BG = Beaufort Gyre.

2.3. Sedimentation

The Mackenzie River is the third largest river in the Arctic rivers in terms of freshwater discharge (280 km^3/yr ± 25 %; Melling, 2000), but the first in terms of sediment discharge (~ 127 Mt/yr; Macdonald et al., 2004; O'Brian et al., 2006). The suspended sediment discharge of the Mackenzie River forms a large sediment plume (generally 2–3 m thick; Hill et al., 1991) over the Canadian Beaufort Shelf (Figure 1). The transport of suspended sediments within this plume is affected by the sea-ice cover, winds, and currents (Carmack and Macdonald, 2002). In winter, the Mackenzie River discharge is trapped over the inner shelf by the stamukhi (fields of ice fragments), which acts as an inverted dam and causes the formation of the "floating freshwater" lake Herlinveaux (Macdonald et al., 1995). In summer, the position of the plume is greatly affected by prevailing winds, with winds from the northwest pushing the plume along the Tuktoyaktuk Peninsula (Giovando and Herlinveaux, 1981), and winds from the southeast pushing the plume westward, beyond the Mackenzie Trough (MacNeil and Garrett, 1975). Although coastal erosion is an important local sediment supply near the shoreline, its estimated contribution (~ 7 Mt/yr) is dwarfed by that of the Mackenzie River (Carmack and Macdonald, 2002). Overall, modern sedimentation rates are high within the Mackenzie Trough (~ 40 – 320 cm/ka; Macdonald et al., 1998; Richerol et al., 2008a; Durantou et al., 2012) and on the nearby continental shelf and slope (~ 100 – 200 cm/ka; Barletta et al., 2008; Scott et al., 2009; Bringué and Rochon, 2012). On the Canadian Beaufort shelf, most of the surficial seabed sediments are predominantly composed of Holocene marine olive-grey silts and clays (e.g., Pelletier, 1975; Hill et al., 1991; Barletta et al., 2008; Scott et al,. 2009).

2.4. Oceanic and atmospheric circulation

The Mackenzie Shelf nearshore dynamics are tightly linked to the air–sea heat exchange reflected in seasonal sea-ice cover and freshwater discharge (Dunton et al., 2006).

The winds, associated with the high-pressure cell of the central Arctic, push the Beaufort Gyre clockwise, which affects the outer shelf and slope (Figure 1). Thus, the surface circulation over the slope is dominated by the westward branch of the Beaufort Gyre, but beneath the upper 50 m, the flow reverses and forms the Beaufort Undercurrent (Aagaard, 1984; Pickart, 2004). This event, which allows the transport of Pacific and Atlantic origin waters, has been observed for the last 30 years (Lukovich and Barber, 2006). Moreover, the relatively warm Alaskan Coastal Current flows eastward along the shore (Nikolopoulos et al., 2009). At the regional level, these surface circulation regimes are mainly controlled by changes in the phases of large-scale atmospheric patterns such as the AO (MacDonald and Case, 2005; Darby et al., 2012) or the PDO (Overland et al., 1999; Durantou et al., 2012), which are important natural patterns in global climate variability.

The AO controls the configuration of the two major Arctic surface circulation features: (1) The Beaufort Gyre and (2) the Transpolar Drift (TPD; Darby and Bischof, 2004) (Figure 1). During strong negative AO, the TPD shifts east and the Beaufort Gyre expands and strengthens. Whereas, during strong positive AO, the TPD shifts west and the Beaufort Gyre is suppressed, enhancing inflow of North Pacific water through the Bering Strait (e.g., McLaughlin et al., 2002). Therefore, changes in the Beaufort Gyre and TPD dynamic affect Arctic sedimentation at different times (e.g., Darby et al., 2012). The AO was also identified as a mechanism responsible for changes in the wind patterns, and consequently the ice drift regime in the Arctic at multidecadal to century timescales (e.g., Darby et al., 2001; Darby and Bischof, 2004).

On the other hand, The PDO pattern (a major mode of North Pacific climate variability) controls most of the daily precipitations in the Mackenzie and Yukon River basin (Cassano and Cassano, 2010) and the Bering Sea oceanic advection (Danielson et al., 2011). During the positive phase of the PDO, sea surface temperatures tend to be anomalously cool in the central North Pacific and anomalously warm along the west coast of North America. These conditions promote large precipitation events within the Mackenzie and Yukon River watersheds (e.g., Okkonen et al., 2004; Pickart et al., 2009; Bringué and Rochon, 2012;

Durantou et al., 2012). These conditions are reversed during a negative PDO phase (MacDonald and Case, 2005). Furthermore, the Aleutian Low (AL) is influenced by Arctic and subtropical ocean-atmosphere processes making its temporal and spatial variance more complex (Anderson et al., 2016). Thus, the intensity and geographical position of the AL is in constant variation. It strengthens (weakens) concomitantly with a more eastern (western) location (Sugimoto and Hanawa, 2009). Therefore, when a strong AL is positioned eastward, it tends to intensify the PDO phase conditions (Schneider and Cornuelle, 2005; Rodionov et al., 2007; Wills et al., 2019).

3. MATERIAL AND METHODS

3.1. Samples and chronology

Two short sedimentary sequences, box core AMD0214-03BC (hereafter referred to as core 03BC; length 45 cm; location: 70 ° 33.055 ’ N; 137 ° 31.997 ’ W; water depth: 1048 m) and trigger weight core AMD0214-03TWC (hereinafter referred to as 03TWC; length 172 cm; location: 70 °33.032 ’ N; 137 °31.910 ’ W; water depth: 1051 m), were recovered in front of the Mackenzie River delta on board the Canadian Coast Guard icebreaker Amundsen during the 2014 ArcticNet expedition (Montero-Serrano et al., 2014). All coring sites were targeted using high-resolution seismic profiles (3.5 kHz) that indicated high sediment accumulation not influenced by mass wasting events (Figure S1). The physical and magnetic properties of the sediment core 03BC and 03TWC have been previously described in Deschamps et al. (2018a,b)

The chronology of box core 03BC was determined from excess ^{210}Pb in the top 20 cm (Figure 2A-C). Measurements were made by counting the activity of the daughter isotope ^{210}Po, ^{210}Po ($t_{1/2}$ = 138.4 days, a = 5.30 MeV) at the GEOTOP research Centre (Montréal, Canada). The constant rate of supply model (CRS model; Appleby and Oldfieldz, 1983; Ruiz-Fernández and Hillaire-Marcel, 2009) was used to calculate the sedimentation rates (Figure

2C). Likewise, the sediment chronology of core 03TWC was established (Figure 3C) by comparing the magnetic susceptibility and a * profiles of the core with the well-dated nearby piston core 03PC (data obtained by Deschamps, 2018). Indeed, characteristic peaks in declination and inclination curves have been identified in order to transfer the age model of core 03PC to core 03TWC below 12 cm, where no radiocarbon ages are available. In addition, the correlation of the physical and magnetic parameters measured on cores 03BC and 03TWC suggests that the sediment – water interface has been well preserved at the top of core 03TWC (Figure 3A,B). Thus, cores 03BC and 03TWC were combined into a composite sequence (hereafter referred to as core 03CS) in order to obtain a complete sedimentary sequence covering the last 2000 years (Figure 4). The first 44 cm of the composite core correspond to the BC and the rest of the sequence corresponds to the TWC.

The R software package BACON (Blaauw and Christen, 2011) was used to produce the “best fit” linearly interpolated age model (Figure 4). BACON uses a Bayesian approach to estimate the best fit or weighted mean age for each depth with a 95 % confidence interval that allows to consider all chronostratigraphic markers (^{210}Pb, as well as physical and magnetic properties tie points). Thus, based on this age model, the sediment core 03BC was subsampled evenly every 1 cm, whereas the core 03TWC was subsampled every 4 cm below 48 cm for a total of 59 samples. Overall, we estimate the temporal resolution of ~ 7 years in core 03BC, and ~ 100 years in core 03TWC.

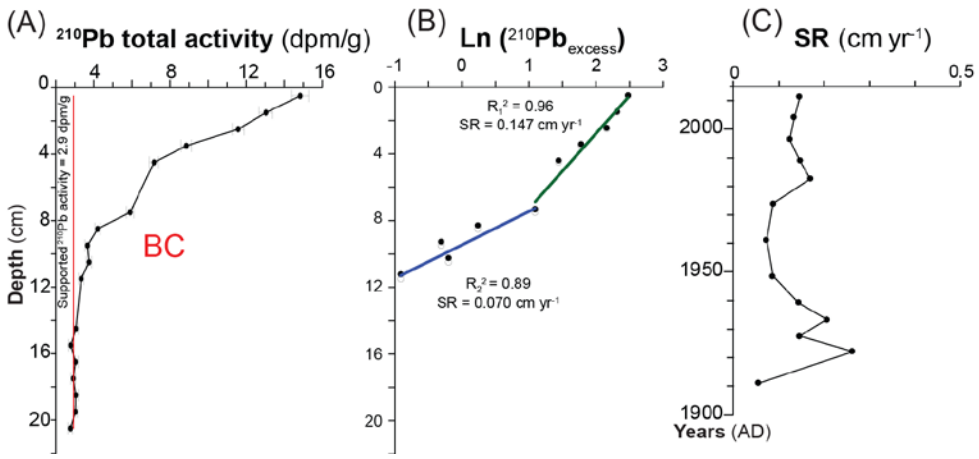

Figure 2. Chronology of box core (03BC) determined from excess ^{210}Pb. (A) ^{210}Pb total activity (dpm/g). (B) Ln (^{210}Pb$_{excess}$). (C) SR = Sedimentation rate (cm yr^{-1}).

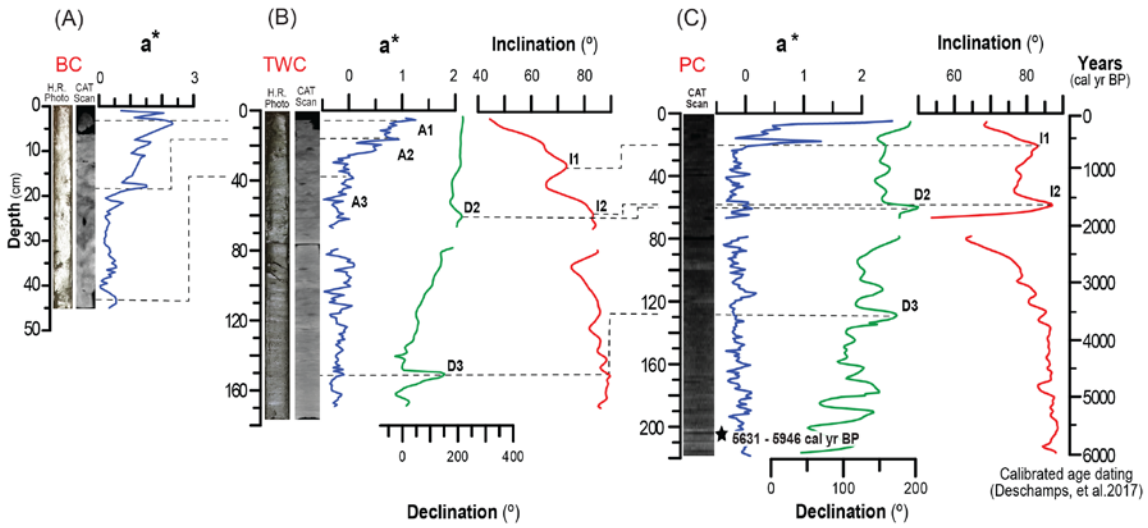

Figure 3. Correlation between piston and trigger weight and box cores using a *, inclination and declination for cores AMD2014-03. (A) a * of the box core (BC). (B) a *, declination and inclination of the trigger weight core (TWC). (C) a *, declination and inclination of the piston core (PC).

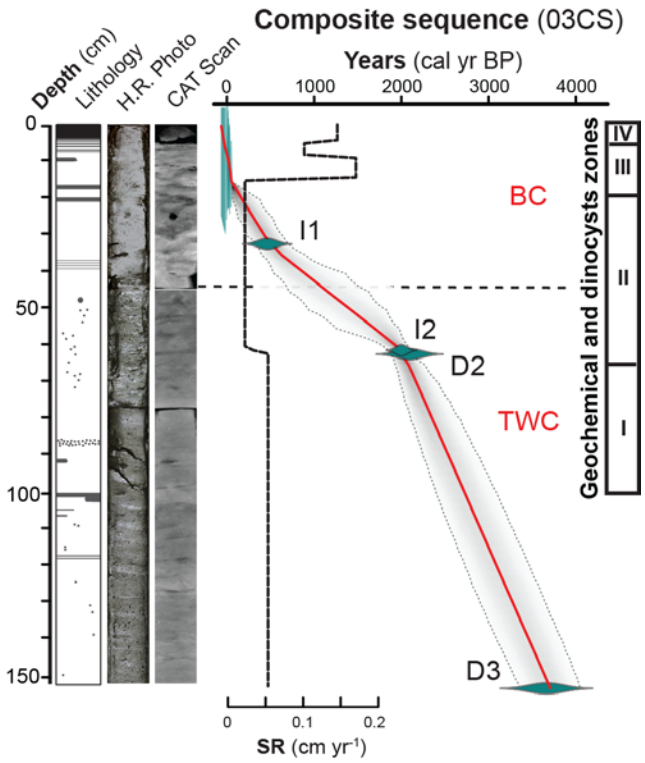

Figure 4. Age-depth relationship of composite sediment core (03CS) with Bacon. Dashed line: limit between BC and TWC.

3.2. **Analytical procedure**

3.2.1. Grain size analyses

Sediment grain-size analyses were performed on the detrital fraction using a Beckman Coulter LS13320 laser diffraction grain-size analyzer, which has a detection range of 0.04–2000 µm. Samples were deflocculated by successive washing with distilled water after the removal of organic matter with 10 mL of hydrogen peroxide (30 % H_2O_2). Biogenic silica was not removed as it appeared to be negligible (likely less than 1 %, as suggested by its non-detection in the bulk sediment XRD diffractograms; Deschamps et al., 2018a). The grain-

size distribution and statistical parameters (e.g., mean, sorting) were calculated using the moment methods in logarithmic (phi - ϕ) scale and the GRADISTAT software (Blott and Pye, 2001).

3.2.2. Mineralogical and geochemical analyses

Before mineralogical and geochemical analyses, the sediment samples (< 2 mm) were rinsed five times with distilled water after the removal of the organic matter fraction with 10 mL of hydrogen peroxide (30 % H_2O_2). Subsequently, a portion of this processed sediment sample was used as the bulk fraction, whereas another portion was used to separate the clay-sized fraction (< 2 μm). Portions of the bulk sediment samples were oven-dried overnight at approximately 60 °C and then slightly homogenized with an agate mortar. These homogenized sediment samples were used for bulk mineralogical and geochemical analysis.

Quantitative bulk mineralogy. - Bulk mineral associations were studied by quantitative X-ray diffraction (qXRD) following the method developed by Eberl (2003) and used in other Quaternary glacial marine studies that address sediment mineralogy (Darby et al., 2011; Andrews et al., 2015, 2016; Stein et al., 2017; Deschamps et al., 2018a). For this, dry sediment samples (1 g) and 0.25 g of corundum were grinded for 10 min with a McCrone micronizing mill adding ethanol (5 mL) to obtain a homogeneous powder. The slurry was oven-dried overnight at about 60 °C and then slightly re-homogenized with an agate mortar. Subsequently, 0.5 mL of Vertrel was added to the mixture to prevent the possible agglomeration of finer particles. The powder sample was then sieved (< 300 μm), back-loaded into the holders and analyzed on a PANalytical X'Pert Powder diffractometer. Samples were scanned from 5 ° to 65 ° two-theta in steps of 0.02° two-theta, with a counting time of 4 seconds per step. For the quantification of the major mineralogical components, sediment XRD scans obtained were converted into mineral weight percent (wt. %) using the Excel macro program ROCKJOCK v11 (Eberl, 2003). This program uses a full-pattern fitting method that permits the quantification of whole-sediment mineralogy with a precision of ± 3

wt % (Eberl, 2003). The calculated total mineral wt. % was normalized to a sum of 100 %. We focused on 15 key minerals: quartz, K-feldspar, plagioclase, calcite, dolomite, amphibole, Fe-bearing (pyrite, hematite), amorphous silica, kaolinite, chlorite, illite, biotite, muscovite, smectite and vermiculite, which represented more than 96 % of the overall mineral concentration in the bulk sediment sample.

A ternary plot of illite+kaolinite, feldspars, and dolomite was created to compare the general mineralogical composition of the sediments from core 03CS and the potential source areas (Deschamps et al., 2018a). Likewise, the relative abundance of dolomite, and the following ratios were used to trace detrital input changes over time (Gamboa et al., 2017; Deschamps et al., 2018a): illite/feldspar or I/Fsp, total clays/dolomite or total clays/dol, smectite+vermiculite/illite or S+V/I and illite/kaolinite+chlorite or I/K+C.

Clay mineralogy. - Clay minerals were quantified in the bulk sediment fraction (< 2 mm) using the Excel macro program RockJock. However, nearly all previous clay-mineral provenance studies in the Arctic Ocean used oriented mounts of the < 2 μm sediment fraction to identify and semi-quantify the clay-mineral abundance, notably illite, kaolinite, chlorite, and smectite (Naidu et al., 1971, 1982; Naidu and Mowatt, 1983). Therefore, in this study, the clay-size fraction of all sediment samples was isolated and analyzed in this manner for comparison. Indeed, clay mineral associations were studied using XRD following established protocols (Bout-Roumazeilles et al., 1999; El Ouahabi et al., 2017). Deflocculation of clays was achieved in all samples by successive washing with distilled water. The clay-size fraction was separated by settling according to Stokes's law, concentrated by centrifugation, and oriented by wet smearing on glass slides. The analyses were run from 2.49 ° to 32.49 ° 2θ on a PANalytical X'Pert Powder diffractometer. The sample was air-dried, and then ethylene glycol vapor saturation was completed for 12 h, followed by heating at 490 °C for 2 h. Semi-quantitative estimation of clay mineral abundances (smectite, illite, chlorite, kaolinite, vermiculite and chlorite/smectite mixed layer) based on peak areas on the X-ray diagrams was performed using the MacDiff® 4.2.5 software (Petschick, 2000). Similar to other Arctic clay mineral studies (Wahsner et al., 1999; Schoster et al., 2000; Deschamps et al., 2018a),

clay mineral contents were calculated using the weighting factors introduced by Biscaye (1965) and calculated to a sum of 100 %. The error on the reproducibility of measurements is estimated to be 5 % for each clay mineral, as measured during the analysis of replicate samples. Overall, the combinations of both RockJock and oriented mounted methods support each other and give independent information (e.g., Darby et al., 2011; Deschamps et al., 2018a).

Bulk elemental concentration. - A total of 15 elements (Al, Si, K, Mg, Ca, Ti, Mn, Fe, P, Sr, V, Cr, Zn, As and Zr) were analyzed on both bulk and clay-sized fractions by energy dispersive X-ray fluorescence (EDXRF) spectrometry using a PANalytical Epsilon 3-XL. Samples were treated by borate fusion in an automated fusion furnace (CLAISSE® M4 Fluxer) before EDXRF analysis. The analytical procedures were similar to Gamboa et al. (2017). Analytical accuracy and precision were found to be better than 1 – 5 % for major elements and 5 – 10 % for the other elements, as checked against an international standard (USGS SDC-1) and analysis of replicate samples.

Because Al and Si are associated with clay minerals, aluminosilicates, and quartz, and Ca is associated with carbonates, the ternary plot Al, Si, and Ca (expressed as oxides; Figure 6A) was used to obtain a general geochemical classification of the sediments (Brumsack, 1989; Deschamps et al., 2018a). Based on previous geochemical studies carried out in the Canadian Beaufort margin (Gamboa et al., 2017; Deschamps et al., 2018a), Si/Al, Al/Ca, Fe/Al and As/Al ratios are used to elucidate downcore variations in the Mackenzie River discharges. In addition, to compare the relative enrichment of redox-sensitive elements (Mn, Fe, V, Cr, Zn, As), we calculated enrichment factors (EF) by comparing Al-normalized metal concentrations to those of average shale (Wedepohl, 1991): $X_{EF} = [(X/Al)_{sample}/(X/Al)_{average\ shale}]$. In practical terms, EF > 3 represents a detectable authigenic enrichment of an element over average shale concentrations, whereas EF > 10 represents a moderate to strong degree of authigenic enrichment (e.g., Tribovillard et al., 2006).

3.2.1. Palynological analyses

Each core was sub-sampled every 2 cm (box core) and 8 cm (trigger weight core) for palynological analyses, according to the standard preparation method described in Rochon et al. (1999). A volume of ~ 5 cm^3 of sediment was measured for each sub-sample by water displacement. One tablet of marker grain (*Lycopodium clavatum*, University of Lund, Sweden) of known concentration (12100 spores ± 1892, batch # 414831) was added to each sample, allowing for the calculation of palynomorph concentrations (Matthews, 1969; Price et al., 2016).

Wet sieving was performed using Nytex ® sieves of 100 μm and 10 μm mesh to remove coarse sands, fine silts, and clays. The fraction between 100 and 10 μm was subjected alternately to four hydrochloric acid (HCl 10 %) and three hydrofluoric acid (HF 49 %) treatments on a hot plate under a fume hood, including an overnight HF treatment. A final sieving at 100 μm and 10 μm was performed to eliminate fine and coarse particles as well as fluorosilicates gels formed during the chemical treatments. Finally, each sample was centrifuged, and the supernatant was removed. A drop of the residue was mounted between slide and coverslip in glycerin jelly to be observed under a microscope.

Dinocysts, pollen grains, spores, foraminifer organic linings, pre-Quaternary and freshwater palynomorphs were systematically counted using a transmitted light microscope (LEICA DM5500B, magnification factor of 400×). The nomenclature used for identifying the dinocyst taxa followed Rochon et al. (1999), de Vernal et al. (2001), Head et al. (2001), Radi et al. (2001,2013) and Williams et al. (2017). In this study, *Operculodinium centrocarpum* s.l. refers to all morphotypes (*O. centrocarpum* sensu Wall & Dale, 1966, *O. centrocarpum* short processes and *O. centrocarpum* arctic morphotype); *Islandinium minutum* s.l. includes *I. minutum*, *I. brevispinosum*, *Echinidinium karaense* and *Echinidinium* spp; *Brigantedinium* spp. includes *B. simplex*, *B. cariacoense* and *Brigantedinium* sp; *Spiniferites elongatus* includes *S. elongatus* and *S. frigidus* (cf. Rochon et al., 1999).

3.3. Statistical approach

Constrained cluster analysis was performed using the elemental geochemical and palynological data to determine the sedimentary facies. Prior to cluster analyses, a log-centered (clr) transform was applied to the data set (Aitchison, 1990). Constrained hierarchical cluster was carried out with R software using the packages “cluster” (Maechler et al., 2018; https://cran.r-project.org/web/packages/cluster/cluster.pdf), “rioja” (Juggins, 2019) and Ward’s method (Ward, 1963). Results are shown on figure S6.

A minimum of 300 dinocysts were counted to obtain a significant statistical representation of the dinocyst population. Dinocyst assemblages were used for the quantitative reconstruction of past sea-surface conditions based on transfer functions and the modern analogue technique (MAT) using a modern dinocyst reference database (GEOTOP data: n = 1492). The MAT method (Prell, 1985; Guiot, 1990; de Vernal et al., 2001, 2005) is based on the similarity between fossil dinocyst spectra and modern samples from the reference database n = 1492 available on the website (http://www.geotop.ca/en/bases-de-donnees/dinokystes.html). The reconstructed values and the associated confidence interval were obtained with the five best modern analogues using the statistical software R version 3.3.3 and the BIOINDIC package. de Vernal et al. (2013) applied the validation tests on the n = 1492 database (with 66 dinocyst taxa), confirming the suitability of the MAT method in paleoenvironmental reconstruction studies. Modern environmental data used for statistical analysis consist in sea-ice cover, sea-surface temperature and salinity (for winter and summer) values at 10 m depth compiled from the 2001 version of the World Ocean Atlas (NODC, 2001), in addition to mean annual productivity obtained from MODIS satellite observations (http://modis.gsfc.nasa.gov/index.php/; Radi and de Vernal, 2008).

Sea-surface temperature (SST) is reconstructed with errors of prediction of ± 1.3/1.7 °C for winter/summer, and of ± 2.1/2.3 for sea-surface salinity (SSS). Sea-ice cover extent is expressed as the number of months with more than 50 % coverage (based on the 1953 – 2003 mean) with an error of prediction of ± 1.4 months/yea. The error of prediction for productivity

is ± 57.8 gC m^{-2} yr^{-1}. However, for 3 (T°, S, sea-ice cover extent) of the 4 reconstructed parameters the error of prediction is larger than the variability of the reconstructed values. Therefore, we have decided not to use the transfer functions (Figure S7) in our interpretations.

4. RESULTS

4.1. Sediment characteristics

Core 03CS (Figure 4) is mainly composed of homogeneous dark grey (5Y 4/1) mud to olive brown (2.5Y 4/3) mud with dark yellowish brown (10YR 4/6) laminations (1 cm thick) and occasional spots. These color laminations are abundant in the upper 20 cm of the core. The upper 6 cm of the core is slightly darker (5Y 3/1). All sediment samples are poorly sorted (values of $1.40 < \phi < 1.69$). The sediment grain size remains relatively constant (~ 2.8 µm; Figure 5) through the composite core suggesting no significant variations in the depositional environment during the last 2000 cal yr BP.

4.2. Mineralogical and geochemical composition

Stratigraphic distributions of the bulk and clay mineralogical and elemental geochemical data from the composite sequence studied here are shown in Figure S3. In general, total clays (60 – 70 %), quartz (18 – 24 %), plagioclase (2 – 5 %) and K-feldspar (1 – 6 %) represent more than 97 % of the overall mineral concentration. Likewise, the clay mineral assemblage consists of a few minerals (Figure S3B): illite (28 – 47 %), kaolinite (10 – 21 %), chlorite (14 – 25 %), vermiculite (3 – 14 %) and smectite/chlorite mixed layers (9 – 41 %). These mineralogical results are consistent with those reported for modern surface sediments of the Beaufort Shelf (e.g., Naidu et al., 1982; Naidu and Mowatt, 1983; Wahsner

et al., 1999; Gamboa et al., 2017; Deschamps et al., 2018a). The Al_2O_3-SiO_2-CaO and illite+kaolinite-total feldspars-dolomite ternary plots (Figure 6A-C) show that bulk sediments from core 03CS have a chemical and mineralogical composition similar to the sediments of the Mackenzie River and average shale (Pourmand et al., 2012). Furthermore, Fe/Al and Mn/Al display a positive linear correlation ($r^2 = 0.54$; Figure S4) below Zone IV, indicating a geochemical relationship most likely similar to Fe–Mn oxyhydroxide phases. Fe/Al and As/Al also display a positive linear correlation ($r^2 = 0.85$). The enrichment factors (EF) of redox-sensitive elements (V, Zn, As and Fe) reveal modest authigenic enrichment (1 – 3) in core 03CS compared to average shale values (Figure S5). In general, Cr shows no detectable authigenic enrichment (~ 1). Whereas Mn is authigenically depleted (EF < 1) with respect to detrital values, except in Zone IV, which shows a moderate-to-strong authigenic enrichment (EF = 5 – 11).

4.3. Palynological assemblages

Dinocysts (mean of 142 cysts cm^{-2} yr^{-1}) and pre-Quaternary palynomorphs (115 cells cm^{-2} yr^{-1}; reworked spores, pollen, dinocysts and acritarchs) are the most abundant organic-walled microfossils present in the samples (Figure 7). Foraminifer organic linings and pollen/spore were also well represented, with means of 53 linings cm^{-2} yr^{-1} and 39 grains cm^{-2} yr^{-1}, respectively (Figure 7). Influxes of freshwater palynomorphs (e.g. *Zygnema*, *Pediastrum*, *Halodinium* and Tintinnids) are about two orders of magnitude lower (means of 5.0 cells cm^{-2} yr^{-1}) than dinocyst and pre-Quaternary palynomorphs (Figure 7). Pollen assemblages are represented by four genus and one family: *Picea* (41 %); *Alnus* (mean of 19 %); Cyperaceae (16 %); *Betula* (13 %) and *Pinus* (7 %). The spores are dominated by trilete spores (78 %), followed by monolete spores (22 %).

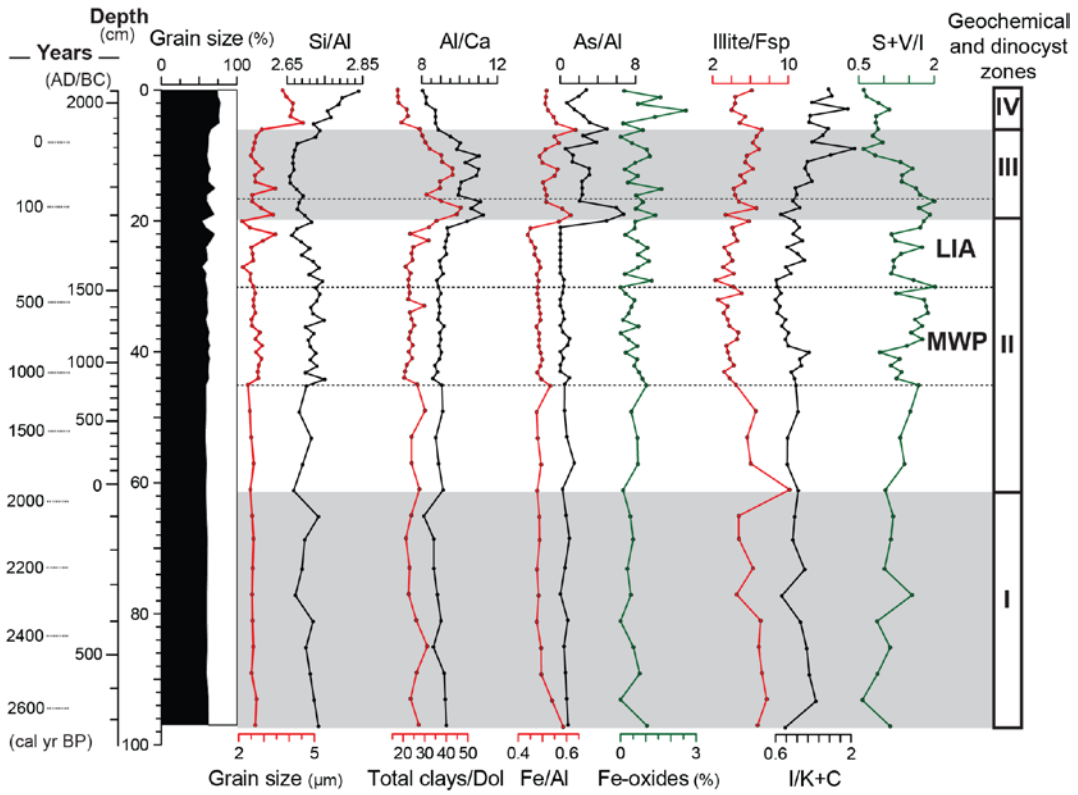

Figure 5. Mean grain size (µm), elemental geochemical and bulk mineralogical ratios for the composite sediment core 03CS. Silt-size (black pattern), clay-size (white pattern). LIA = Little Ice Age, MWP = Medieval Warm Period.

A total of 23 dinocyst taxa were identified in the samples. However, 8 taxa comprised more than 96 % of the assemblage, which is consistent with previous work in the Canadian Arctic Ocean (e.g., Mudie and Rochon, 2001; Richerol et al., 2008a; Pieńkowski et al., 2011; Bringué and Rochon, 2012; Durantou et al., 2012). The assemblages are dominated by four taxa: cysts of *Pentapharsodinium dalei* (mean of 41 %), *O. centrocarpum* s.l. (25 %), *I. minutum* s.l. (19 %) and *Brigantedinium* spp. (7 %), which are common in Arctic regions (Kunz-Pirrung et al., 2001, Mudie and Rochon, 2001) (Figure 8). Additionally, the mean relative abundances of *I. minutum* var. *cezare*, cysts of *Polykrikos* sp. var. *arctic/quadratus*, *Spiniferites elongatus/frigidus*, *Impagidinium pallidum* and cysts of *Protoperidinium americanum* range between 0.2 and 2.7 %. Other taxa (*Spiniferites ramosus*,

Nematosphaeropsis labyrinthus and *Selenopemphix nephroides*) are present in low proportions (≤ 0.1 %).

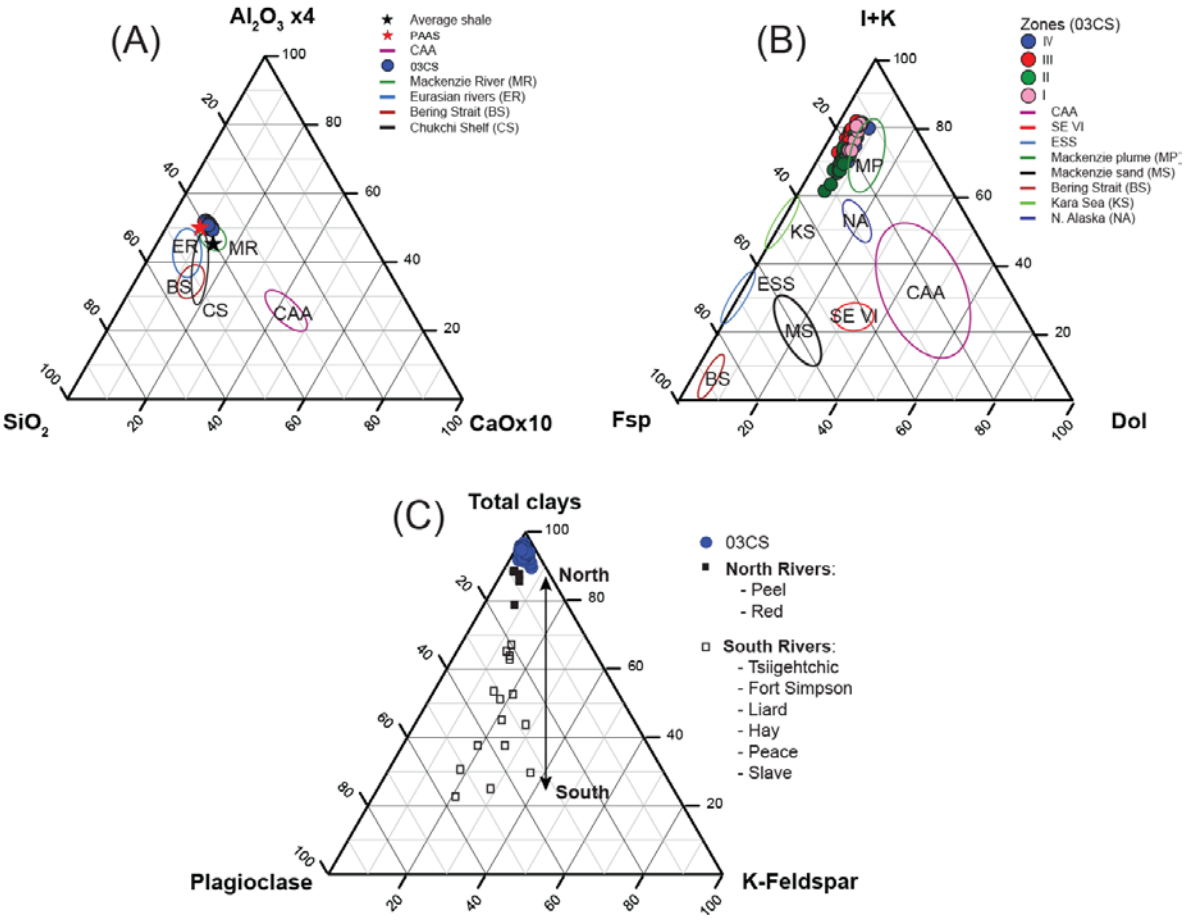

Figure 6. (A) Al_2O_3-SiO_2-CaO ternary plot showing the overall composition (bulk and clay fractions) of the 03CS composite core in comparison to the average shale and circum-Arctic source areas. PAAS: Post-Archaean Average Shale. (B) illite+kaolinite (I+K) – total feldspars (Fsp) – dolomite (Dol) ternary plot for the 03CS composite core based on bulk mineralogy. (C) Total clays-plagioclase-K-feldspar ternary plot of sand samples from the main tributaries of the Mackenzie River (Gamboa et al., 2017). Note that the northern tributaries are enriched in total clays while the southern tributaries are enriched in total feldspars. (Data sources - Beaufort Sea, Mackenzie Delta and Canadian Arctic Archipelago (CAA): Gamboa et al., 2017. Chukchi Sea: Khim, 2003. Bering Strait: Kalinenko, 2001. Eastern Siberian Sea: Khim, 2003, Viscosi-Shirley et al., 2003).

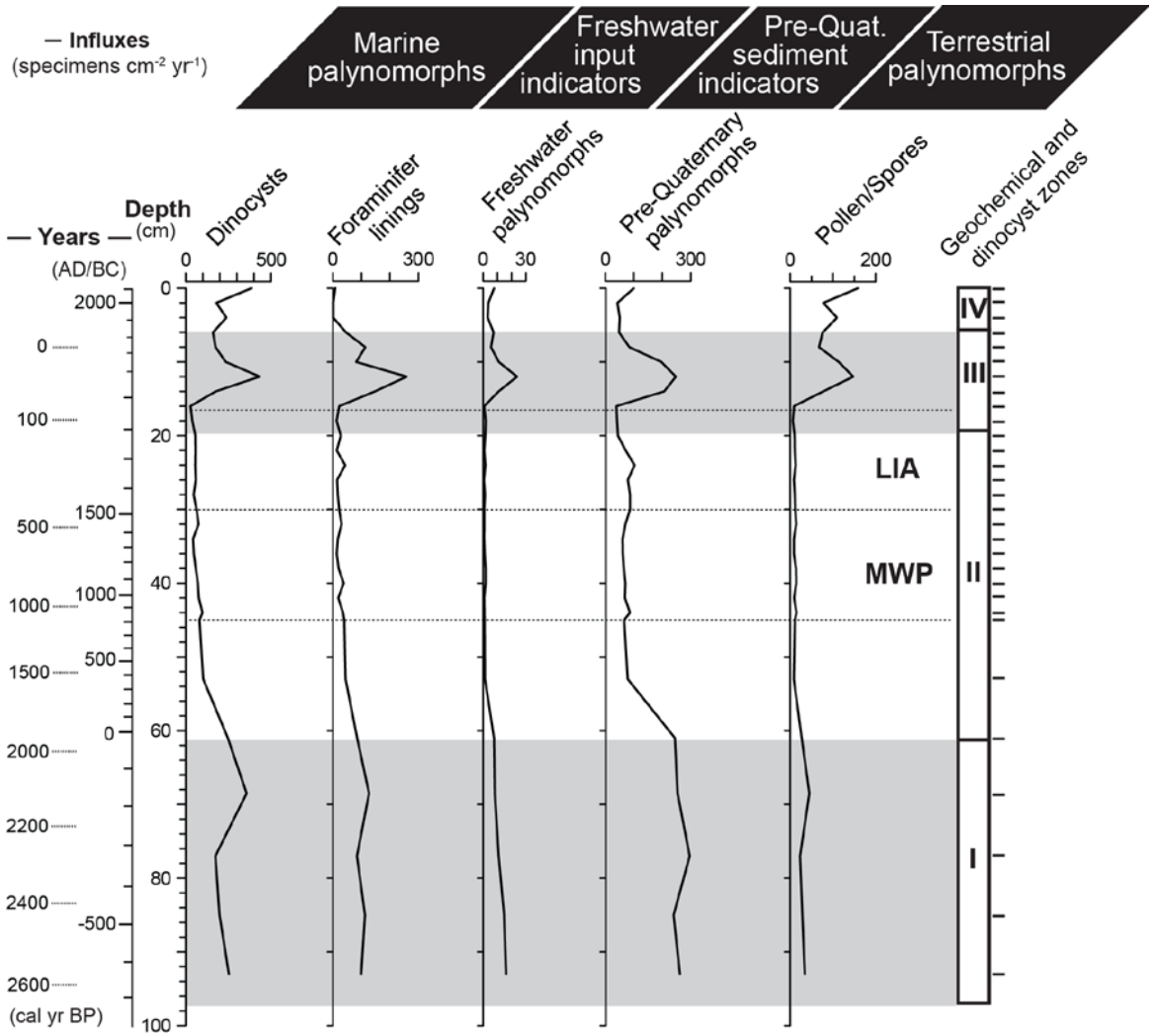

Figure 7. Main organic-walled microfossils influxes in core 03CS. Thick horizontal ticks on the right-hand side indicate the depths where samples were taken. The freshwater palynomorphs include *Zygnema*, *Pediastrum*, *Halodinium* and Tintinnids, while the pre-Quaternary palynomorphs include reworked spores, pollen, dinocysts and acritarchs.

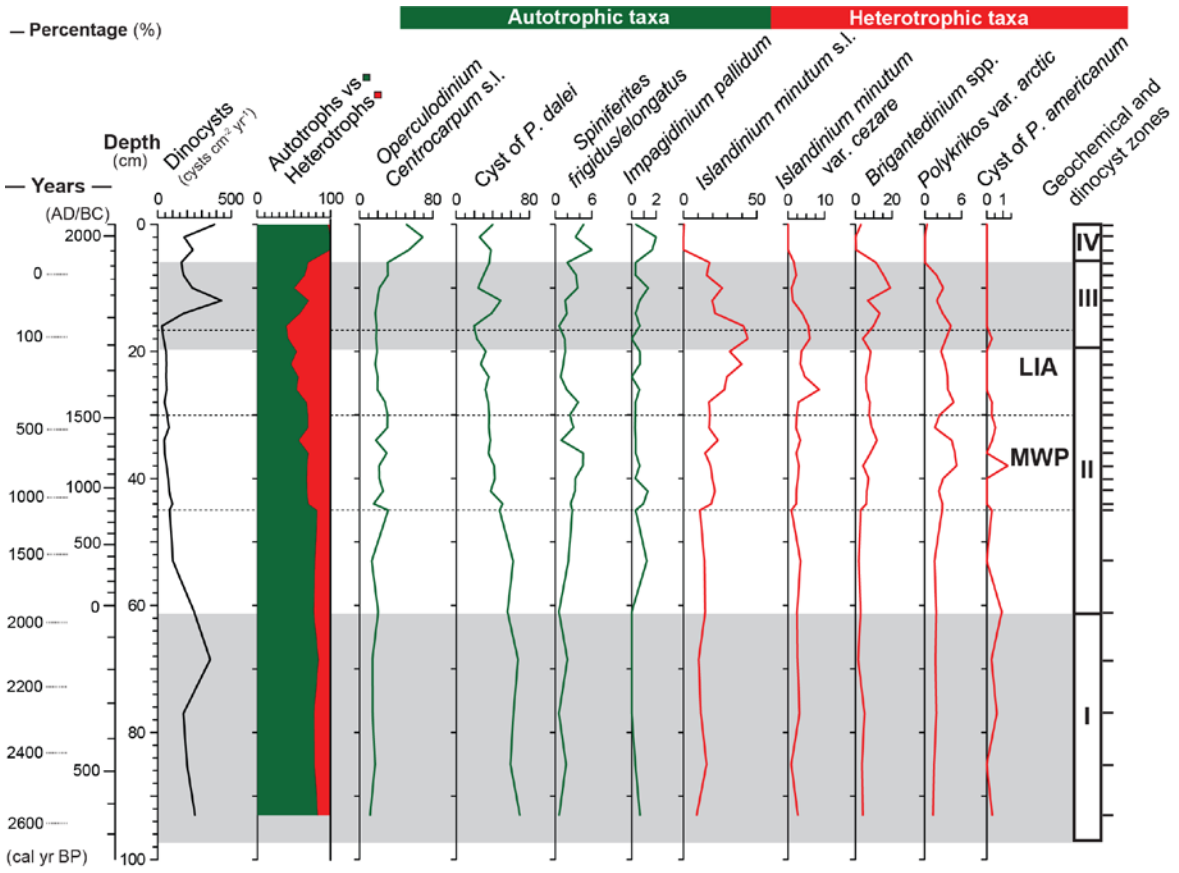

Figure 8. Dinocyst influx, proportion of autotrophs vs heterotrophs taxa and relative abundance of the main dinocyst taxa. Depths where samples were taken are indicated with thick horizontal ticks on the right-hand side. The dotted lines represent Medieval Warm Period (MWP) and Little Ice Age (LIA) limitation age.

4.4. Sedimentary zones

Four main sedimentary zones are identified on the basis of the constrained cluster analyses performed on the elemental geochemical and palynological data (Figure S6). Although some inverted or distorted hierarchical levels are observed in the cluster, due to the

constrained nature of the clustering process (only stratigraphically adjacent samples can be clustered during the agglomerative procedure; Grimm, 1987), these dendrograms show similar sedimentary zones. The dendrograms also show a continuity between the 03BC and the 03TWC sample, justifying the implementation of the composite sequence 03CS. The sedimentary zones labeled 1 – 4 from base to top, are described below according to both core depth and age (derived from the age-depth model; Figure 4).

Zone I: 200–62 cm (2700 – 2000 cal yr BP) – The sedimentation rates is about 53 cm/ka (Table 1). This zone is characterized by having the highest abundance in kaolinite (mean of 18 %; Table 4) and the lowest abundances in plagioclase (mean of 2.7 %; Table 3). All geochemical elements reveal relative constant values. It is also characterized by the dominance of the autotrophic taxa cysts of *P. dalei* (mean of 65 %; Table 2), accompanied by *O. centrocarpum* s.l. (14 %) and *I. minutum* s.l. (12 %).

Zone II: 62–21 cm (2000 – 200 cal yr BP) – Zone II displays a lower sedimentation rate (from 53 to 23 cm/ka; Table 1). It displays the highest smectite (23 %; Table 4) and K-feldspar (3.1 %), lowest illites (26 %) mean abundances. All geochemical elements reveal relative constant values. In this zone, the relative abundances of cysts of *P. dalei* (65 to 41 %; Table 2) decrease in favor of *O. centrocarpum* s.l. (14 to 23 %), *S. frigidus/elongatus* and *I. pallidum*. Heterotrophic taxa, such as *I. minutum* s.l. (12 to 20 %), *Brigantedinium* spp. (3 to 6 %) and cysts of *Polykrikos* sp. var. *arctic/quadratus* (1.6 to 3.2 %) increase after about 1000 cal yr BP.

Zone III: 21–6 cm (AD 1800 – 1950) - The strong increase of the sedimentation rate (up to 167 cm/ka; Table 1) is the most prominent feature in this zone. Also, the smectite has the highest mean abundance (21 %; Table 3) as well as the vermiculite (3.4 %; Table 3). This zone displays the highest ratios in Clays/Dol, I/Fsp, I/K+C, Al/Ca, Fe/Al and As/Al (Figure 5). Likewise, overall abundances of peridinioid taxa *I. minutum* s.l. (20 to 29 %; Table 2) and *Brigantedinium* spp. (6 to 11 %) are high in this zone, however *I. minutum* s.l. shows a decreasing trend. Cysts of *Pentapharsodinium dalei* show peaks in the middle of the zone.

Operculodinium centrocarpum s.l., *S. frigidus/elongatus* and *I. pallidum* all show increasing trends in the upper part of the zone.

Zone IV: 6–0 cm (AD 1950 – modern) – This zone also displays a high sedimentation rate (143 cm/ka; Table 1). The smectite and the kaolinite decrease to their lowest mean abundances (16 % and 2.9 %, respectively). However, the plagioclase and the dolomite present their maximum mean abundance (3.6 % and 3.2 %, respectively) as well as the Fe-oxides (1.4 %) and amphibole (1.4 %). The illite and the chlorite present their maximum mean abundance (42 % and 21 %, respectively; Table 4). This zone displays the highest ratios in Fe/Al and Si/Al (Figure 5). It is dominated by autotrophic taxa *O. centrocarpum* s.l. (51 %) and cysts of *P. dalei* (35 %) (Figure 8). *Impagidinium pallidum* and *S. frigidus/elongatus* reach their highest abundances of all heterotrophic taxa.

4.5. Palynological data

Since the assemblages and autotrophic/heterotrophic ratio do not necessarily reflect dinoflagellate productivity in estuarine zones (Radi et al., 2007), in the present study dinocyst influxes are also presented to better characterize dinoflagellate productivity changes throughout the period covered by core 03CS (Figure 7-8). Thus, dinocyst influxes vary between 28 and 434 cysts cm^{-2} yr^{-1} (mean of 142 cysts cm^{-2} yr^{-1}; Table 2). From 2700 to 2000 cal yr BP (Zone I) dinocyst influxes mean is 246 cysts cm^{-2} yr^{-1}, with a maximum value around 2100 cal yr BP. Then, the influxes decrease (79 cysts cm^{-2} yr^{-1}) from 2000 to 200 cal yr BP (Zone II) and increase again (163 cysts cm^{-2} yr^{-1}) to reach their modern value of 241 cysts cm^{-2} yr^{-1} at the top of the core. A short-lived maximum around AD 1900 is also identified. Influxes of pre-Quaternary palynomorphs (mean of 115 cells cm^{-2} yr^{-1}; Table 2) and foraminifer linings (53 cells cm^{-2} yr^{-1}) vary in parallel to those of dinocysts, except for Zone IV, in which foraminifer linings are decreasing rather than increasing.

5. DISCUSSION

5.1. General mineralogical and geochemical characteristics and sedimentary source in the Mackenzie Slope

The ternary plot of Al_2O_3-SiO_2-CaO (Figure 6A) suggests that our sediment samples are composed of detrital material similar to average shale (Pourmand et al., 2012) and Mackenzie River sediments (Gamboa et al., 2017). Likewise, the ternary plot of illite+kaolinite, total feldspars, and dolomite (Figure 6B), also illustrates that slope sediments have a dominant influence from the Mackenzie River. Additionally, the total clays-plagioclase-K-feldspar ternary plot (Figure 6C) illustrates a predominance in total clays in our sediments, suggesting a marked contribution from northern tributaries (notably from the Peel and Red Arctic rivers; Figure 1) relative to the southern tributaries of the Mackenzie Basin. Alternatively, this clay enrichment in the slope can also reflect weaker hydrodynamic conditions in the Mackenzie Slope, such as a decrease in the influence of currents and waves in the deeper environment (e.g., Pavlidis and Shirshov, 1996; Osborne & Forest, 2016). The coarser grains of K-feldspar and plagioclase likely settle more rapidly in the shelf whereas the lighter grains of clays are transported over a longer distance (e.g., Gamboa et al., 2017). However, this hypothesis cannot be validated or rejected with the data currently available. Further sedimentological investigations are required to precisely understand the possible influence of hydrodynamic regime to the sediment distribution in the Canadian Beaufort Shelf.

The moderate enrichment factors of redox sensitive elements (Fe, As, V, Cr, Zn) suggest that the authigenic phases in core 03CS are negligible (Figure S5). This implies that oxic bottom water conditions prevailed over the last 2000 years in the Mackenzie Slope area. Moreover, the moderate to high authigenic Mn enrichment values (5 to 11) in the upper core (Zone IV) can be attributed to precipitation of authigenic Mn oxyhydroxide or oxide at the

Mn redox boundary (e.g., Burdige, 1993; März et al., 2011; Macdonald and Gobeil, 2012; Sundby et al., 2015; Meinhardt et al., 2016). Conversely, the good correlation observed between Fe/Al and Mn/Al in Zones I to III (Figure S4) and between Fe/Al and As/Al (Figure 5) indicates a dominant detrital source for these elements. As the Mackenzie River discharge clearly plays a predominant role in the input of detrital sediments into the Canadian Beaufort margin, we hypothesize that Fe, Mn and As signatures represent mainly pre-formed continental Fe–Mn oxyhydroxides (e.g., Bayon et al., 2004) derived from the sedimentary platform along the Mackenzie Valley.

Overall, in agreement with previous sediment provenance studies on the Mackenzie-Beaufort Sea Slope (e.g., Gamboa et al., 2017; Deschamps et al., 2018a), these results suggest that core 03CS is representative of the sedimentation in the offshore part of the Canadian Beaufort margin. In addition, this part collects fine grained land-derived detrital particles delivered mainly by the Mackenzie River.

5.2. Dinocyst assemblage zones and paleoenvironmental interpretations

ZONE I (100 – 62 cm; 2700 to 2000 cal yr BP)

Mean dinocyst influx is relatively high during this period (246 cysts cm^{-2} yr^{-1}) and dominated by autotrophic taxa (cysts of *Pentapharsodinium dalei* and *Operculodinium centrocarpum* s.l.), accompanied by high mean foraminifer lining influx (106 linings cm^{-2} yr^{-1}), suggesting a period of high surface primary and benthic productivities (Figure 7). This and the relatively high mean freshwater palynomorph influx (13 cells cm^{-2} yr^{-1}; Figure 7), implies a relatively important freshwater input, probably coming from the Mackenzie River, which decreases gradually from the beginning to the end of the zone. Besides, the highest mean pre-Quaternary palynomorph influx (263 cells cm^{-2} yr^{-1}; Figure 7) in this zone suggests

sediment input from the Mackenzie River, possibly from the northern Basin, which is characterized by sedimentary rocks from Cambrian to Cretaceous age (Millot et al., 2003). The mineralogical ratios I/Fsp (maximum) and S+V/I (minimum) are other evidence confirming that sediments originate from the north, since illites are representative of this part of the Mackenzie Basin (Figure 5). Thus, precipitations in the northern part of the Mackenzie Basin were probably important during this period. Previous investigations on the regional hydrologic responses to atmospheric circulation patterns during the Holocene (e.g., MacDonald and Case, 2005; Barron and Anderson, 2011; Anderson et al., 2016) suggest that variations in precipitations on western North America could be controlled by changes in the large-scale atmospheric climate modes, similar to the modern PDO and AO. Warmer temperatures in the central North Pacific during PDO- and a weak AL induce northerly wind anomalies across the Bering Strait, increasing heat and moisture transport to the western Canadian Arctic (Lapointe et al., 2017) including the Yukon Territory and the northern part of the Mackenzie Basin (Figures 9,10A; Hook et al., 2015).

Furthermore, based on the source of ice-rafted iron grains in a sediment core off the coast of Alaska, Darby et al. (2012) suggested strong positive AO-like conditions between 3000 and 1200 cal yr BP. Low atmospheric pressure prevalent during positive AO phases promotes a weakening in the Beaufort Gyre (Darby et al., 2012), as well as an enhanced inflow of North Pacific water through the Bering Strait (e.g., McLaughlin et al., 2002). Within this context, we hypothesize that Pacific water inputs constrained and deflected the Mackenzie River plume eastward, enhancing light availability and allowing a rise in productivity during this period. Thus, upwelling conditions (e.g., Osborne and Forest, 2016) and on-shelf transport of nutrient-rich Pacific water along the Mackenzie Slope may have contributed to increase the primary productivity in this region. This is in agreement with the $\delta^{15}N$ results in a composite core in Bringué and Rochon (2012), suggesting higher Pacific water input from 4600 to 1300 cal yr BP associated with centennial scale shifts of the AO phases.

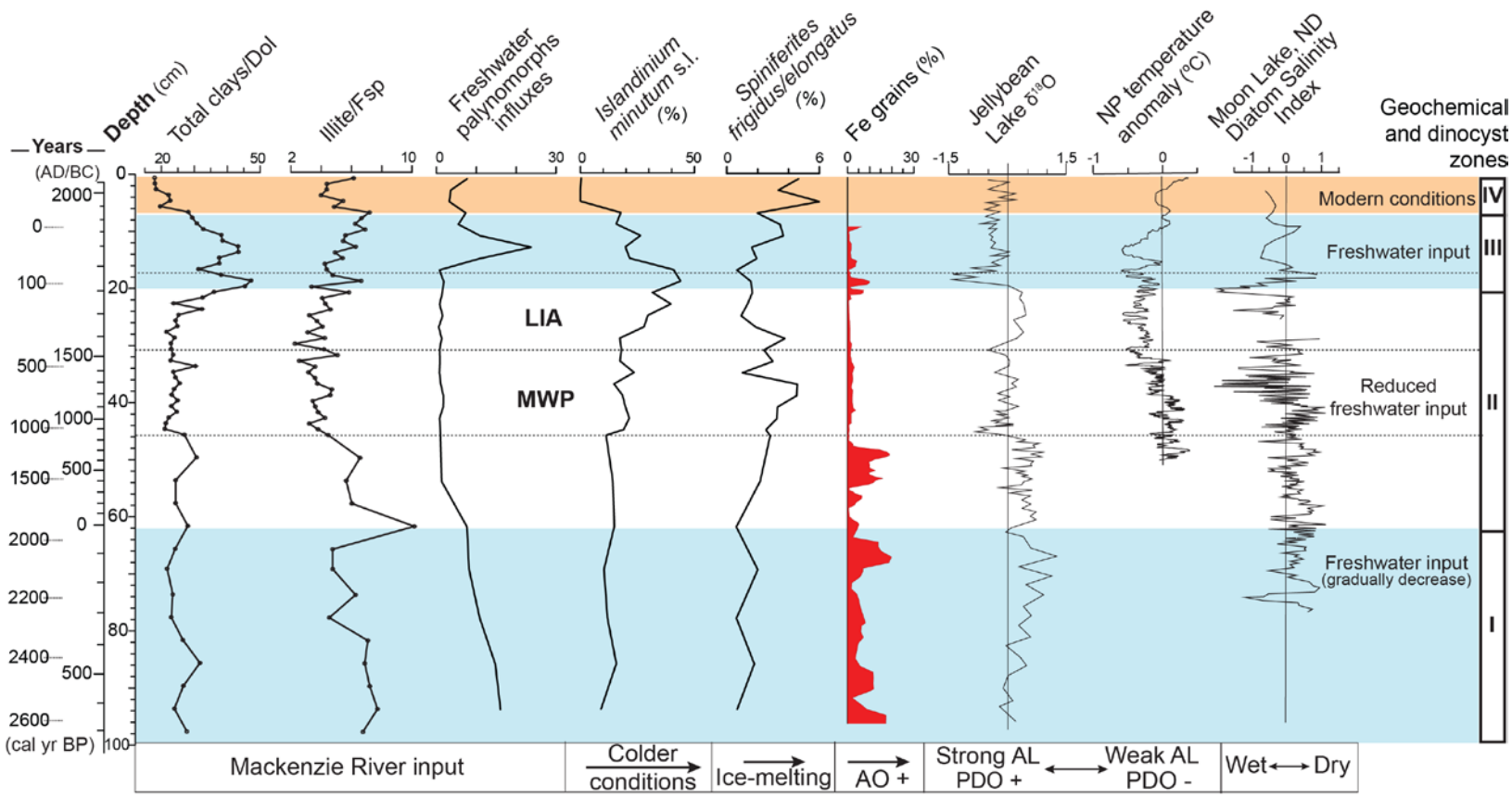

Figure 9. Comparison of multi proxie indicators of core 03CS and reconstructed climatic variations. Fe grains = abundances of iron grains (Darby et al., 2012), oxygen isotope from Jellybean Lake (Anderson et al., 2005), North Pacific (NP) temperature anomaly (Mann et al., 2009), Moon Lake (Laird et al., 1998) in . AL = Aleutian Low, PDO = Pacific Decadal Oscillation. LIA = Little Ice Age. MWP = Medieval Warm Period. The location of Moon Lake and Jellybean Lake is shown on figure 10.

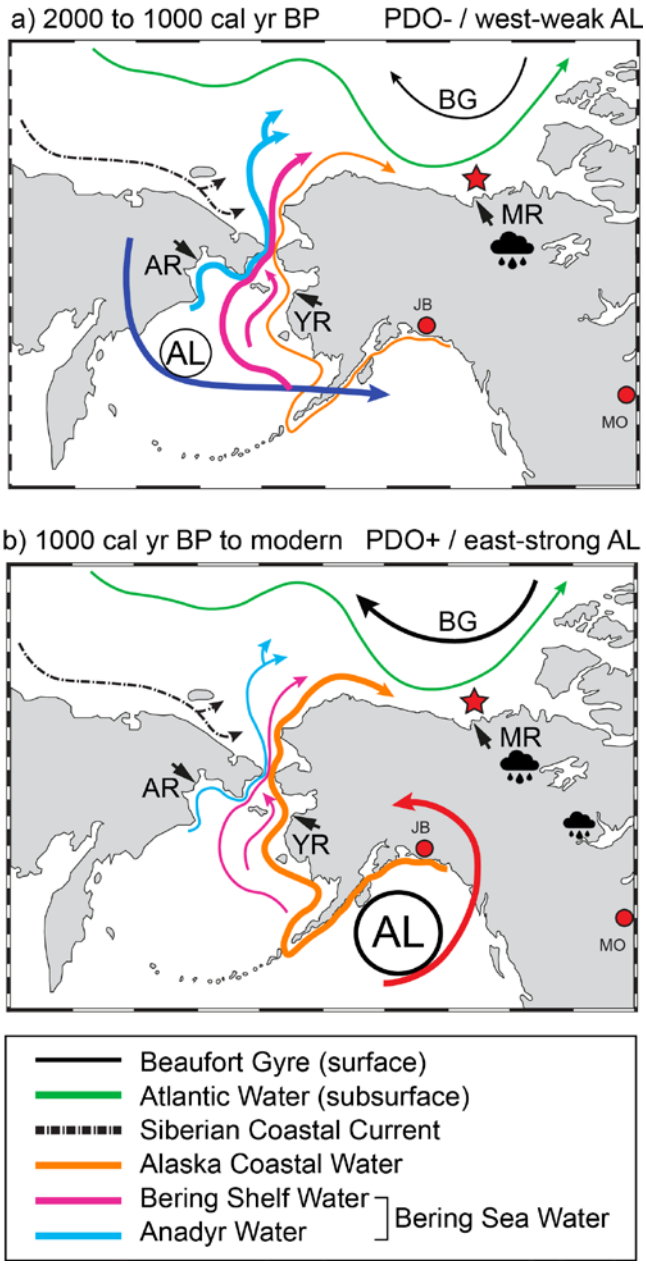

Figure 10. Hypothesized influence of the position and intensity of the Aleutian Low (AL) associated with the PDO phases over the last 2000 years on the Mackenzie River Basin and the Canadian Beaufort Sea. Composite core: 03CS (red star). BG = Beaufort Gyre, AL = Aleutian Low, PDO = Pacific Decadal Oscillation, AR = Anadyr River, YR =Yukon River, MR = Mackenzie River, JB = Jellybean Lake, MO = Moon Lake. 🌧 Pluvial conditions. Modified from Grebmeier et al., 2006; Anderson et al., 2016; Deschamps et al., 2019.

ZONE II (62 – 21 cm; 2000 to 200 cal yr BP)

All palynomorph influxes decreased steadily from the base to approximately the middle part of this zone where they reach their minimum values (Figure 7), which suggests decreasing surface (dinocysts; 247 to 43 cysts cm^{-2} yr^{-1}) and benthic (foraminifer linings; 85 to 13 cells cm^{-2} yr^{-1}) productivities during that period (~ 2000 to 200 cal yr BP). Moreover, pollen/spores relatively low contribution as well as freshwater and pre-Quaternary palynomorphs decrease suggest reduced input from the Mackenzie River during this period. We hypothesize that lower discharge from the Mackenzie River and a decrease in the advection of nutrient-rich Pacific waters could have reduced the nutrient supply to the shelf and slope. This is also in agreement with the effect of a weaker signal of AO (Darby et al., 2012), reflected in a strengthened Beaufort Gyre which reduce the advection of Pacific waters by the Bering Strait (Figure 9) (e.g., Yamamoto et al., 2017). Considering this, autotrophic taxa are limited by the reduction in nutrients, but diatoms can still use the silica reserves accumulated in their frustules to survive. For this reason, heterotrophic taxa are probably controlled by the presence of diatoms (principal heterotrophic prey) and other primary producers. Consequently, heterotrophic taxa still have access to a food source and the decrease of nutrients in the environment had a smaller impact on their population. This is evidenced in the decreasing autotroph/heterotroph ratio shown in figure 8.

Likewise, the relative abundance of cysts of *P. dalei* gradually decreases in this zone (Figure 8). Since this species often dominates in areas characterized by reduced surface salinity (Zonneveld et al., 2013), the decrease of this species thus further supports our interpretation that reduced freshwater discharge prevailed in the area during that period. Moreover, the mineralogical ratios I/Fsp and S+V/I show a gradual increase in feldspars and smectite-vermiculite within this Zone (Figure 5), which are the characteristic minerals from the southern Mackenzie Basin. These modifications in the detrital sources likely suggest that the atmospheric configuration allowed for more moisture transfer to the southern part of Mackenzie basin during this period. Several paleoclimate studies based on terrestrial records from western North America (e.g., Laird et al., 1998; Anderson et al., 2005,2016; MacDonald

and Case, 2005; Barron and Anderson, 2011; Bird et al., 2017) suggest that the period between 2000 and 200 cal yr BP was characterized by (1) changes from a PDO- state to a strong PDO+ state (~ 1000 cal yr BP) and (2) a gradual decrease in the amount of precipitation probably linked to a major change in the Aleutian Low intensity and position over the North Pacific. Figure 9 shows this PDO state change in the Jellybean Lake curve and the precipitation conditions with the wet-dry indicator from Moon Lake. In this context, we speculate that predominantly positive PDO-like conditions allowed the main moisture transfer to reach the southern part of the Mackenzie Basin, promoting a major remobilization and transport of sediments from that region. However, the PDO signal displays greater variability than in Zone I (Figure 9) suggesting more variable Pacific ocean–atmosphere modes than a single PDO type analogue (Anderson et al., 2016). This variability is also observed by Baron and Anderson (2011) and Stone et al. (2016).

In core 03CS, the transition from an autotrophic-dominated assemblage to one dominated by heterotrophic takes place between the beginning of the MWP and the end of the LIA (Figure 8). Cold environment assemblages (e.g., *S. elongatus/frigidus, I. minutum* s.l., *I. minutum* var. *cezare and Polykrikos* sp. var. *arctic/quadratus*) are dominant during the same interval. However, the MWP is marked by the increase in relative abundance of the autotrophic taxa *S. elongatus/ frigidus* (Figure 9; 1 to 5 %), which could be also an indicator of sea-ice reduction possibly due to milder sea-surface conditions, as this species is associated with cold water generated from ice-melting (Zonneveld et al., 2013). Then, *I. minutum* s.l. becomes dominant during the period corresponding to the LIA, suggesting longer sea-ice duration and colder conditions arising from sea-water freeze (Figure 8). Overall, this zone is characterized by reduced freshwater input by the Mackenzie River Basin and milder sea-surface conditions, associated with the MWP (AD 800 – 1525), and followed by a cooler period tentatively associated with the LIA (AD 1525 – 1865).

ZONE III (21 – 6 cm; AD 1800 to 1950)

Dinocyst influxes reach their maximum value in Zone III (434 cysts cm^{-2} yr^{-1}; Figure 7), together with foraminifer linings (259 linings cm^{-2} yr^{-1}), freshwater palynomorphs (24 cells cm^{-2} yr^{-1}) and pollen/spores (147 grains cm^{-2} yr^{-1}). All these, in conjunction with the high sedimentation rate (up to 167 cm/ka) suggest a period of high Mackenzie River discharge. The freshwater input stratifies the water column and induces the nutrients supply in the euphotic zone and promote an increase in primary productivity. The heterotrophic taxa *I. minutum* s.l. reaches it maximum relative abundance at the transition between Zones II and III, which corresponds with the end of the LIA (Figure 8). It then decreases gradually throughout the zone and is replaced by autotrophic taxa probably because of greater nutrient availability from the Mackenzie River. Additionally, there is a gradual increase in *Brigantedinium* spp. in this period, a taxa controlled by nutrients and prey availability (Figure 8).

Moreover, this zone displays a marked increase of certain elemental (e.g., Al/Ca, As/Al and Fe/Al) and mineralogical ratios (total clays/Dol, I/Fsp and I/K+C), and a decrease in S+V/I ratio (Figure 5), suggesting increasing detrital input from the northern Mackenzie River basin. However, the beginning of the zone is marked by relatively high values of smectite and vermiculite (S+V/I; Figure 5), which indicate some contribution from the southern basin. Overall, these data suggest higher precipitations in the Mackenzie River basin between AD 1800 and 1950 (Figures 9,10B), possibly associated with a positive phase of the PDO and a strong AL in an eastern position (Figure 10B). Thus, prevailing westerly winds from the central northern part of the Pacific during the PDO+ (Zhang and Delworth, 2015), likely transport North Pacific water vapor eastward along the west coast of North America. These PDO-like conditions are likely responsible for enhanced precipitation in the southern part of the Mackenzie River basin.

ZONE IV (6 – 0 cm; AD 1950 to modern)

The dinocyst assemblages in this zone are dominated by autotrophic species (Figure 8), possibly due to the oxic conditions prevailing in the area (see section 5.1.) Cysts of *Islandinium minutum* s.l. species are shown to be extremely sensitive to oxygen availability in bottom sediments, *I. pallidum* and cysts of *P. dalei* are considered very sensitive, while *Operculodinium centrocarpum* is moderately sensitive (Zonneveld et al., 2001). Thus, the absence of *Islandinium minutum* s.l. and maximum values of *Operculodinium centrocarpum* s.l. in this section may reflect taphonomic processes rather than climatic variations. Furthermore, lower sample resolution in this zone makes it difficult to evaluate the possible influence of the PDO and the AL on the sea-surface conditions and sediment dynamics.

In summary, dinocyst and terrestrial palynomorph (pollen/spores) influxes fluctuate in a similar manner, suggesting synchronous variations in terrestrial and marine habitats. In general, autotrophic taxa dominate between 2700 and 1000 cal yr BP, while heterotrophic taxa increase between AD 1000 and 1950 (Figure 5), with maximum abundance during the LIA period (AD 1525 – 1865). Autotrophic taxa also dominate in the modern zone. This trophic transition is also observed in Mackenzie Trough and Slope cores studied by Richerol et al. (2008b) and Bringué et al. (2012). Overall, we hypothesize that major changes in the Pacific Ocean–atmospheric dynamics (such as PDO) likely influence the evolution of sea-surface conditions and sediment dynamics in the Canadian Beaufort Shelf (Figure 10).

CONCLUSIONS

This study allowed us to determine hydroclimatic changes using a multiproxy approach to estimate sea-surface conditions, detrital input and freshwater discharge from the Mackenzie River in the recent Holocene over the Mackenzie Slope in the Canadian Beaufort Sea.

- Dinocyst assemblages reveal relatively stable oceanographic conditions in the Canadian Beaufort Sea over the last 2000 years, with occasional warm (MWP) and cold (LIA) periods, which are constrained over the slope between AD 800 – 1525 and AD 1525 – 1865, respectively.
- Mineralogical, geochemical and palynological proxies used in this study suggest an enhanced freshwater input from the Mackenzie River between AD 1800 and 1950 likely related with a persistent PDO+ phase and a strong east AL.
- The mineralogical and geochemical ratios (S+V/I, I/K+C, I/Fsp, total clays/Dol, Al/Ca, Si/Al, and Fe/Al), together with a discriminant diagram based on Al-Si-Ca and I+K-Fds-Dol, suggest that Late Holocene sediments on the slope of the Canadian Beaufort Sea derive mainly from the northern tributaries of the Mackenzie Basin, with the southern tributaries acting as secondary source areas.
- Four assemblage zones are identified based on changes in the mineralogical, geochemical and palynological compositions and constrained cluster analysis, as follows: Zone I (2700 – 2000 cal yr BP) is characterized by an important freshwater input from the Mackenzie River; Zone II (2000 – 200 cal yr BP) suggests drier weather conditions with a decrease in the Mackenzie River discharge likely associated with the PDO+ state; Zone III (AD 1800 – 1950) corresponds to increasing freshwater and detrital input from the northern tributaries of the Mackenzie River relative to the southern tributaries and is associated with predominantly positive PDO-like conditions; and Zone IV (AD 1950 – modern) records taphonomic processes rather than climatic variations.

- Evolution of sea-surface conditions and sedimentary dynamics on the Mackenzie Slope over the last 2000 years seem to be likely influenced by major changes in the atmospheric climate mode, such as PDO and AO.

ACKNOWLEDGEMENTS

We are grateful to the captain, officers, crew and scientists on board the CCGS Amundsen during the 2014 ArcticNet expedition for the recovery of cores used in this study. We also thank Quentin Beauvais (UQAR-ISMER), Charles-Édouard Deschamps (UQAR-ISMER), Adriana Gamboa (UPTOSCR) and Maria-Emilia Rodriguez-Cuicas (UQAR-ISMER and UCV) and Thomas Richerol (ISMER-UQAR) for their technical support and advice in the laboratory. This research was funded by the Network of Centers of Excellence (ArcticNet) and by the Natural Sciences and Engineering Research Council of Canada (NSERC) through Discovery and Northern Supplement Grants to A. Rochon and J.-C. Montero-Serrano.

CONCLUSION GÉNÉRALE

Les variations des différents traceurs analysés (minéralogiques, géochimiques et palynologiques) dans une séquence sédimentaire composite (03CS) qui couvre les derniers 2000 ans ont permis de reconstituer l'évolution des conditions océaniques de surface et la dynamique sédimentaire au cours l'Holocène récent sur le talus du Mackenzie (mer de Beaufort, Arctique canadien). L'ensemble des traceurs détritiques suggère que les sédiments sur le talus proviennent principalement du fleuve Mackenzie.

Quatre zones ont été déterminées sur la base d'une analyse de regroupement hiérarchique des données géochimiques et de l'abondance relative des dinokystes : La **Zone I** (2700 – 2000 cal yr BP) montre une granulométrie et des valeurs de l'ensemble des éléments géochimiques relativement constantes. Cette zone est dominée par des espèces autotrophes (kyste de *Pentapharsodinium dalei* et *Operculodinium centrocarpum* s.l.), de palynomorphes d'eau douce et pré-quaternaires. Les valeurs élevées de flux de dinokystes et de réseaux organiques de foraminifères suggèrent des productivités primaires et benthiques élevées, alors que les palynomorphes d'eau douce et pré-quaternaires suggèrent des apports importants d'eau douce en provenance du fleuve Mackenzie. Les rapports minéralogiques élevés d'illite/K-feldspath+plagioclase (I/Fsp) et faible de smectite+vermiculite/illite (S+V/I) suggèrent une provenance de sédiments du nord du bassin du fleuve Mackenzie probablement lié à de fortes précipitations septentrionales induites par une configuration ODP- et à une faible dépression des Aléoutiennes-ouest. L'ODP- ainsi que l'OA+ (affaiblissement du gyre de Beaufort) au cours de cette période suggèrent également une augmentation des apports des eaux du Pacifique Nord (riche en nutriments); La **Zone II** (2000 – 200 cal yr BP) montre une diminution du taux de sédimentation (de 53 à 23 cm/ka), du flux des dinokystes ainsi que de l'ensemble des palynomorphes, ce qui suggère des conditions climatiques plus sèches en lien avec une diminution de la décharge du fleuve

Mackenzie, ainsi qu'une productivité primaire diminuée. Les rapports I/Fsp et S+V/I indiquent une augmentation progressive des feldspaths et des smectites-vermiculites (minéraux caractéristiques du sud du bassin du fleuve Mackenzie). De plus, cette zone est caractérisée par une diminution graduelle des espèces autotrophes vers la dominance des hétérotrophes qui devient plus marquée (productivité primaire possiblement dominée par des diatomées) dans une période qui correspond au début de l'OCM (~ AD 800 – 1525) et à la fin de la PAG (~ AD 1525 – 1865). L'OCM et le PAG sont marqués, respectivement, par l'augmentation des abondances relatives de *S. elongatus/frigidus* (conditions plus douces) et de l'*I. minutum* s.l. (conditions plus froides). Ces résultats sont en accord avec un signal plus faible de l'OA (gyre de Beaufort renforcé) et d'un changement d'une phase ODP- (faible dépression des Aléoutiennes-ouest) à une phase ODP+ (forte dépression des Aléoutiennes-est) qui correspond à une diminution des précipitations au nord du Pacifique. Par contre, la Z**one III** (AD 1800 – 1950) montre une augmentation du Ts (jusqu'à 167 cm/ka), de certains rapports élémentaires (ex., Al/Ca, As/Al et Fe/Al) et minéralogiques (Argiles/Dol, I/Fsp et illite/kaolinite+chlorite) et une diminution du rapport S+V/I, ce qui indique une forte augmentation des apports sédimentaires du bassin nord du fleuve Mackenzie par rapport au bassin sud. Cependant, les valeurs relativement élevées en smectite et vermiculite (S+V/I) au début de cette zone montrent aussi une certaine contribution du bassin sud. Ceci est probablement contrôlé par une configuration ODP+ (forte dépression des Aléoutiennes-est), ce qui induit un plus important transport d'humidité vers le nord-ouest du continent nord-américain et à une augmentation des précipitations au sud du bassin du fleuve Mackenzie. Cette augmentation d'apport d'eau douce est également marquée par l'augmentation des flux de palynomorphes d'eau douce et pré-quaternaires. On y observe la co-dominance d'espèces autotrophes et hétérotrophes. Finalement, la **Zone IV** (AD 1950 – moderne) est caractérisée par un taux de sédimentation élevé (143 cm/ka) et une augmentation de la taille des grains (2.7 à 4.1 µm). Les espèces autotrophes (*Operculodinium centrocarpum* s.l. et kyste de *Pentapharsodinium dalei*) et les conditions oxiques (augmentation de Fe-oxides) dominent. Ces conditions sont principalement influencées par les variations des apports du fleuve Mackenzie au niveau du talus de la mer de Beaufort dues aux précipitations dans les

différents secteurs du bassin versant du fleuve. Dans le cas présent, il semble que ce soient les processus taphonomiques qui aient influencé la composition des assemblages récents de dinokystes (Zone IV), et non le climat.

Les reconstitutions des paramètres de conditions de masses d'eau de surface (température, salinité, durée du couvert de glace, productivité primaire) obtenues par les fonctions de transfert et la technique des analogues modernes (MAT) n'ont pas été utilisées dans l'interprétation des résultats parce que les variations des valeurs de ces paramètres sont inférieures à l'erreur de prédiction respective de plusieurs paramètres, ce qui limite l'interprétation des résultats dans notre séquence sédimentaire. Les assemblages de dinokystes ont tout de même permis de réaliser des interprétations qualitatives des conditions de masses d'eau de surface. D'autre part, cette étude donne des informations sur les changements de la provenance des sédiments dans le bassin du fleuve Mackenzie ainsi que sur les variations climatiques qui affectent le nord-ouest de l'Amérique du Nord. Ainsi, au cours des 2000 dernières années, l'évolution des conditions de surface et la dynamique sédimentaire ont été influencées par l'OA et l'OPD. Ces variations climatiques modifient l'intensité de l'apport sédimentaire et d'eau douce du fleuve Mackenzie, ainsi que l'entrée des masses d'eau du Pacifique lorsque celles-ci affaiblissent le gyre de Beaufort.

Pour conclure, cette étude multi-traceurs a permis de documenter la possible influence des variations climatiques et atmosphériques (notamment, OA et ODP) sur l'évolution des conditions paléo-environnementales dans le talus canadien de la mer de Beaufort au cours l'Holocène récent. Cependant, bien que le modèle chronostratigraphique obtenu par la corrélation de propriétés physiques et magnétiques ait permis de documenter des variations paléoenvironnementales dans le talus du Mackenzie au cours l'Holocène récent, ceci pourrait être amélioré. En effet, des datations au radiocarbone seraient utiles pour déterminer précisément les taux de sédimentation de la séquence composite et valider avec plus de précision les différents faciès sédimentologiques proposés ici. D'autre part, des données sédimentologiques à haute fréquence (ex. scanner de fluorescence des rayons X) couplées à

des analyses en ondelettes pourraient aider à confirmer des patrons et périodes similaires à la PDO et AO et ainsi la possible influence des oscillations climatiques sur les conditions océaniques de surface et la dynamique sédimentaire dans le talus du Mackenzie.

Table 1. Chronology and sedimentation rates from age modelling constructed (Figure 4) using the R package BACON (Blaauw & Christen 2011).

Depth 03CS (cm)	Core	Age AD	Age cal yr BP	Average sedimentation rate (cm/ka)	ZONE
0	BC	2014	-65	143	
1	BC	2008	-58	143	
2	BC	2000	-50	143	
3	BC	1993	-43	143	IV
4	BC	1986	-36	143	
5	BC	1978	-28	143	
6	BC	1968	-18	100	
7	BC	1958	-8	100	
8	BC	1947	3	100	
9	BC	1937	13	100	
10	BC	1926	24	167	
11	BC	1920	30	167	
12	BC	1915	35	167	
13	BC	1909	41	167	
14	BC	1904	46	167	III
15	BC	1898	52	167	
16	BC	1876	74	23	
17	BC	1854	96	23	
18	BC	1833	117	23	
19	BC	1811	139	23	
20	BC	1789	161	23	
21	BC	1761	189	23	
22	BC	1731	219	23	
23	BC	1703	247	23	
24	BC	1676	274	23	
25	BC	1650	300	23	
26	BC	1625	325	23	
27	BC	1597	353	23	
28	BC	1569	381	23	
29	BC	1540	410	23	
30	BC	1513	437	23	
31	BC	1478	472	23	
32	BC	1438	512	23	
33	BC	1401	549	23	
34	BC	1366	584	23	
35	BC	1333	617	23	
36	BC	1279	671	23	
37	BC	1226	724	23	
38	BC	1176	774	23	II
39	BC	1126	824	23	
40	BC	1079	871	23	
41	BC	1024	926	23	
42	BC	967	983	23	
43	BC	909	1041	23	
44	BC	856	1094	23	
45	TWC	804	1146	23	
46	TWC	747	1203	23	
47	TWC	686	1264	23	
48	TWC	628	1322	23	
49	TWC	569	1381	23	
50	TWC	509	1441	23	
51	TWC	457	1493	23	
52	TWC	403	1547	23	
53	TWC	345	1605	23	
54	TWC	287	1663	23	

Table 1 (continued)

Depth 03CS (cm)	Core	Age AD	Age cal yr BP	Average sedimentation rate (cm/ka)	ZONE
55	TWC	228	1722	23	II
56	TWC	184	1766	23	II
57	TWC	141	1809	23	II
58	TWC	96	1854	23	II
59	TWC	48	1902	23	II
60	TWC	-3	1953	23	II
61	TWC	-28	1978	23	II
62	TWC	-54	2004	53	I
63	TWC	-80	2030	53	I
64	TWC	-105	2055	53	I
65	TWC	-126	2076	53	I
66	TWC	-145	2095	53	I
67	TWC	-164	2114	53	I
68	TWC	-182	2132	53	I
69	TWC	-199	2149	53	I
70	TWC	-216	2166	53	I
71	TWC	-234	2184	53	I
72	TWC	-253	2203	53	I
73	TWC	-273	2223	53	I
74	TWC	-291	2241	53	I
75	TWC	-309	2259	53	I
76	TWC	-328	2278	53	I
77	TWC	-345	2295	53	I
78	TWC	-364	2314	53	I
79	TWC	-382	2332	53	I
80	TWC	-399	2349	53	I
81	TWC	-418	2368	53	I
82	TWC	-437	2387	53	I
83	TWC	-457	2407	53	I
84	TWC	-477	2427	53	I
85	TWC	-495	2445	53	I
86	TWC	-514	2464	53	I
87	TWC	-532	2482	53	I
88	TWC	-552	2502	53	I
89	TWC	-571	2521	53	I
90	TWC	-588	2538	53	I
91	TWC	-607	2557	53	I
92	TWC	-626	2576	53	I
93	TWC	-645	2595	53	I
94	TWC	-664	2614	53	I
95	TWC	-683	2633	53	I
96	TWC	-702	2652	53	I
97	TWC	-721	2671	53	I

CS = composite core; BC = box core; TWC = trigger weight core

Table 2. Palynological results. Relative abundance of dinocyst taxa in our sample (%). Palynomorph influxes (specimens cm^{-2} yr^{-1}). Quantitative reconstruction of sea-surface conditions (ºC, psu, months yr^{-1}, gC m^{-2} yr^{-1}).

Depth 03CS (cm)	Core	Age (AD)	Age (cal yr BP)	A	H	Ocen	Pdal	Imin	Imic	Bspp	Selo	Parc	Ipal	Pame	Dino.	Foram. linings	Fresh.	pre-Quat. palyno.	Pollen Spore	Twin	Tsum	Ssum	Ice cover	Prim. prod.	Zone
0	BC	2014	-65	96	4	51	40	0	0	3	5	0	0	0	387	8	8	100	159	-1.7	5.1	28	7.1	162	
2	BC	2000	-50	100	0	69	26	0	0	0	3	0	2	0	180	1	4	43	77	-1.5	0.0	29	11.3	28	IV
4	BC	1986	-36	100	0	54	38	0	0	0	6	0	2	0	238	1	3	51	109	-1.6	3.2	29	8.4	88	
6	BC	1968	-18	70	30	31	36	18	2	11	2	0	0	0	160	46	7	48	76	-1.6	4.2	25	8.7	154	
8	BC	1947	3	65	35	31	30	16	2	15	3	2	0	0	175	114	5	85	67	-1.4	3.3	23	9.5	160	
10	BC	1926	24	51	49	22	24	26	1	19	4	3	1	0	235	81	11	197	113	-1.6	4.1	24	9.2	156	
12	BC	1915	35	70	30	19	49	20	1	7	2	2	1	0	434	259	24	248	147	-1.3	3.7	25	9.3	136	
14	BC	1904	46	58	42	17	39	22	4	13	2	3	0	0	177	147	11	207	77	-1.6	3.9	24	9.2	160	III
16	BC	1876	74	40	60	19	20	41	6	10	1	4	1	0	28	22	1	39	9	-1.6	3.9	24	9.3	150	
18	BC	1833	117	42	58	18	23	44	6	4	2	3	0	0	39	13	2	41	6	-1.5	4.4	26	9.0	139	
20	BC	1789	161	54	46	19	33	32	4	8	2	3	1	0	56	28	1	44	10	-1.6	3.7	24	9.4	151	
22	BC	1731	219	46	54	17	27	40	3	7	1	3	1	0	58	13	1	71	11	-1.6	3.8	24	9.4	151	
24	BC	1676	274	56	44	20	36	30	5	6	1	4	0	0	56	43	2	103	13	-1.5	4.4	26	9.0	141	
26	BC	1625	325	54	46	19	32	28	8	6	2	4	1	0	59	14	1	79	9	-1.6	3.7	24	9.4	149	
28	BC	1569	381	67	33	28	35	17	3	8	4	5	0	0	46	17	1	87	11	-1.3	4.3	23	9.3	173	
30	BC	1513	437	69	31	31	36	18	2	8	2	2	0	0	64	22	1	87	12	-1.5	4.6	22	9.5	191	
32	BC	1438	512	69	31	30	36	17	2	9	3	2	0	1	75	30	1	71	14	-1.3	5.2	22	9.6	218	
34	BC	1366	584	57	43	18	38	23	3	12	1	4	0	0	43	17	1	61	8	-1.5	4.9	22	9.5	199	
36	BC	1279	671	70	30	30	35	15	2	8	5	5	0	0	47	13	1	62	8	-1.1	3.8	25	9.1	148	II
38	BC	1176	774	68	32	21	41	18	3	4	5	5	1	1	59	20	2	65	14	-1.3	5.3	22	9.6	220	
40	BC	1079	871	67	33	21	42	20	3	7	3	3	0	0	71	37	2	71	14	-1.3	3.5	25	9.3	147	
42	BC	967	983	68	32	26	38	21	2	6	3	2	1	0	77	19	1	69	9	-1.4	3.4	25	9.4	134	
44	BC	856	1094	70	30	16	51	19	2	6	3	3	1	0	98	35	1	87	15	-1.3	3.5	25	9.4	141	
45	TWC	804	1146	82	18	31	48	11	1	3	3	3	0	0	81	40	1	66	11	-0.6	5.1	26	8.9	173	
53	TWC	345	1605	79	21	13	62	14	3	2	2	2	1	0	102	44	1	79	8	-1.3	3.2	27	9.5	110	
61	TWC	-28	1978	77	23	20	56	15	2	3	1	2	0	1	247	85	8	244	27	-0.9	4.6	27	9.1	165	
68.5	TWC	-182	2132	84	16	14	68	10	3	1	2	2	0	0	357	127	8	254	45	-0.9	4.2	28	8.9	135	
77	TWC	-345	2295	78	22	14	63	12	3	5	1	2	0	1	174	84	11	296	23	-0.9	4.5	27	8.9	152	I
85	TWC	-495	2445	78	22	17	59	16	1	4	2	1	0	0	198	112	15	240	28	-0.8	3.8	26	9.1	131	
93	TWC	-645	2595	83	17	12	70	9	3	4	1	1	1	0	253	99	16	262	34	-1.5	4.4	23	9.7	178	

Table 2 (continued)

		A	H	Ocen	Pdal	Imin	Imic	Bspp	Selo	Parc	Ipal	Pame	Dino.	Foram. lining	Fresh.	pre-Quat. palyno.	Pollen Spore	Twin	Tsum	Ssum	Ice cover	Prim. prod.
Mean		69	31	25	41	19	2.7	7	2.5	2.5	0.6	0.2	142	53	5.0	115	39	-1.3	4.0	25	9.3	156
Max		100	60	69	70	44	8.5	19	6.0	5.2	2.0	1.3	434	259	24	296	159	-0.6	5.3	29	11	227
Min		40	0	12	20	0	0.0	0	0.6	0.0	0.0	0.0	28	1	1	39	6	-1.7	0.1	21	7	28
Mean of each zone	IV	91	9	51	35	5	0.4	4	4.0	0.1	1.1	0.0	241	14	5.5	60	105	-1.6	3.0	28	9.0	108
	III	54	46	21	31	29	3.4	11	2.1	2.9	0.6	0.0	163	95	7.9	123	61	-1.5	3.8	24	9.3	153
	II	67	33	23	41	20	3.1	6	2.5	3.2	0.5	0.3	79	30	1.5	87	12	-1.3	4.2	24	9.4	169
	I	81	19	14	65	12	2.3	3	1.3	1.6	0.2	0.3	246	106	12.5	263	33	-1.1	4.4	26	9.2	160

CS = composite core; BC = box core; TWC = trigger weight core; A = Autotrophs; H = Heterotrophs; Ocen = *Operculodinium centrocarpum* sensu Wall & Dale 1966 + *O. centrocarpum* short processes + *O. centrocarpum* arctic morphotype; Pdal = cyst of *Pentapharsodinium dalei*; Imin = *Islandinium minutum* + *I. brevispinosum* + *Echinidinium karaense* + *Echinidinium* spp; Imic = *I. minutum* var. *cezare*; Bspp = *B. simplex* + *B. cariacoense* + *Bringantedinium* sp.; Selo= *Spiniferites elongatus* + *S. frigidus*; Parc = cyst of *Polykrikos* spp. arctic/quadratus morphotypes; Ipal = *Impagidinium pallidum*; Pame = cyst of *Protoperidinium americanum*. Palynomorphs influxes (Dino. = Dinocyst; Foram.lining = Foraminifer linings; Fresh.= Freshwater palynomorphs; pre-Quat.palyno. = pre-Quaternary palynomorph). Quantitative reconstruction of sea-surface conditions (Twin = Winter sea-surface temperature (ºC); Tsum = Summer sea-surface temperature (ºC); Ssum = Summer sea-surface salinity (psu); Ice cover = Sea-ice cover (months yr^{-1}); Prim.prod. = primary productivity (gC m^{-2} yr^{-1}).

Table 3. Grain size (µm) and bulk mineralogical abundance (%) results.

Depth 03CS (cm)	Core	Age AD	Age cal yr BP	Grain size (µm)	Qz	FeldsK	Plag	Dol	Amph	Fe-oxides	Amorph Silica	Biotite-chlorite	Illites	Kaol	Smectite	Vermiculite	Zone
0	BC	2014	-65	3.7	24	2.1	3.2	3.7	0.7	0.1	1.1	14	32	3.0	14	1.5	
1	BC	2008	-58	3.9	23	2.2	5.3	3.5	1.7	1.6	0.0	11	33	2.8	15	0.4	
2	BC	2000	-50	4.2	22	4.0	2.5	3.5	1.0	0.7	2.6	14	28	2.6	16	1.8	
3	BC	1993	-43	4.1	23	3.4	4.0	2.8	0.6	2.6	2.1	11	29	0.0	20	0.9	IV
4	BC	1986	-36	4.0	21	1.5	4.2	2.9	1.6	1.4	1.4	14	31	3.5	16	0.8	
5	BC	1978	-28	4.6	21	2.6	3.4	3.3	2.7	0.1	3.7	13	29	3.5	15	2.0	
6	BC	1968	-18	2.9	22	1.5	2.9	2.4	1.5	0.9	1.1	12	32	3.1	17	3.5	

Table 3 (continued)

Depth 03CS (cm)	Core	Age AD	Age cal yr BP	Grain size (μm)	Qz	FeldsK	Plag	Dol	Amph	Fe-oxides	Amorph Silica	Biotite-chlorite	Illites	Kaol	Smectite	Vermiculite	Zone
7	BC	1958	-8	2.7	21	1.2	3.6	2.3	1.7	0.0	1.9	12	32	4.1	16	3.0	III
8	BC	1947	3	2.6	21	1.4	3.6	2.3	1.3	0.5	1.9	12	31	4.9	16	4.4	
9	BC	1937	13	2.6	21	1.2	3.9	2.0	1.3	1.0	3.3	10	36	3.9	15	1.3	
10	BC	1926	24	2.5	22	2.3	3.4	1.8	0.6	1.2	0.4	12	32	3.1	18	2.4	
11	BC	1920	30	2.7	22	2.2	3.0	1.8	0.3	0.6	0.2	12	28	3.5	22	3.4	
12	BC	1915	35	2.9	21	1.1	3.2	1.6	0.8	0.2	3.0	13	27	2.0	22	4.4	
13	BC	1909	41	2.6	22	2.2	3.3	1.5	1.9	0.7	1.8	12	27	2.5	20	4.6	
14	BC	1904	46	2.7	22	2.3	3.0	1.9	0.1	0.3	0.7	11	29	3.5	22	4.0	
15	BC	1898	52	3.4	21	2.2	3.2	1.7	1.6	1.6	1.9	12	23	4.2	21	4.7	
16	BC	1876	74	2.5	22	1.8	3.8	2.2	0.9	0.6	0.5	12	24	3.8	23	4.3	
17	BC	1854	96	2.5	23	1.5	3.8	1.8	0.2	0.9	0.0	11	25	4.4	23	5.3	
18	BC	1833	117	2.9	22	0.7	3.1	1.5	0.8	0.6	2.3	13	26	2.7	26	0.9	
19	BC	1811	139	3.4	21	3.6	2.9	1.5	1.5	1.4	1.2	15	22	4.3	24	1.6	
20	BC	1789	161	2.1	20	1.3	2.8	1.9	0.4	0.6	4.9	13	24	3.2	25	2.9	
21	BC	1761	189	2.4	22	3.2	3.2	2.1	0.8	0.6	0.0	12	26	3.1	27	0.3	
22	BC	1731	219	3.4	23	2.6	3.8	2.8	0.7	0.2	0.0	14	27	4.8	18	1.7	
23	BC	1703	247	2.9	21	2.5	3.6	2.1	1.6	0.7	0.7	13	28	4.2	20	2.9	
24	BC	1676	274	2.5	20	4.4	3.1	2.6	0.7	1.1	3.5	13	24	3.4	20	3.3	
25	BC	1650	300	2.5	22	2.8	4.1	2.7	0.9	0.7	2.3	13	25	4.3	20	1.6	
26	BC	1625	325	2.6	22	3.2	3.3	2.6	0.9	1.1	3.6	13	26	3.0	19	1.8	
27	BC	1597	353	2.2	23	4.4	3.4	3.0	0.9	0.7	2.0	15	24	4.4	19	0.0	
28	BC	1569	381	2.5	23	3.2	3.2	2.8	0.0	0.2	2.2	15	27	4.0	18	0.8	
29	BC	1540	410	2.5	21	6.3	3.5	2.7	0.0	1.2	4.0	15	22	3.8	18	0.8	
30	BC	1513	437	2.6	23	2.3	3.5	2.8	0.9	0.0	3.1	13	24	4.2	22	0.0	
31	BC	1478	472	2.7	18	1.9	2.9	2.7	2.4	0.2	8.9	16	24	3.8	17	0.6	
32	BC	1438	512	2.6	21	5.8	3.2	2.9	0.6	0.6	1.3	17	23	3.4	21	0.0	
33	BC	1401	549	2.6	23	2.6	3.8	2.2	0.7	0.4	1.2	15	23	3.0	22	0.5	
34	BC	1366	584	2.7	22	3.6	3.9	2.9	0.4	0.3	0.3	15	24	4.7	22	0.6	
35	BC	1333	617	2.5	23	3.7	3.4	2.7	1.4	0.1	0.5	14	25	3.6	22	0.3	
36	BC	1279	671	2.5	24	2.9	4.1	2.6	0.0	0.7	0.8	14	26	3.3	20	0.3	

Table 3 (continued)

Depth 03CS (cm)	Core	Age AD	Age cal yr BP	Grain size (µm)	Qz	FeldsK	Plag	Dol	Amph	Fe-oxides	Amorph Silica	Biotite-chlorite	Illites	Kaol	Smectite	Vermiculite	Zone
37	BC	1226	724	2.8	23	2.4	3.4	2.8	1.0	0.0	0.7	13	27	3.7	19	2.2	
38	BC	1176	774	2.7	21	1.5	4.2	3.0	0.4	0.3	2.1	15	26	2.7	22	1.6	
39	BC	1126	824	2.9	23	4.6	2.9	2.6	0.4	0.7	1.2	14	26	3.6	21	0.0	
40	BC	1079	871	2.7	23	2.2	2.5	2.9	1.3	0.2	1.0	16	25	3.1	20	1.8	
41	BC	1024	926	2.9	22	3.3	3.7	2.7	0.2	0.7	0.7	14	27	2.5	19	3.5	
42	BC	967	983	2.8	23	2.8	3.6	3.0	0.4	0.5	1.3	14	27	3.3	19	2.0	
43	BC	909	1041	2.7	21	3.3	4.5	3.1	0.4	0.7	1.9	14	25	3.6	19	2.1	II
44	BC	856	1094	2.8	22	3.1	4.1	3.2	0.5	0.9	0.4	14	27	3.6	20	1.2	
45	TWC	804	1146	2.4	22	3.5	2.4	2.5	0.3	1.0	1.2	11	27	3.6	21	4.0	
49	TWC	569	1381	2.4	23	0.9	3.3	2.2	1.3	0.4	1.3	12	28	3.1	21	3.3	
53	TWC	345	1605	2.5	23	2.1	2.9	2.8	0.2	0.7	1.2	14	29	4.4	18	2.0	
57	TWC	141	1809	2.6	22	2.6	2.1	2.8	0.9	0.7	1.0	14	29	3.5	20	0.9	
61	TWC	-28	1978	2.5	20	1.1	1.8	2.4	0.6	0.1	8.4	14	30	3.3	15	3.0	
65	TWC	-126	2076	2.5	24	3.1	2.8	2.7	0.2	0.4	1.1	15	28	2.4	17	2.7	
68.5	TWC	-19	2141	2.6	23	3.2	2.5	3.1	0.4	0.5	1.1	15	27	4.3	18	1.3	
73	TWC	-273	2223	2.5	21	1.8	3.0	2.9	0.4	0.3	3.5	13	30	3.9	17	2.8	
77	TWC	-345	2295	2.5	22	3.8	2.0	3.0	0.0	0.4	0.0	15	26	4.3	21	0.4	
81	TWC	-418	2368	2.5	19	1.5	2.5	2.5	1.3	0.0	8.3	15	28	4.0	17	0.8	I
85	TWC	-495	2445	2.6	23	1.3	2.8	2.2	0.1	0.5	1.7	13	28	3.5	21	1.1	
89	TWC	-571	2521	2.5	22	1.7	2.6	2.5	1.0	0.8	1.1	14	31	3.9	17	0.8	
93	TWC	-645	2595	2.7	22	1.5	3.4	2.8	0.6	0.0	2.6	13	37	3.9	12	0.0	
97	TWC	-721	2671	2.6	21	2.9	2.6	2.5	1.3	1.1	0.6	13	37	3.2	11	3.2	
Mean				2.8	22.0	2.6	3.3	2.5	0.8	0.6	2.1	13	28	3.5	19	1.9	
Max				4.6	24.0	6.3	5.3	3.7	2.7	2.6	13.6	17	37	4.9	27	5.3	
Min				2.1	18.4	0.7	1.8	1.5	0.0	0.0	0.0	10	22	0.0	11	0.0	
Mean of each zone			IV	3.9	22.3	2.5	3.6	3.2	1.4	1.1	1.7	13	31	2.6	16	1.6	
			III	2.7	21.6	1.8	3.3	1.8	1.0	0.7	1.7	12	27	3.6	21	3.4	
			II	2.6	22.2	3.1	3.4	2.7	0.7	0.5	2.4	14	26	3.6	20	1.5	
			I	2.6	21.9	2.3	2.7	2.7	0.6	0.4	2.2	14	30	3.7	17	1.5	

CS = composite core; BC = box core; TWC = trigger weight core; Qz = quartz; FeldsK = K-feldspar; Plag = plagioclase; Dol = dolomite; Amph = amphipole; Amorph Silica = amorphous silica; Kaol = kaolinite

Table 4. Clay mineralogical (%) results.

Depth 03CS (cm)	Core	Age AD	Age cal yr BP	Smectite	Illite	Chlorite	Kaolinite	Vermiculite	Zone
0	BC	2014	-65	19	40	21	13	7	
1	BC	2008	-58	17	42	25	10	6	
2	BC	2000	-50	16	44	20	17	3	
3	BC	1993	-43	9	47	20	15	9	IV
4	BC	1986	-36	12	42	20	17	10	
5	BC	1978	-28	11	45	25	13	6	
6	BC	1968	-18	22	38	14	18	8	
7	BC	1958	-8	25	40	17	15	3	
8	BC	1947	3	21	43	17	16	3	
9	BC	1937	13	28	31	19	14	8	
10	BC	1926	24	18	34	17	16	14	
11	BC	1920	30	18	43	17	14	7	
12	BC	1915	35	20	42	19	17	3	
13	BC	1909	41	11	40	22	15	11	III
14	BC	1904	46	30	35	16	13	6	
15	BC	1898	52	26	38	15	15	5	
16	BC	1876	74	16	39	19	17	10	
17	BC	1854	96	14	39	19	17	11	
18	BC	1833	117	27	36	14	14	9	
19	BC	1811	139	33	33	16	13	5	
20	BC	1789	161	29	37	14	16	4	
21	BC	1761	189	23	38	18	15	6	
22	BC	1731	219	41	33	15	11	3	
23	BC	1703	247	26	36	17	16	5	
24	BC	1676	274	19	37	19	20	5	
25	BC	1650	300	19	37	21	13	11	
26	BC	1625	325	21	35	18	18	9	
27	BC	1597	353	24	34	17	19	7	
28	BC	1569	381	24	34	18	15	9	
29	BC	1540	410	32	28	15	14	11	
30	BC	1513	437	30	32	16	14	7	
31	BC	1478	472	22	39	16	18	6	
32	BC	1438	512	18	37	21	18	7	
33	BC	1401	549	16	38	19	19	7	
34	BC	1366	584	25	34	20	15	6	
35	BC	1333	617	17	38	20	21	4	II
36	BC	1279	671	22	37	21	13	7	
37	BC	1226	724	25	36	21	14	4	
38	BC	1176	774	22	34	22	16	6	
39	BC	1126	824	26	28	15	18	13	
40	BC	1079	871	31	33	17	14	5	
41	BC	1024	926	23	35	17	18	8	
42	BC	967	983	22	35	18	17	8	
43	BC	909	1041	25	36	16	15	9	
44	BC	856	1094	21	34	18	15	12	
45	TWC	804	1146	21	38	17	17	7	
49	TWC	569	1381	18	41	20	15	5	
53	TWC	345	1605	22	39	19	15	5	
57	TWC	141	1809	18	40	19	16	7	
61	TWC	-28	1978	14	43	17	21	5	

Table 4 (continued)

Depth 03CS (cm)	Core	Age AD	Age cal yr BP	Smectite	Illite	Chlorite	Kaolinite	Vermiculite	Zone
65	TWC	-126	2076	20	40	16	20	4	
68.5	TWC	-19	2141	15	41	19	17	8	
73	TWC	-273	2223	15	42	18	19	7	
77	TWC	-345	2295	17	39	17	20	6	
81	TWC	-418	2368	18	38	19	18	6	I
85	TWC	-495	2445	18	41	18	19	4	
89	TWC	-571	2521	22	37	22	15	4	
93	TWC	-645	2595	14	44	18	17	6	
97	TWC	-721	2671	36	36	15	13	3	
Mean				21	38	18	16	7	
Max				41	47	25	21	14	
Min				9	28	14	10	3	
Mean of each zone			IV	15	42	21	15	7.0	
			III	23	38	17	15	7.0	
			II	23	36	18	16	7.0	
			I	20	40	18	18	5.3	

CS = composite core; BC = box core; TWC = trigger weight core

Table 5. Elemental geochemical results.

Depth 03CS (cm)	Core	Age AD	Age cal yr BP	L.O.I.	Mg (%)	Al (%)	Si (%)	P (%)	K (%)	Ca (%)	Ti (%)	Mn (%)	Fe (%)	V ppm	Cr ppm	Cu ppm	Zn ppm	Sr ppm	Zr ppm	As ppm	Zone
0	BC	2014	-65	9.4	1.0	9.9	28.2	0.08	2.8	1.2	0.49	0.70	5.1	304	111	23	157	167	152	28	
1	BC	2008	-58	9.5	1.0	9.9	27.6	0.07	2.8	1.2	0.48	0.80	5.1	296	208	23	162	164	150	19	
2	BC	2000	-50	10.6	1.0	9.7	27.1	0.08	2.8	1.2	0.48	0.97	5.0	278	111	64	191	168	154	7	IV
3	BC	1993	-43	9.5	0.9	9.8	27.0	0.08	2.8	1.1	0.48	1.95	5.1	298	109	71	163	175	157	15	
4	BC	1986	-36	9.5	0.9	9.8	27.0	0.10	2.8	1.1	0.48	1.41	5.3	304	96	41	158	166	143	24	
5	BC	1978	-28	11.6	1.1	9.8	26.8	0.09	2.9	1.1	0.47	0.54	5.5	303	112	65	162	170	143	31	
6	BC	1968	-18	9.2	0.9	9.9	27.2	0.16	2.8	1.1	0.48	0.20	6.3	294	135	23	165	171	147	49	
7	BC	1958	-8	8.3	0.9	10.1	27.5	0.11	2.9	1.1	0.50	0.08	5.6	282	129	23	157	149	152	25	
8	BC	1947	3	8.4	0.9	10.3	27.5	0.12	2.9	1.0	0.49	0.08	5.8	294	120	63	160	153	151	40	
9	BC	1937	13	8.3	0.9	10.3	27.6	0.11	2.9	1.0	0.49	0.08	5.3	295	147	60	158	147	154	6	
10	BC	1926	24	8.0	0.9	10.6	28.3	0.03	3.0	1.0	0.51	0.05	5.2	290	213	81	168	144	155	15	
11	BC	1920	30	8.2	0.9	10.4	27.8	0.11	2.9	1.0	0.50	0.05	5.2	275	134	72	167	149	160	14	
12	BC	1915	35	8.0	0.8	10.4	27.7	0.09	2.9	0.9	0.50	0.06	5.8	303	145	81	174	145	150	32	
13	BC	1909	41	8.2	0.8	10.4	27.7	0.11	2.9	1.0	0.50	0.06	5.7	302	127	65	166	145	148	32	III
14	BC	1904	46	8.2	0.9	10.5	27.9	0.11	2.9	1.0	0.50	0.05	5.3	308	138	74	156	144	153	24	
15	BC	1898	52	8.2	1.0	10.4	27.9	0.10	2.9	1.0	0.50	0.05	5.3	294	141	70	157	143	153	24	
16	BC	1876	74	8.2	1.0	10.4	28.0	0.08	2.9	1.0	0.50	0.05	5.4	280	144	67	158	143	153	24	
17	BC	1854	96	8.0	0.8	10.4	28.0	0.09	2.9	0.9	0.50	0.05	5.4	290	115	74	172	145	148	21	
18	BC	1833	117	8.2	0.8	10.3	27.6	0.14	2.9	1.0	0.49	0.05	6.0	303	121	73	164	157	145	61	
19	BC	1811	139	8.2	0.8	10.2	27.5	0.09	2.9	0.9	0.49	0.06	6.3	304	136	75	167	142	159	69	
20	BC	1789	161	8.2	0.8	10.2	27.8	0.09	2.9	1.0	0.49	0.05	5.8	303	191	74	162	140	149	50	
21	BC	1761	189	8.3	1.0	10.5	28.1	0.10	3.0	1.1	0.50	0.04	4.7	300	123	23	156	148	153	1	
22	BC	1731	219	8.8	1.0	10.6	28.2	0.05	3.0	1.1	0.50	0.04	4.6	325	125	23	156	142	149	0	
23	BC	1703	247	8.2	1.0	10.4	28.0	0.03	3.0	1.1	0.50	0.04	4.7	300	162	67	158	137	145	0	
24	BC	1676	274	8.2	0.9	10.4	28.1	0.06	3.0	1.1	0.50	0.04	4.9	328	129	72	159	143	157	0	
25	BC	1650	300	8.3	1.0	10.4	27.8	0.08	3.0	1.1	0.49	0.05	4.8	303	120	56	155	143	151	0	
26	BC	1625	325	8.5	1.1	10.2	27.9	0.02	3.0	1.1	0.49	0.04	5.0	301	141	70	156	143	150	0	
27	BC	1597	353	8.4	1.0	10.2	27.8	0.06	2.9	1.1	0.49	0.04	5.0	308	134	70	151	138	147	0	
28	BC	1569	381	8.3	1.0	10.3	27.8	0.00	3.0	1.1	0.49	0.03	4.9	290	122	66	152	141	150	0	
29	BC	1540	410	8.2	1.0	10.2	28.0	0.08	2.9	1.2	0.49	0.04	4.9	287	120	23	163	138	145	4	
30	BC	1513	437	8.4	1.0	10.2	27.8	0.06	2.9	1.1	0.49	0.04	4.9	308	136	61	155	142	154	4	
31	BC	1478	472	8.4	1.0	10.3	28.2	0.05	3.0	1.1	0.50	0.04	4.9	291	156	23	157	141	154	3	

Table 5 (continued)

Depth 03CS (cm)	Core	Age AD	Age cal yr BP	L.O.I.	Mg (%)	Al (%)	Si (%)	P (%)	K (%)	Ca (%)	Ti (%)	Mn (%)	Fe (%)	V ppm	Cr ppm	Cu ppm	Zn ppm	Sr ppm	Zr ppm	As ppm	Zone
32	BC	1438	512	7.9	1.0	10.1	27.7	0.02	2.9	1.1	0.49	0.04	4.9	290	147	64	147	142	153	0	
33	BC	1401	549	8.3	1.0	10.1	27.5	0.05	2.9	1.1	0.49	0.03	4.9	296	129	23	157	147	149	0	
34	BC	1366	584	8.6	1.1	10.3	27.9	0.03	3.0	1.2	0.50	0.04	5.0	320	142	66	155	138	160	3	
35	BC	1333	617	8.3	1.0	10.2	28.0	0.05	3.0	1.2	0.49	0.03	5.0	317	151	23	156	145	156	4	
36	BC	1279	671	8.2	1.0	10.2	27.6	0.08	2.9	1.1	0.49	0.03	4.9	291	129	63	150	141	146	0	
37	BC	1226	724	8.5	1.0	10.2	27.8	0.05	2.9	1.1	0.49	0.03	5.0	292	131	61	144	140	141	3	
38	BC	1176	774	8.5	0.9	10.2	27.7	0.05	2.9	1.1	0.49	0.03	5.0	303	134	64	158	139	152	10	
39	BC	1126	824	8.5	1.0	10.2	27.7	0.04	2.9	1.1	0.49	0.04	4.9	290	197	69	157	141	155	8	
40	BC	1079	871	8.4	1.0	10.3	28.0	0.05	3.0	1.1	0.49	0.04	5.1	312	149	74	160	143	158	0	
41	BC	1024	926	8.6	1.0	10.3	27.8	0.04	3.0	1.1	0.49	0.04	5.1	298	139	70	158	146	151	4	
42	BC	967	983	8.9	1.0	10.1	27.4	0.06	2.9	1.2	0.48	0.04	4.9	311	207	69	154	145	156	0	
43	BC	909	1041	8.9	1.1	10.2	27.5	0.04	3.0	1.2	0.49	0.03	4.9	310	147	23	152	140	151	0	
44	BC	856	1094	9.1	1.0	10.1	27.7	0.05	3.0	1.2	0.49	0.05	5.0	320	126	23	144	142	145	10	
45	TWC	804	1146	8.2	0.9	10.1	27.4	0.06	2.9	1.1	0.48	0.04	5.4	317	128	68	155	142	140	5	
49	TWC	569	1381	8.1	1.0	10.3	27.7	0.06	3.0	1.1	0.49	0.04	4.9	309	119	67	166	137	146	5	
53	TWC	345	1605	8.2	1.0	10.2	27.7	0.07	3.0	1.2	0.49	0.04	4.9	301	142	57	157	146	150	7	
57	TWC	141	1809	8.2	1.0	10.3	27.6	0.05	3.0	1.2	0.50	0.05	5.1	327	145	59	162	146	152	15	
61	TWC	-28	1978	8.2	0.9	10.4	27.9	0.07	3.0	1.1	0.50	0.04	5.0	322	139	65	161	147	160	3	
65	TWC	-126	2076	9.2	1.1	10.0	27.4	0.02	3.0	1.2	0.49	0.05	4.9	312	126	62	118	149	153	6	
68.5	TWC	-19	2141	9.1	1.1	10.1	27.2	0.02	3.0	1.2	0.49	0.05	4.9	302	121	67	157	141	157	10	
73	TWC	-273	2223	8.3	1.1	10.3	27.6	0.05	3.0	1.2	0.50	0.05	4.9	298	130	70	158	141	148	5	
77	TWC	-345	2295	8.3	1.0	10.3	27.6	0.09	3.0	1.2	0.50	0.05	5.0	309	145	65	152	142	144	0	
81	TWC	-418	2368	8.2	0.9	10.2	27.7	0.05	3.0	1.1	0.49	0.05	4.9	317	119	31	150	143	150	8	I
85	TWC	-495	2445	8.7	1.0	10.1	27.3	0.04	3.0	1.2	0.49	0.05	5.0	301	118	64	144	145	152	4	
89	TWC	-571	2521	8.1	1.0	10.2	27.8	0.09	3.0	1.1	0.49	0.04	5.1	318	127	23	152	139	155	6	
93	TWC	-645	2595	8.4	1.0	10.1	27.5	0.07	3.0	1.1	0.49	0.07	5.5	309	139	31	151	140	150	7	
97	TWC	-721	2671	8.7	1.0	10.0	27.2	0.06	2.9	1.1	0.48	0.10	5.8	300	152	61	150	141	144	8	

Table 5 (continued)

		L.O.I.	Mg	Al	Si	P	K	Ca	Ti	Mn	Fe	V	Cr	Cu	Zn	Sr	Zr	As
Mean		8.5	1.0	10.2	27.7	0.1	2.9	1.1	0.5	0.2	5.2	302	138	56	157	146	151	13
Max		11.6	1.1	10.6	28.3	0.2	3.0	1.2	0.5	2.0	6.3	328	213	81	191	175	160	69
Min		7.9	0.8	9.7	26.8	0.0	2.8	0.9	0.5	0.0	4.6	275	96	23	118	137	140	0
Mean of each zone	IV	9.9	1.0	9.8	27.3	0.1	2.8	1.2	0.48	0.9	5.4	297	126	44	165	169	149	25
	III	8.2	0.9	10.4	27.8	0.1	2.9	1.0	0.50	0.1	5.6	294	143	68	163	146	152	31
	II	8.4	1.0	10.3	27.8	0.1	3.0	1.1	0.49	0.0	4.9	306	140	54	155	142	151	3
	I	8.5	1.0	10.1	27.5	0.1	3.0	1.1	0.49	0.1	5.1	307	131	52	148	142	150	6

CS = composite core; BC = box core; TWC = trigger weight core

ANNEXES

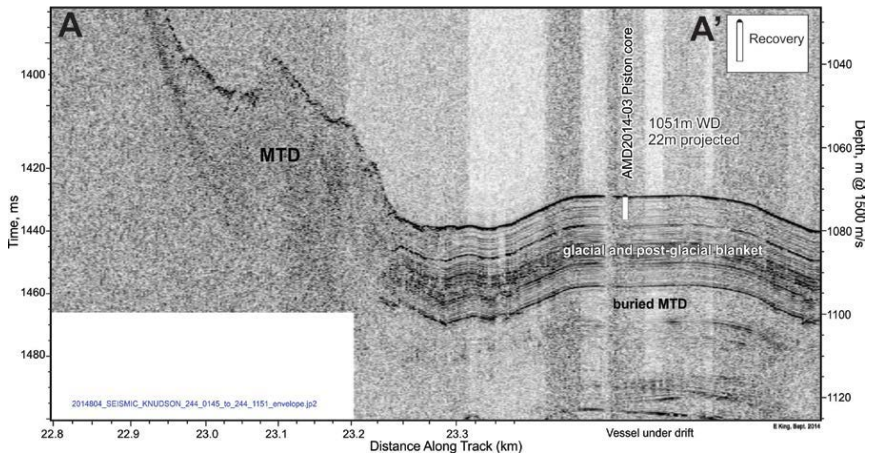

Figure S1. Trigger weight core and box core sampling site AMD2014-03 in relation to 3.5 kHz sub-bottom profiler.

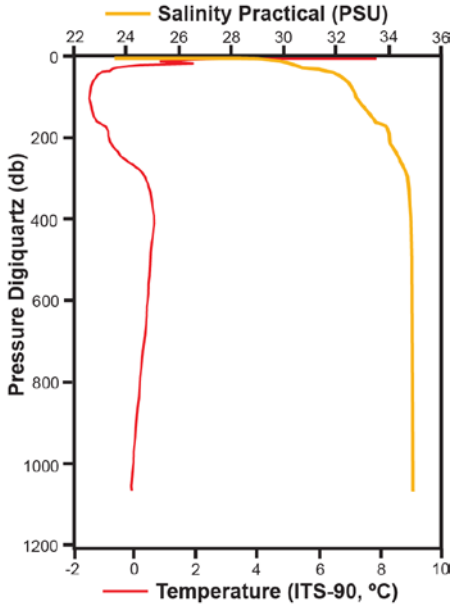

Figure S2. Temperature and salinity profiles (CTD data) from the station AMD0214-03 in August 2014.

(A)

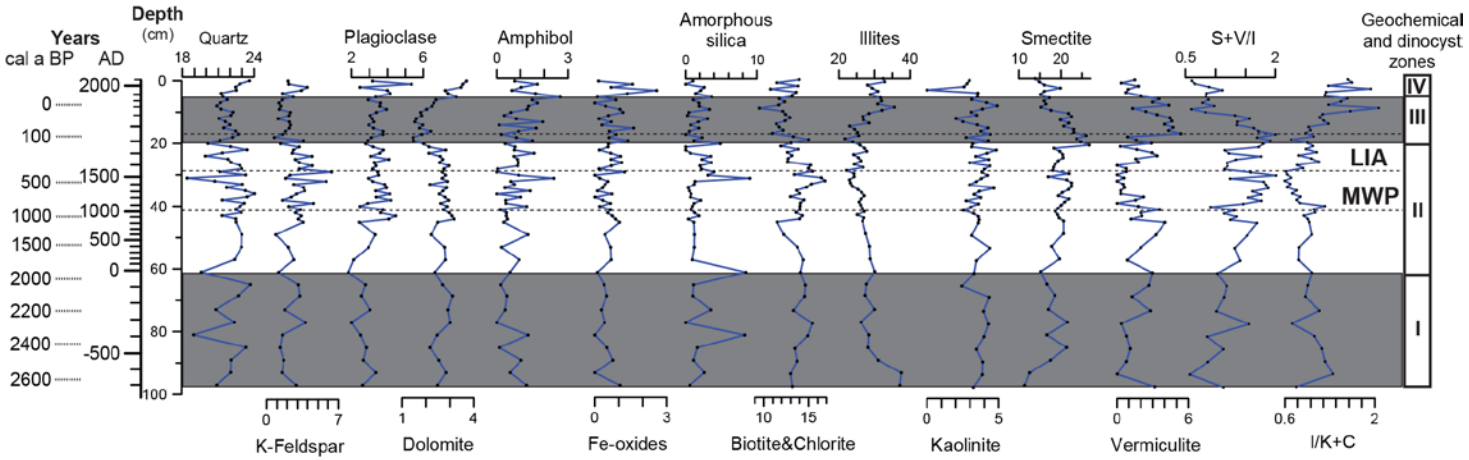

Figure S3. Relative abundances of a) bulk mineralogy, b) clay mineralogy and c) elemental geochemistry from the composite sequence 03CS.

(B)

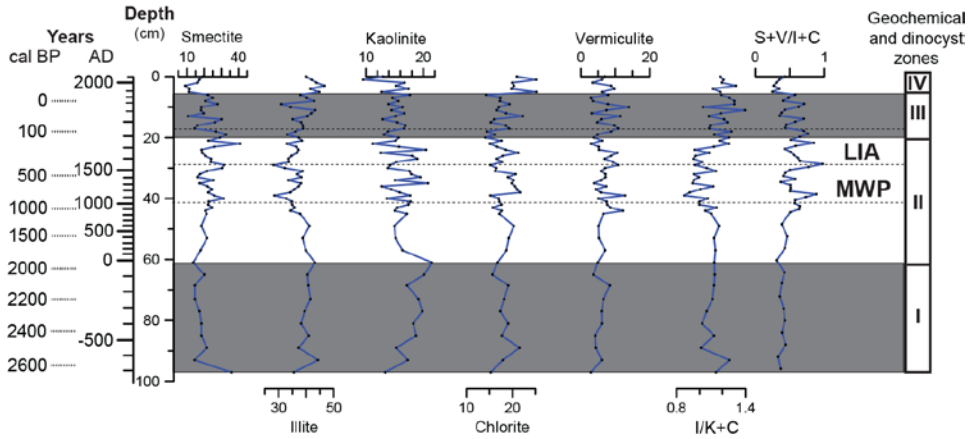
Depth
(cm)
Years
cal BP AD
Smectite
Kaolinite
Vermiculite
S+V/I+C
Geochemical and dinocyst zones
LIA
MWP
IV
III
II
I
Illite
Chlorite
I/K+C

(C)

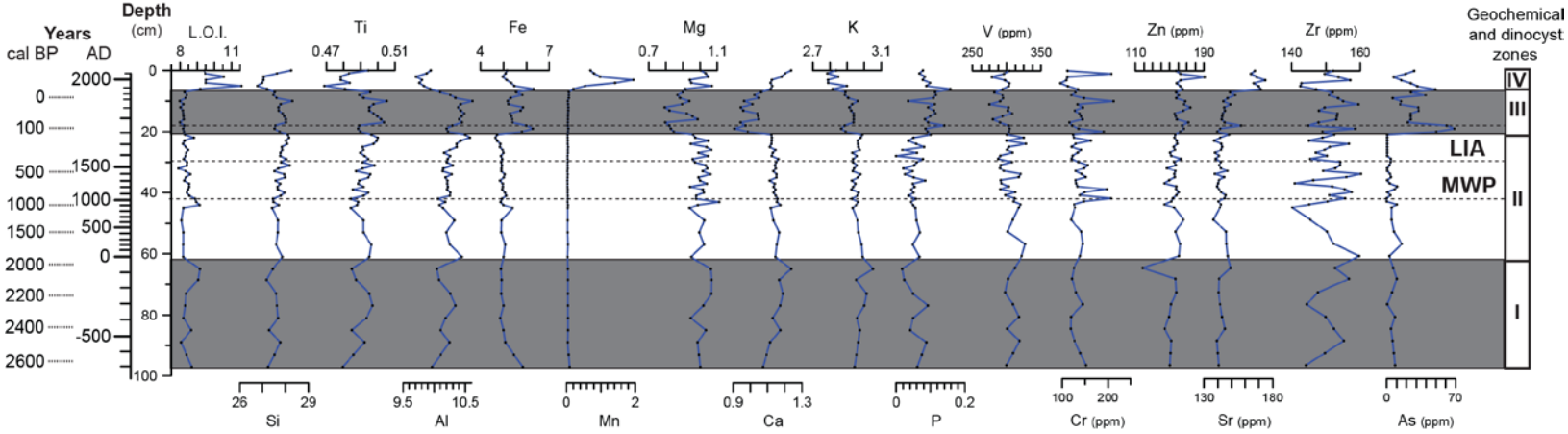
Depth
(cm)
Years
cal BP AD
L.O.I.
Ti
Fe
Mg
K
V (ppm)
Zn (ppm)
Zr (ppm)
Geochemical and dinocyst zones
LIA
MWP
IV
III
II
I
Si
Al
Mn
Ca
P
Cr (ppm)
Sr (ppm)
As (ppm)

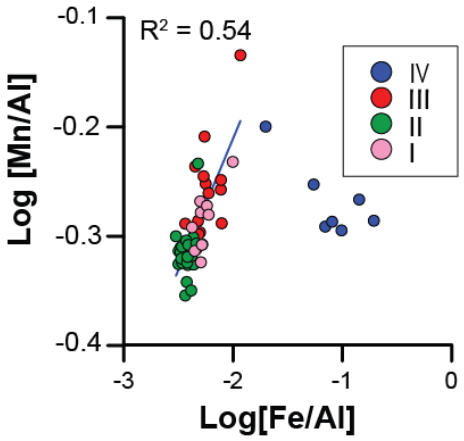

Figure S4. Log[Fe/Al)] versus Log[Mn/Al] from each zone (I, II, III and IV).

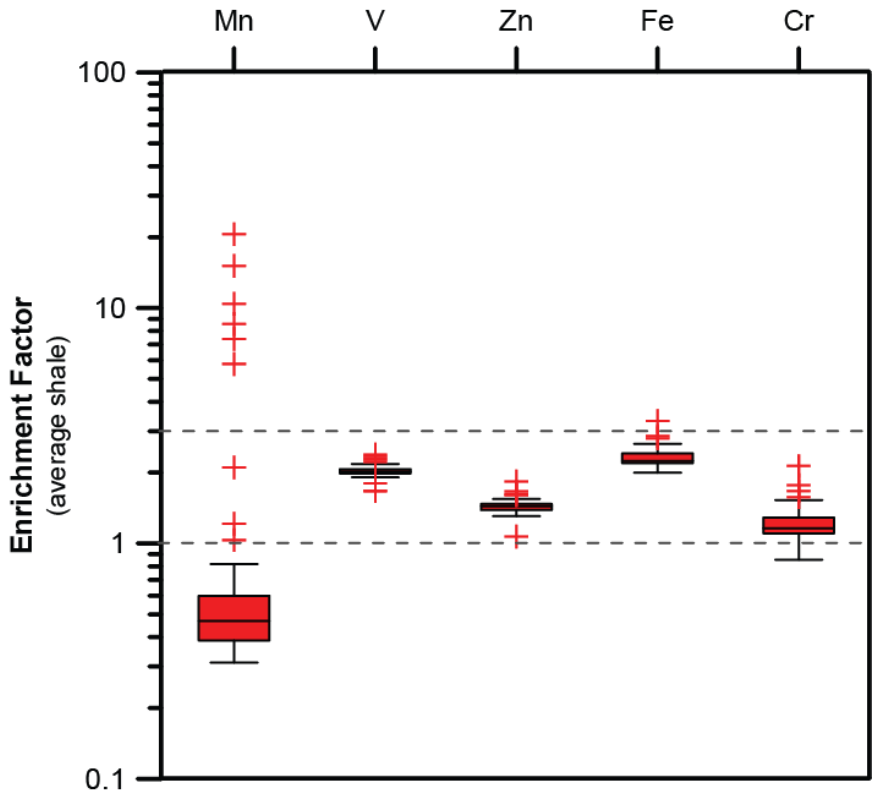

Figure S5. Box plots of the enrichment factors (EF) of redox-sensitive elements (Mn, Fe, V, Cr, Zn) from the Mackenzie Slope.

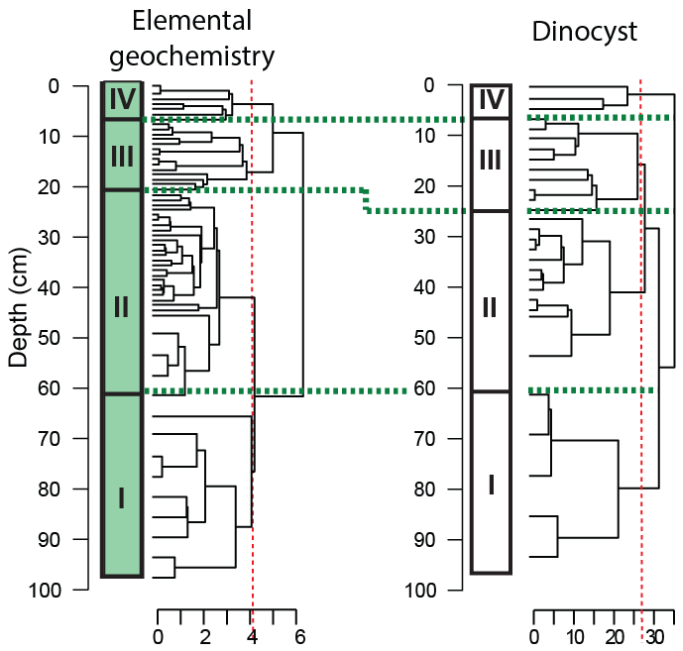

Figure S6. Zonation established using constrained cluster analysis on the geochemical and palynological data.

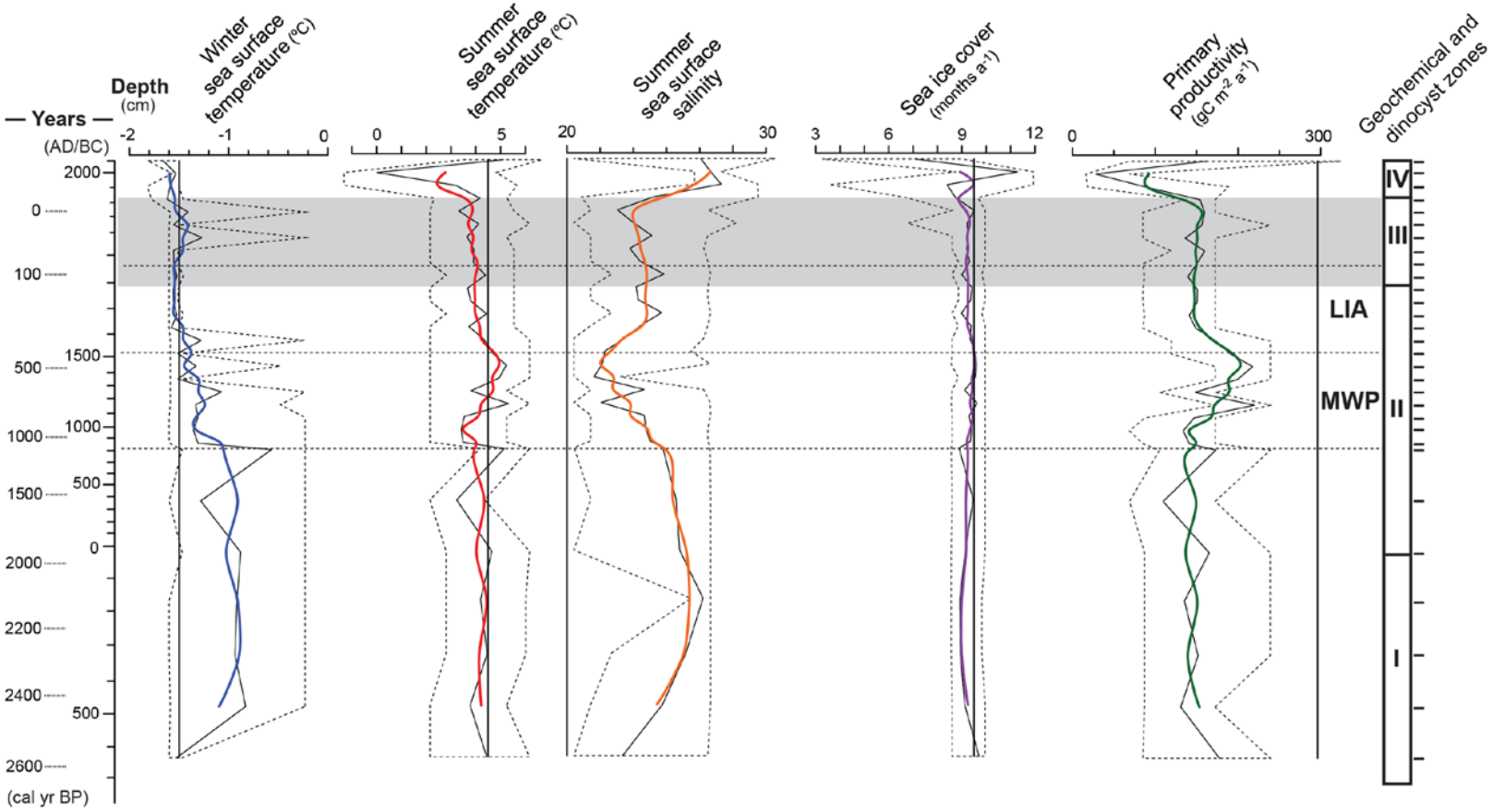

Figure S7. Quantitative reconstruction of sea-surface conditions of composite core 03CS using the modern analogue technique (MAT). The thick curves represent a running average over 3 data points. Dotted areas indicate confidence interval of reconstructions (minimum and maximum reconstructed value according to the set of 5 modern analogues). Solid vertical lines indicate modern sea-surface condition values.

RÉFÉRENCES BIBLIOGRAPHIQUES

Aagaard, K., 1984. The beaufort undercurrent. In: Barnes, P.W., Schell, D.M., Reimnitz, E. (Eds.), The Alaskan Beaufort Sea: Ecosystems and Environments. Elsevier, 47–71.

Aitchison, J., 1990. Relative variation diagrams for describing patterns of compositional variability. Mathematical Geology 22, 487–511.

Anderson, L., Abbott, M.B., Finney, B.P., Burns, S.J., 2005. Regional atmospheric circulation change in the North Pacific during the Holocene inferred from lacustrine carbonate oxygen isotopes, Yukon Territory, Canada. Quaternary Research 64, 21–35.

Anderson, L., Berkelhammer, M., Barron, J.A., Steinman, B.A., Finney, B.P., Abbott, M.B., 2016. Lake oxygen isotopes as recorders of North American Rocky Mountain hydroclimate: Holocene patterns and variability at multi-decadal to millennial time scales. Global and Planetary Change 137, 131–148.

Andrews, J.T., Bjork, A.A., Eberl, D.D., Jennings, A.E., Verplanck, E.P., 2015. Significant differences in late Quaternary bedrock erosion and transport: East versus West Greenland~ 70° N–evidence from the mineralogy of offshore glacial marine sediments. Journal of Quaternary Science 30, 452–463.

Andrews, J.T., Stein, R., Moros, M., Perner, K., 2016. Late Quaternary changes in sediment composition on the NE Greenland margin (~ 73 N) with a focus on the fjords and shelf. Boreas 45, 381–397.

Appleby, P.G., Oldfieldz, F., 1983. The assessment of 210Pb data from sites with varying sediment accumulation rates. Hydrobiologia 103, 29–35.

Barber, D.G., Hanesiak, J.M., 2004. Meteorological forcing of sea ice concentrations in the southern Beaufort Sea over the period 1979 to 2000. Journal of Geophysical Research C: Oceans 109, 16. https://doi.org/10.1029/2003JC002027

Barletta, F., St-Onge, G., Channell, J.E.T., Rochon, A., Polyak, L., Darby, D., 2008. High-resolution paleomagnetic secular variation and relative paleointensity records from the western Canadian Arctic: implication for Holocene stratigraphy and geomagnetic field behaviour. Canadian Journal of Earth Sciences 45, 1265–1281. https://doi.org/10.1139/E08-039

Barron, J.A., Anderson, L., 2011. Enhanced Late Holocene ENSO/PDO expression along the margins of the eastern North Pacific. Quaternary International 235, 3–12.

Bayon, G., German, C.R., Burton, K.W., Nesbitt, R.W., Rogers, N., 2004. Sedimentary Fe–Mn oxyhydroxides as paleoceanographic archives and the role of aeolian flux in regulating oceanic dissolved REE. Earth and Planetary Science Letters 224, 477–492.

Bird, B.W., Wilson, J.J., Gilhooly III, W.P., Steinman, B.A., Stamps, L., 2017. Midcontinental Native American population dynamics and late Holocene hydroclimate extremes. Scientific Reports 7, 41628.

Biscaye, P.E., 1965. Mineralogy and sedimentation of recent deep-sea clay in the Atlantic Ocean and adjacent seas and oceans. Geological Society of America Bulletin 76, 803–832.

Bischof, J., Clark, D.L., Vincent, J.-S., 1996. Origin of ice-rafted debris: Pleistocene paleoceanography in the western Arctic Ocean. Paleoceanography 11, 743. https://doi.org/10.1029/96PA02557

Blaauw, M., Christen, J.A., 2011. Flexible paleoclimate age-depth models using an autoregressive gamma process. Bayesian Analysis 6, 457–474.

Blott, S.J., Pye, K., 2001. GRADISTAT: a grain size distribution and statistics package for

the analysis of unconsolidated sediments. Earth Surface Processes and Landforms 26, 1237–1248.

Bourke, R.H., Garrett, R.P., 1987. Sea ice thickness distribution in the Arctic Ocean. Cold Regions Science and Technology 13, 259–280.

Bout-Roumazeilles, V., Cortijo, E., Labeyrie, L., Debrabant, P., 1999. Clay mineral evidence of nepheloid layer contributions to the Heinrich layers in the northwest Atlantic. Palaeogeography, Palaeoclimatology, Palaeoecology 146, 211–228.

Bradley, R.S., Jonest, P.D., 1993. “Little Ice Age” summer temperature variations: their nature and relevance to recent global warming trends. The Holocene 3, 367–376.

Bringué, M., Rochon, A., 2012. Late Holocene paleoceanography and climate variability over the Mackenzie Slope (Beaufort Sea, Canadian Arctic). Marine Geology 291–294, 83–96. https://doi.org/10.1016/j.margeo.2011.11.004

Brugler, E.T., Pickart, R.S., Moore, G.W.K., Roberts, S., Weingartner, T.J., Statscewich, H., 2014. Seasonal to interannual variability of the Pacific water boundary current in the Beaufort Sea. Progress in Oceanography 127, 1–20.

Brumsack, H.-J., 1989. Geochemistry of recent TOC-rich sediments from the Gulf of California and the Black Sea. Geologische Rundschau 78, 851–882.

Burdige, D.J., 1993. The biogeochemistry of manganese and iron reduction in marine sediments. Earth-Science Reviews 35, 249–284.

Carmack, E., Wassmann, P., 2006. Food webs and physical–biological coupling on pan-Arctic shelves: unifying concepts and comprehensive perspectives. Progress in Oceanography 71, 446–477.

Carmack, E.C., Macdonald, R.W., 2002. Oceanography of the Canadian shelf of the Beaufort Sea: A setting for marine life. Arctic 55, 29–45. https://doi.org/10.1126/science.100.2596.291

Carmack, E.C., Macdonald, R.W., Jasper, S., 2004. Phytoplankton productivity on the Canadian Shelf of the Beaufort Sea. Marine Ecology Progress Series 277, 37–50.

Carson, M.A., Jasper, J.N., Conly, P.M., 1998. Magnitude and sources of sediment input to the Mackenzie Delta, Northwest Territories, 1974-94. Arctic 51, 116–124.

Cassano, E.N., Cassano, J.J., 2010. Synoptic forcing of precipitation in the Mackenzie and Yukon River basins. International Journal of Climatology 30, 658–674. https://doi.org/10.1002/joc.1926

Cavalieri, D.J., Parkinson, C.L., 2012. Arctic sea ice variability and trends, 1979-2010. The Cryosphere 6, 881.

Cohen, J., Screen, J.A., Furtado, J.C., Barlow, M., Whittleston, D., Coumou, D., Francis, J., Dethloff, K., Entekhabi, D., Overland, J., 2014. Recent Arctic amplification and extreme mid-latitude weather. Nature Geoscience 7, 627.

Crowley, T.J., Lowery, T.S., 2000. How warm was the medieval warm period? AMBIO: A Journal of the Human Environment 29, 51–54.

Danielson, S., Curchitser, E., Hedstrom, K., Weingartner, T., Stabeno, P., 2011. On ocean and sea ice modes of variability in the Bering Sea. Journal of Geophysical Research: Oceans 116.

Dansgaard, W., Johnsen, S.J., Clausen, H.B., Dahl-Jensen, D., Gundestrup, N.S., Hammer, C.U., Hvidberg, C.S., Steffensen, J.P., Sveinbjörnsdottir, A.E., Jouzel, J., 1993. Evidence for general instability of past climate from a 250-kyr ice-core record. Nature 364, 218.

Darby, D., Bischof, J., Cutter, G., de Vernal, a., Hillaire-Marcel, C., Dwyer, G., McManus, J., Osterman, L., Polyak, L., Poore, R., 2001. New record shows pronounced changes in Arctic Ocean circulation and climate. Eos, Transactions American Geophysical Union 82, 601–601. https://doi.org/10.1029/01EO00345

Darby, D.A., Bischof, J.F., 2004. A Holocene record of changing Arctic Ocean ice drift analogous to the effects of the Arctic Oscillation. Paleoceanography 19, 1–9. https://doi.org/10.1029/2003PA000961

Darby, D.A., Myers, W.B., Jakobsson, M., Rigor, I., 2011. Modern dirty sea ice characteristics and sources: the role of anchor ice. Journal of Geophysical Research: Oceans 116.

Darby, D.A., Ortiz, J.D., Grosch, C.E., Lund, S.P., 2012. 1,500-year cycle in the Arctic Oscillation identified in Holocene Arctic sea-ice drift. Nature Geoscience 5, 897–900. https://doi.org/10.1038/ngeo1629

de Vernal, A., Eynaud, F., Henry, M., Hillaire-Marcel, C., Londeix, L., Mangin, S., Matthiessen, J., Marret, F., Radi, T., Rochon, A., Solignac, S., Turon, J.L., 2005. Reconstruction of sea-surface conditions at middle to high latitudes of the Northern Hemisphere during the Last Glacial Maximum (LGM) based on dinoflagellate cyst assemblages. Quaternary Science Reviews 24, 897–924. https://doi.org/10.1016/j.quascirev.2004.06.014

de Vernal, A., Henry, M., Matthiessen, J., Mudie, P.J., Rochon, A., Boessenkool, K.P., Eynaud, F., Grosfjeld, K., Guiot, J., Hamel, D., Harland, R., Head, M.J., Kunz-Pirrung, M., Levac, E., Loucheur, V., Peyron, O., Pospelova, V., Radi, T., Turon, J.L., Voronina, E., 2001. Dinoflagellate cyst assemblages as tracers of sea-surface conditions in the Northern North Atlantic, Arctic and sub-Arctic seas: The new “n = 677” data base and its application for quantitative palaeoceanographic reconstruction. Journal of Quaternary Science 16, 681–698. https://doi.org/10.1002/jqs.659

de Vernal, A., Hillaire-Marcel, C., Rochon, A., Fréchette, B., Henry, M., Solignac, S., Bonnet, S., 2013. Dinocyst-based reconstructions of sea ice cover concentration during the Holocene in the Arctic Ocean, the northern North Atlantic Ocean and its adjacent seas. Quaternary Science Reviews 79. https://doi.org/10.1016/j.quascirev.2013.07.006

Dellinger, M., Bouchez, J., Gaillardet, J., Faure, L., Moureau, J., 2017. Tracing weathering regimes using the lithium isotope composition of detrital sediments. Geology 45, 411–414.

Deschamps, C.-É., 2018. Dynamique sédimentaire et paléocéanographie le long des marges continentales des mers de beaufort et des Tchouktches (Océan Arctique) depuis la dernière déglaciation. Université du Québec à Rimouski.

Deschamps, C., Montero-Serrano, J., St-Onge, G., Poirier, A., 2019. Holocene changes in deep-water circulation inferred from authigenic Nd and Hf isotopes in sediment records from the Chukchi-Alaskan and Canadian Beaufort margins. Paleoceanography and Paleoclimatology.

Deschamps, C.E., Montero-Serrano, J.-C., St-Onge, G., 2018a. Sediment Provenance Changes in the Western Arctic Ocean in Response to Ice Rafting, Sea Level, and Oceanic Circulation Variations Since the Last Deglaciation. Geochemistry, Geophysics, Geosystems 19, 2147–2165. https://doi.org/10.1029/2017GC007411

Deschamps, C.E., St-Onge, G., Montero-Serrano, J.-C., Polyak, L., 2018b. Chronostratigraphy and spatial distribution of magnetic sediments in the Chukchi and Beaufort seas since the last deglaciation. Boreas 47, 544–564. https://doi.org/10.1111/bor.12296

Dumas, J., Carmack, E., Melling, H., 2005. Climate change impacts on the Beaufort shelf landfast ice. Cold Regions Science and Technology 42, 41–51.

Dunton, K.H., Weingartner, T., Carmack, E.C., 2006. The nearshore western Beaufort Sea ecosystem: circulation and importance of terrestrial carbon in arctic coastal food webs. Progress in Oceanography 71, 362–378.

Durantou, L., Rochon, A., Ledu, D., Massé, G., Schmidt, S., Babin, M., 2012. Quantitative reconstruction of sea-surface conditions over the last 150 yr in the Beaufort Sea based on dinoflagellate cyst assemblages: the role of large-scale atmospheric circulation

patterns. Biogeosciences 9, 5391–5406. https://doi.org/10.5194/bg-9-5391-2012

Eberl, D.D., 2003. User guide to RockJock-A program for determining quantitative mineralogy from X-ray diffraction data. US Geological Survey.

Ekwurzel, B., Schlosser, P., Mortlock, R.A., Fairbanks, R.G., Swift, J.H., 2001. River runoff, sea ice meltwater, and Pacific water distribution and mean residence times in the Arctic Ocean. Journal of Geophysical Research: Oceans 106, 9075–9092.

El Ouahabi, M., Hubert-Ferrari, A., Fagel, N., 2017. Lacustrine clay mineral assemblages as a proxy for land-use and climate changes over the last 4 kyr: The Amik Lake case study, Southern Turkey. Quaternary International 438, 15–29.

Fagel, N., Not, C., Gueibe, J., Mattielli, N., Bazhenova, E., 2014. Late Quaternary evolution of sediment provenances in the Central Arctic Ocean: mineral assemblage, trace element composition and Nd and Pb isotope fingerprints of detrital fraction from the Northern Mendeleev Ridge. Quaternary Science Reviews 92, 140–154.

Galley, R.J., Key, E., Barber, D.G., Hwang, B.J., Ehn, J.K., 2008. Spatial and temporal variability of sea ice in the southern Beaufort Sea and Amundsen Gulf: 1980–2004. Journal of Geophysical Research: Oceans 113.

Gamboa, A., Montero-Serrano, J., St-Onge, G., Rochon, A., Desiage, P., 2017. Mineralogical, geochemical and magnetic signatures of surface sediments from the Canadian Beaufort Shelf and Amundsen Gulf (Canadian Arctic). Geochemistry, Geophysics, Geosystems 25.

Giovando, L.F., Herlinveaux, R.H., 1981. A Discussion of Factors Influencing Dispersion of Pollutants in the Beaufort Sea. Pacific Marine Science Report. Canada. Department of Fisheries and Oceans. Institute of Ocean Sciences, BC, Sidney, 198.

Grebmeier, J.M., Cooper, L.W., Feder, H.M., Sirenko, B.I., 2006. Ecosystem dynamics of the Pacific-influenced northern Bering and Chukchi Seas in the Amerasian Arctic.

Progress in Oceanography 71, 331–361.

Grimm, E.C., 1987. CONISS: a FORTRAN 77 program for stratigraphically constrained cluster analysis by the method of incremental sum of squares. Computers & Geosciences 13, 13–35.

Guiot, J., 1990. Methods and programs of statistics for paleoclimatology and paleoecology. Quantification Des Changements Climatiques: Methode et Programmes. Institut National Des Sciences de l'Univers (INSU-France), Monographie.

Head, M.J., Harland, R., Matthiessen, J., 2001. Cold marine indicators of the late Quaternary: the new dinoflagellate cyst genus Islandinium and related morphotypes. Journal of Quaternary Science: Published for the Quaternary Research Association 16, 621–636.

Hill, P.R., Blasco, S.M., Harper, J.R., Fissel, D.B., 1991. Sedimentation on the Canadian Beaufort Shelf. Continental Shelf Research 11, 821–842. https://doi.org/10.1016/0278-4343(91)90081-G

Hill, P.R., Lewis, C.P., Desmarais, S., Kauppaymuthoo, V., Rais, H., 2001. The Mackenzie Delta: Sedimentary processes and facies of a high-latitude, fine-grained delta. Sedimentology 48, 1047–1078.

Hook, B.A., Halfar, J., Gedalof, Z., Bollmann, J., Schulze, D.J., 2015. Stable isotope paleoclimatology of the earliest Eocene using kimberlite-hosted mummified wood from the Canadian Subarctic. Biogeosciences 12.

Jakobsson, M., Mayer, L., Coakley, B., Dowdeswell, J.A., Forbes, S., Fridman, B., Hodnesdal, H., Noormets, R., Pedersen, R., Rebesco, M., Schenke, H.W., Zarayskaya, Y., Accettella, D., Armstrong, A., Anderson, R.M., Bienhoff, P., Camerlenghi, A., Church, I., Edwards, M., Gardner, J. V., Hall, J.K., Hell, B., Hestvik, O., Kristoffersen, Y., Marcussen, C., Mohammad, R., Mosher, D., Nghiem, S. V., Pedrosa, M.T., Travaglini, P.G., Weatherall, P., 2012. The International Bathymetric Chart of the Arctic Ocean (IBCAO) Version 3.0. Geophysical Research Letters 39, 1–6.

https://doi.org/10.1029/2012GL052219

Juggins, S., 2019. Analysis of Quaternary Science Data: Package ‘rioja.’

Kalinenko, V. V, 2001. Clay minerals in sediments of the Arctic seas. Lithology and Mineral Resources 36, 362–372.

Khim, B.-K., 2003. Two modes of clay-mineral dispersal pathways on the continental shelves of the East Siberian Sea and western Chukchi Sea. Geosciences Journal 7, 253–262.

Laird, K.R., Fritz, S.C., Cumming, B.F., 1998. A diatom-based reconstruction of drought intensity, duration, and frequency from Moon Lake, North Dakota: a sub-decadal record of the last 2300 years. Journal of Paleolimnology 19, 161–179.

Lamb, H.H., 1965. The early medieval warm epoch and its sequel. Palaeogeography, Palaeoclimatology, Palaeoecology 1, 13–37.

Lapointe, F., Francus, P., Lamoureux, S.F., Vuille, M., Jenny, J.-P., Bradley, R.S., 2017. Influence of North Pacific decadal variability on the western Canadian Arctic over the past 700 years. Climate of the Past 13, 411–420.

Lindsay, R., Schweiger, A., 2015. Arctic sea ice thickness loss determined using subsurface, aircraft, and satellite observations. Cryosphere 9, 269–283. https://doi.org/10.5194/tc-9-269-2015

Lukovich, J. V, Barber, D.G., 2006. Atmospheric controls on sea ice motion in the southern Beaufort Sea. Journal of Geophysical Research: Atmospheres 111.

MacDonald, G.M., Case, R.A., 2005. Variations in the Pacific Decadal Oscillation over the past millennium. Geophysical Research Letters 32.

Macdonald, R.W., Gobeil, C., 2012. Manganese sources and sinks in the Arctic Ocean with reference to periodic enrichments in basin sediments. Aquatic Geochemistry 18, 565–591. https://doi.org/10.1007/s10498-011-9149-9

Macdonald, R.W., Naidu, A.S., Yunker, M.B., Gobeil, C., 2004. The Beaufort Sea: distribution, sources, fluxes and burial of organic carbon. The Organic Carbon Cycle in the Arctic Ocean. Springer Publishing Company, Berlin. 177–193.

Macdonald, R.W., Paton, D.W., Carmack, E.C., 1995. The freshwater budget and under-ice spreading of Mackenzie River water in the Canadian Beaufort Sea based on salinity and 18O/16O measurements in water and ice. Journal of Geophysical Research: Oceans 100, 895–919.

Macdonald, R.W., Solomon, S.M., Cranston, R.E., Welch, H.E., Yunker, M.B., Gobeil, C., 1998. A sediment and organic carbon budget for the Canadian beaufort shelf. Marine Geology 144, 255–273. https://doi.org/10.1016/S0025-3227(97)00106-0

MacNeil, M.R., Garrett, J.R., 1975. Open water surface currents in the southern Beaufort Sea. Beaufort Sea Project, Victoria, BC.

Maechler, M., Rousseeuw, P., Struyf, A., Hubert, M., Hornik, K., 2018. Package 'cluster'. Finding Groups in Data: Cluster Analysis Extended Rousseeuw et al., Dosegljivo na.

Mann, M.E., Zhang, Z., Rutherford, S., Bradley, R.S., Hughes, M.K., Shindell, D., Ammann, C., Faluvegi, G., Ni, F., 2009. Global signatures and dynamical origins of the Little Ice Age and Medieval Climate Anomaly. Science 326, 1256–1260.

Manson, G.K., Solomon, S.M., 2007. Past and future forcing of Beaufort Sea coastal change. Atmosphere-Ocean 45, 107–122. https://doi.org/10.3137/ao.450204

März, C., Stratmann, A., Matthießen, J., Meinhardt, A.-K., Eckert, S., Schnetger, B., Vogt, C., Stein, R., Brumsack, H.-J., 2011. Manganese-rich brown layers in Arctic Ocean sediments: composition, formation mechanisms, and diagenetic overprint. Geochimica et Cosmochimica Acta 75, 7668–7687.

Matthews, J., 1969. The assessment of a method for the determination of absolute pollen frequencies. New Phytologist 68, 161–166.

McBean, G., Alekseev, G., Chen, D., Foerland, E., Fyfe, J., Groisman, P.Y., King, R., Melling, H., Vose, R., Whitfield, P.H., 2005. Chapter 2. Arctic Climate: past and present, impact of a warming Arctic. Arctic Climate Impact Assessment (ACIA), Arctic Climate Impact Assessment (ACIA). Canbridge.

McLaughlin, F., Carmack, E., Macdonald, R., Weaver, A.J., Smith, J., 2002. The Canada Basin, 1989–1995: Upstream events and far-field effects of the Barents Sea. Journal of Geophysical Research: Oceans 107, 20.

McLaughlin, F.A., Carmack, E.C., Macdonald, R.W., Melling, H., Swift, J.H., Wheeler, P.A., Sherr, B.F., Sherr, E.B., 2004. The joint roles of Pacific and Atlantic-origin waters in the Canada Basin, 1997–1998. Deep Sea Research Part I: Oceanographic Research Papers 51, 107–128.

Meinhardt, A.-K., Pahnke, K., Böning, P., Schnetger, B., Brumsack, H.-J., 2016. Climate change and response in bottom water circulation and sediment provenance in the Central Arctic Ocean since the Last Glacial. Chemical Geology 427, 98–108.

Melling, H., 2000. Exchanges of freshwater through the shallow straits of the North American Arctic. The Freshwater Budget of the Arctic Ocean. Springer, Dordrecht, 479–502.

Millot, R., Gaillardet, J., Dupré, B., Allègre, C.J., 2003. Northern latitude chemical weathering rates: clues from the Mackenzie River Basin, Canada. Geochimica et Cosmochimica Acta 67, 1305–1329.

Montero-Serrano, J.-C., Deschamps, C.E., Jaegle, M., 2014. Amundsen Expedition Report: Geology and paleoceanography leg 2a, ArctiNet, Université Laval.

Mudie, P.J., Rochon, A., 2001. Distribution of dinoflagellate cysts in the Canadian Arctic marine region. Journal of Quaternary Science 16, 603–620.

Naidu, A.S., Burrell, D.C., Hood, D.W., 1971. Clay mineral composition and geologic

significance of some Beaufort Sea sediments. Journal of Sedimentary Research 41, 691–694.

Naidu, A.S., Creager, J.S., Mowatt, T.C., 1982. Clay mineral dispersal patterns in the north Bering and Chukchi Seas. Marine Geology 47, 1–15.

Naidu, A.S., Mowatt, T.C., 1983. Sources and dispersal patterns of clay minerals in surface sediments from the continental-shelf areas off Alaska. Geological Society of America Bulletin 94, 841–854.

Nikolopoulos, A., Pickart, R.S., Fratantoni, P.S., Shimada, K., Torres, D.J., Jones, E.P., 2009. The western Arctic boundary current at 152 W: Structure, variability, and transport. Deep Sea Research Part II: Topical Studies in Oceanography 56, 1164–1181.

NODC, N.O.D.C., 2001. World Ocean Atlas. National Oceanographic Data Center.

O'Brien, M.C., Macdonald, R.W., Melling, H., Iseki, K., 2006. Particle fluxes and geochemistry on the Canadian Beaufort Shelf: Implications for sediment transport and deposition. Continental Shelf Research 26, 41–81. https://doi.org/10.1016/j.csr.2005.09.007

Okkonen, S.R., Schmidt, G.M., Cokelet, E.D., Stabeno, P.J., 2004. Satellite and hydrographic observations of the Bering Sea 'Green Belt.' Deep Sea Research Part II: Topical Studies in Oceanography 51, 1033–1051.

Osborne, P.D., Forest, A., 2016. Sediment dynamics from coast to slope–Southern Canadian Beaufort Sea. Journal of Coastal Research 75, 537–542.

Overland, J.E., Adams, J.M., Bond, N.A., 1999. Decadal variability of the Aleutian low and its relation to high-latitude circulation. Journal of Climate 12, 1542–1548.

Padgham, W.A., Fyson, W.K., 1992. The Slave province: A distinct Archean craton. Canadian Journal of Earth Sciences 29, 2072–2086.

Pelletier, B.R., 1975. Sediment dispersal in the southern Beaufort Sea. Beaufort Sea Project, Victoria, BC.

Petschick, R., 2000. MacDiff 4.2. 5 Manual, Institut für Geologie, Universität Erlangen: 917 Germany.

Pickart, R.S., 2004. Shelfbreak circulation in the Alaskan Beaufort Sea: Mean structure and variability. Journal of Geophysical Research C: Oceans 109, 1–14. https://doi.org/10.1029/2003JC001912

Pickart, R.S., Macdonald, A.M., Moore, G.W.K., Renfrew, I.A., Walsh, J.E., Kessler, W.S., 2009. Seasonal evolution of Aleutian low pressure systems: Implications for the North Pacific subpolar circulation. Journal of Physical Oceanography 39, 1317–1339.

Pieńkowski, A.J., Mudie, P.J., England, J.H., Smith, J.N., Furze, M.F.A., 2011. Late Holocene environmental conditions in Coronation Gulf, southwestern Canadian Arctic Archipelago: evidence from dinoflagellate cysts, other non-pollen palynomorphs, and pollen. Journal of Quaternary Science 26, 839–853.

Podritske, B., Gajewski, K., 2007. Diatom community response to multiple scales of Holocene climate variability in a small lake on Victoria Island, NWT, Canada. Quaternary Science Reviews 26, 3179–3196.

Pourmand, A., Dauphas, N., Ireland, T.J., 2012. A novel extraction chromatography and MC-ICP-MS technique for rapid analysis of REE, Sc and Y: Revising CI-chondrite and Post-Archean Australian Shale (PAAS) abundances. Chemical Geology 291, 38–54.

Prell, W.L., 1985. Stability of low-latitude sea-surface temperatures: an evaluation of the CLIMAP reconstruction with emphasis on the positive SST anomalies. Final report. Brown Univ., Providence, RI (USA). Dept. of Geological Sciences.

Price, A.M., Gurdebeke, P.R., Mertens, K.N., Pospelova, V., 2016. Determining the absolute abundance of dinoflagellate cysts in recent marine sediments III: Identifying the source

of Lycopodium loss during palynological processing and further testing of the Lycopodium marker-grain method. Review of Palaeobotany and Palynology 226, 78–90.

Radi, T., Bonnet, S., Cormier, M.-A., De Vernal, A., Durantou, L., Faubert, É., Head, M.J., Henry, M., Pospelova, V., Rochon, A., 2013. Operational taxonomy and (paleo-) autecology of round, brown, spiny dinoflagellate cysts from the Quaternary of high northern latitudes. Marine Micropaleontology 98, 41–57.

Radi, T., de Vernal, A., 2008. Dinocysts as proxy of primary productivity in mid–high latitudes of the Northern Hemisphere. Marine Micropaleontology 68, 84–114.

Radi, T., Pospelova, V., de Vernal, A., Barrie, J.V., 2007. Dinoflagellate cysts as indicators of water quality and productivity in British Columbia estuarine environments. Marine Micropaleontology 62, 269–297.

Radi, T., Vernal, A. de, Peyron, O., 2001. Relationships between dinoflagellate cyst assemblages in surface sediment and hydrographic conditions in the Bering and Chukchi seas. Journal of Quaternary Science: Published for the Quaternary Research Association 16, 667–680.

Rasmussen, S.O., Andersen, K.K., Svensson, A.M., Steffensen, J.P., Vinther, B.M., Clausen, H.B., Siggaard-Andersen, M., Johnsen, S.J., Larsen, L.B., Dahl-Jensen, D., 2006. A new Greenland ice core chronology for the last glacial termination. Journal of Geophysical Research: Atmospheres 111.

Richerol, T., Rochon, A., Blasco, S., Scott, D.B., Schell, T.M., Bennett, R.J., 2008a. Distribution of dinoflagellate cysts in surface sediments of the Mackenzie Shelf and Amundsen Gulf, Beaufort Sea (Canada). Journal of Marine Systems 74, 825–839. https://doi.org/10.1016/j.jmarsys.2007.11.003

Richerol, T., Rochon, A., Blasco, S., Scott, D.B., Schell, T.M., Bennett, R.J., 2008b. Evolution of paleo sea-surface conditions over the last 600 years in the Mackenzie

Trough, Beaufort Sea (Canada). Marine Micropaleontology 68, 6–20.

Robock, A., 1979. The “Little Ice Age”: Northern hemisphere average observations and model calculations. Science 206, 1402–1404.

Rochon, A., de Vernal, A., Turon, J.-L., Matthießen, J., Head, M.J., 1999. Distribution of recent dinoflagellate cysts in surface sediments from the North Atlantic Ocean and adjacent seas in relation to sea-surface parameters. American Association of Stratigraphic Palynologists Contribution Series 35, 1–146.

Rodionov, S.N., Bond, N.A., Overland, J.E., 2007. The Aleutian Low, storm tracks, and winter climate variability in the Bering Sea. Deep Sea Research Part II: Topical Studies in Oceanography 54, 2560–2577.

Rothrock, D.A., Yu, Y., Maykut, G.A., 1999. Thinning of the Arctic sea-ice cover. Geophysical Research Letters 26, 3469. https://doi.org/10.1029/1999GL010863

Ruiz-Fernández, A.C., Hillaire-Marcel, C., 2009. 210Pb-derived ages for the reconstruction of terrestrial contaminant history into the Mexican Pacific coast: Potential and limitations. Marine Pollution Bulletin 59, 134–145.

Schell, T.M., Moss, T.J., Scott, D.B., Rochon, A., 2008. Paleo – sea ice conditions of the Amundsen Gulf , Canadian Arctic Archipelago : Implications from the foraminiferal record of the last 200 years. 113, 1–14. https://doi.org/10.1029/2007JC004202

Schneider, N., Cornuelle, B.D., 2005. The forcing of the Pacific decadal oscillation. Journal of Climate 18, 4355–4373.

Schoster, F., Behrends, M., Müller, C., Stein, R., Wahsner, M., 2000. Modern river discharge and pathways of supplied material in the Eurasian Arctic Ocean: evidence from mineral assemblages and major and minor element distribution. International Journal of Earth Sciences 89, 486–495.

Scott, D.B., Schell, T., St-Onge, G., Rochon, A., Blasco, S., 2009. Foraminiferal assemblage

changes over the last 15,000 years on the Mackenzie-Beaufort Sea Slope and Amundsen Gulf, Canada: Implications for past sea ice conditions. Paleoceanography 24, 1–20. https://doi.org/10.1029/2007PA001575

Serreze, M.C., Francis, J.A., 2006. The Arctic amplification debate. Climatic Change 76, 241–264.

Serreze, M.C., Meier, W.N., 2018. The Arctic's sea ice cover: trends, variability, predictability, and comparisons to the Antarctic. Annals of the New York Academy of Sciences.

Stein, R., Fahl, K., Schade, I., Manerung, A., Wassmuth, S., Niessen, F., Nam, S., 2017. Holocene variability in sea ice cover, primary production, and Pacific-Water inflow and climate change in the Chukchi and East Siberian Seas (Arctic Ocean). Journal of Quaternary Science 32, 362–379.

Sugimoto, S., Hanawa, K., 2009. Decadal and interdecadal variations of the Aleutian Low activity and their relation to upper oceanic variations over the North Pacific. Journal of the Meteorological Society of Japan. Ser. II 87, 601–614.

Sundby, B., Lecroart, P., Anschutz, P., Katsev, S., Mucci, A., 2015. When deep diagenesis in Arctic Ocean sediments compromises manganese-based geochronology. Marine Geology 366, 62–68.

Treshnikov, A.F., Nikiforov, Y.G., Blinov, N.I., 1977. Results of oceanological investigations by the "north pole"; drifting stations. Polar Geography 1, 22–40.

Tribovillard, N., Algeo, T.J., Lyons, T., Riboulleau, A., 2006. Trace metals as paleoredox and paleoproductivity proxies: an update. Chemical Geology 232, 12–32.

Versteegh, G.J.M., Blokker, P., Bogus, K.A., Harding, I.C., Lewis, J., Oltmanns, S., Rochon, A., Zonneveld, K.A.F., 2012. Infra red spectroscopy, flash pyrolysis, thermally assisted hydrolysis and methylation (THM) in the presence of tetramethylammonium hydroxide

(TMAH) of cultured and sediment-derived Lingulodinium polyedrum (Dinoflagellata) cyst walls. Organic Geochemistry 43, 92–102.

Viscosi-Shirley, C., Mammone, K., Pisias, N., Dymond, J., 2003. Clay mineralogy and multi-element chemistry of surface sediments on the Siberian-Arctic shelf: implications for sediment provenance and grain size sorting. Continental Shelf Research 23, 1175–1200. https://doi.org/10.1016/S0278-4343(03)00091-8

Wahsner, M., Müller, C., Stein, R., Ivanov, G., Levitan, M., Shelekhova, E., Tarasov, G., 1999. Clay-mineral distribution in surface sediments of the Eurasian Arctic Ocean and continental margin as indicator for source areas and transport pathways—a synthesis. Boreas 28, 215–233.

Wall, D., Dale, B., 1966. "Living Fossils" in Western Atlantic Plankton. Nature 211, 1025–1026.

Walsh, J.E., Crane, R.G., 1992. A comparison of GCM simulations of Arctic climate. Geophysical Research Letters 19, 29–32.

Ward, J.H., 1963. Hierarchical grouping to optimize an objective function. Journal of the American Statistical Association 58, 236–244.

Wedepohl, K.H., 1991. The composition of the upper earth's crust and the natural cycles of selected metals. Metals in natural raw materials. Natural Resources. In: Merian, E.(Ed.), Metals and Their Compounds in the Environment. VCH, Weinheim 3–17.

Williams, G.L., Fensome, R.A., Andrew MacRae, R., 2017. The Lentin and Williams index of fossil dinoflagellates, 2017 Edition. Assoc. Strat. Paly., Contributions Series 42, 909.

Wills, R.C.J., Battisti, D.S., Proistosescu, C., Thompson, L., Hartmann, D.L., Armour, K.C., 2019. Ocean Circulation Signatures of North Pacific Decadal Variability. Geophysical Research Letters 46, 1690–1701.

Yamamoto, M., Nam, S.-I., Polyak, L., Kobayashi, D., Suzuki, K., Irino, T., Shimada, K.,

2017. Holocene dynamics in the Bering Strait inflow to the Arctic and the Beaufort Gyre circulation based on sedimentary records from the Chukchi Sea. Climate of the Past 13, 1111–1127.

Zhang, L., Delworth, T.L., 2015. Analysis of the characteristics and mechanisms of the Pacific Decadal Oscillation in a suite of coupled models from the Geophysical Fluid Dynamics Laboratory. Journal of Climate 28, 7678–7701.

Zonneveld, K.A.F., Marret, F., Versteegh, G.J.M., Bogus, K., Bonnet, S., Bouimetarhan, I., Crouch, E., de Vernal, A., Elshanawany, R., Edwards, L., 2013. Atlas of modern dinoflagellate cyst distribution based on 2405 data points. Review of Palaeobotany and Palynology 191, 1–197.

Zonneveld, K.A.F., Versteegh, G.J.M., De Lange, G.J., 2001. Palaeoproductivity and post-depositional aerobic organic matter decay reflected by dinoflagellate cyst assemblages of the Eastern Mediterranean S1 sapropel. Marine Geology 172, 181–195.